Architecture of soil microaggregates: Advanced methodologies to explore properties and functions

Wulf Amelung[1,2] | Ni Tang[1] | Nina Siebers[2] | Michaela Aehnelt[3] | Karin Eusterhues[3] | Vincent J. M. N. L. Felde[4] | Georg Guggenberger[5] | Klaus Kaiser[6] | Ingrid Kögel-Knabner[7,8] | Erwin Klumpp[2] | Claudia Knief[9] | Jens Kruse[2] | Eva Lehndorff[10] | Robert Mikutta[6] | Stephan Peth[4] | Nadja Ray[11] | Alexander Prechtel[12] | Thomas Ritschel[3] | Steffen A. Schweizer[7] | Susanne K. Woche[5] | Bei Wu[2] | Kai U. Totsche[3]

[1]Institute of Crop Science and Resource Conservation (INRES), Soil Science and Soil Ecology, University of Bonn, Bonn, Germany

[2]Institute of Bio- and Geosciences, Agrosphere (IBG-3), Forschungszentrum Jülich GmbH, Jülich, Germany

[3]Department of Hydrogeology, Institute for Geosciences, Friedrich Schiller University Jena, Jena, Germany

[4]Institute of Soil Science, Soil Biophysics, Leibniz University Hannover, Hannover, Germany

[5]Institute of Soil Science, Soil Chemistry, Leibniz University Hannover, Hannover, Germany

[6]Department of Soil Science and Protection, Institute of Agricultural and Nutrition Science, Martin Luther University Halle-Wittenberg, Halle (Saale), Germany

[7]School of Life Sciences, Chair of Soil Science, Technical University Munich, Freising, Germany

[8]Institute for Advanced Study, Technical University of Munich, Garching, Germany

[9]Institute of Crop Science and Resource Conservation (INRES), Molecular Biology of the Rhizosphere, University of Bonn, Bonn, Germany

[10]Department of Soil Ecology, Faculty for Biology, Chemistry, and Earth Science, Bayreuth University, Bayreuth, Germany

[11]Department of Mathematics, Mathematical Institute for Machine Learning and Data Science, Chair of Geomatics and Geomathematics, Catholic University of Eichstätt-Ingolstadt, Ingolstadt, Germany

[12]Department of Mathematics–Modelling and Numerics, Friedrich-Alexander University Erlangen-Nürnberg, Erlangen, Germany

Correspondence
Wulf Amelung and Ni Tang, Institute of Crop Science and Resource Conservation (INRES),Soil Science and Soil Ecology, University of Bonn, Nussallee 13, 53115 Bonn, Germany; Institute of Bio- and Geosciences, Agrosphere (IBG-3), Forschungszentrum Jülich GmbH, Wilhelm-Johnen-Straße, Jülich 52425, Germany.
Email: wulf.amelung@uni-bonn.de and ntang@uni-bonn.de

This article has been edited by Thomas Scholten.

Abstract

The functions of soils are intimately linked to their three-dimensional pore space and the associated biogeochemical interfaces, mirrored in the complex structure that developed during pedogenesis. Under stress overload, soil disintegrates into smaller compound structures, conventionally named aggregates. Microaggregates (<250 µm) are recognized as the most stable soil structural units. They are built of mineral, organic, and biotic materials, provide habitats for a vast diversity of microorganisms, and are closely involved in the cycling of matter and energy. However, exploring the architecture of soil microaggregates and their linkage to soil functions remains a challenging but demanding scientific endeavor. With the advent of complementary spectromicroscopic and tomographic techniques, we can now assess and visualize the size, composition, and porosity of microaggregates and the spatial arrangement of their interior building units. Their combinations with advanced experimental pedology, multi-isotope labeling experiments,

and computational approaches pave the way to investigate microaggregate turnover and stability, explore their role in element cycling, and unravel the intricate linkage between structure and function. However, spectromicroscopic techniques operate at different scales and resolutions, and have specific requirements for sample preparation and microaggregate isolation; hence, special attention must be paid to both the separation of microaggregates in a reproducible manner and the synopsis of the geography of information that originates from the diverse complementary instrumental techniques. The latter calls for further development of strategies for synlocation and synscaling beyond the present state of correlative analysis. Here, we present examples of recent scientific progress and review both options and challenges of the joint application of cutting-edge techniques to achieve a sophisticated picture of the properties and functions of soil microaggregates.

KEYWORDS

aggregate dispersion and fractionation, in silico soil aggregates, microbial biogeography of aggregates, soil interfaces, spectromicroscopy

1 | INTRODUCTION

Soil is a structured porous medium built from various mineral, organic, and biotic constituents, partly retaining the properties of the parent rock. The formation of this structure is mediated by soil organisms, water menisci, as well as by organic "gluing" agents (e.g., proteins and polysaccharides) and inorganic "cementing" agents (e.g., secondary (hydr)oxides of iron, manganese, and aluminum, and carbonates), which, along with other constituents, including clay minerals and organo-mineral associations, form fundamental structural subunits known as aggregates (Tisdall & Oades, 1982; Totsche et al., 2018). Soil microaggregates have, by definition, a size of <250 μm. They can be further classified into the clay- and silt-sized particles (<20 μm) and small- (20–53 μm) and large- (53–250 μm) microaggregates, which are frequently organized in a hierarchical order, and thus, eventually occur within larger structural units, often termed macroaggregates (Jastrow et al., 1996; Oades & Waters, 1991; Tisdall & Oades, 1982). As there is no international consensus on the size of silt, recent reviews just grouped all microaggregates >20 μm as large microaggregates (20–250 μm) and smaller ones as small microaggregates (<20 μm; Totsche et al., 2018). The aggregate hierarchy model, prominently exposed by Jarvis et al. (2012), is widely accepted, though also critically discussed (Baveye, 2006; Baveye, 2021; Vogel et al., 2022). The model applies well to some soils, for example, Mollisols, while hierarchical orders are missing in other soils, such as Oxisols, where low-activity clay minerals are cemented by iron and aluminum (hydr)oxides to pseudo-silt and pseudo-sand structures. In either case, the dynamic spatial arrangement of particles to soil aggregates, being inwrought by intra-aggregate and inter-aggregate pores, finally shapes soil structure (Soil Science Society of America, 1997).

The interconnected pore system allows for the flow of liquids and gases, the transport of dissolved compounds and colloidal particles, and the allocation of soil biota, while physico-chemical niches provide space for the thriving life of soil microorganisms. Changes in aggregate architecture have major implications for many soil functions (Dexter, 1988), for example, water storage and transport, biological activity and habitat, seedbed quality, as well as the storage and biogeochemical cycling of carbon, nitrogen, and other elements, in addition to that also controlling soils' major provision, supporting and regulating functionalities and ecosystem services. Nevertheless, characterizing soil structure solely from the perspective of aggregates has been criticized (Baveye, 2006; Letey, 1991; Rabot et al., 2018; Vogel et al., 2022). One key argument is that soil processes are frequently related to soil aggregates' turnover and mechanical stability rather than the structure itself (Rabot et al., 2018). While this criticism reflects that most previous studies focused mainly on analyzing the size and stability of aggregates instead of their architecture and spatial arrangement, it overlooks the need to focus research on the domain that links the fluid-filled void space with the solids: The biogeochemical interfaces (Totsche et al., 2010) and the roles that the physicochemical and morphological properties play in soil functioning.

Unfortunately, soil's opaque nature limits the direct observation of spatial relationships between soil constituents and, thus, the build-up and functions of its microstructural units. As insitu probing of soil aggregates is usually not possible, common approaches to characterize soil aggregates have to release them from soils using different separation and fractionation techniques, such as mechanical crushing, size or density separation, sonification, or slicing (Díaz-Zorita et al., 2002; Edwards & Bremner, 1967; Felde et al., 2021; Kaiser et al., 2012). The isolated subunits may feature inherent stable properties of the original soil structure, as well as artifacts introduced by the respective fractionation technique (Baveye, 2006), particularly when particles reaggregate (e.g., Siebers et al., 2018).

With the advent of sophisticated spectromicroscopic approaches, advances have been made to image the compositions and forms of soil organic matter (SOM; Weng et al., 2022), soil–root interaction on

micro- and nanoscales (Lippold et al., 2023; Vidal et al., 2018), and soil aggregates of different sizes in two-dimensional (2–D) or three-dimensional (3–D) arrays (Gerke et al., 2021; Lehndorff et al., 2021; Voltolini et al., 2017; Xiao et al., 2019; Young & Crawford, 2004), as well as to characterize microtopography (Gazze et al., 2018) and chemical hotspots at nanoscale resolution (e.g., Lehmann et al., 2007; Rennert et al., 2012; Schweizer et al., 2018; Vogel et al., 2014). In addition, progress has been made in linking aggregate structure to microbial community composition, diversity, or activity (Bach & Hofmockel, 2014; Biesgen et al., 2020; Felde et al., 2021; Upton et al., 2019), and in tracing the evolvement and dynamics of microarchitecture by computational methods (Guhra et al., 2021; Ray et al., 2017; Ritschel & Totsche, 2019; Rupp et al., 2019; Zech et al., 2020, 2022). On an even smaller scale, specific organic matter interactions with mineral surfaces can also be evaluated with the help of molecular modeling, often restricted to simple organic matter fragments as well as short time and length scales (Schaumann & Thiele-Brun, 2011). Although the full diversity of SOM-related aggregation is hardly be captured by these methods, the detailed viewpoint by using quantum or classical molecular mechanics has significantly advanced our understanding of the stability of, for example, organic aggregates or of the interactions of organic matter with reactive mineral surfaces (see Gerzabek et al., 2022, for a review).

The instrumental techniques to explore microaggregates operate at different scales and require different pretreatments, which challenges information integration. Therefore, we aimed to review the state-of-the-art of advanced techniques that are currently utilized in soil aggregate research, including isolation and size differentiation, identification and mapping of chemical composition, visualization of spatial arrangements of, for example, organic matter, minerals, and microorganisms, and related mathematical modeling approaches. Finally, we provide a guideline developed from "lessons learned" and recommend future opportunities to better understand soil aggregates' formation, stability, properties, and functions.

2 | ADVANCEMENTS IN MICROAGGREGATE ISOLATION

2.1 | Soil fractionation

A sampling of aggregates in the field usually follows the method of Peerlkamp (1959). It recommends extracting a spade-sized soil block and gently separating it into aggregates by hand. After that, a range of dry or wet sieving may follow to determine aggregates size distributions and stability (Díaz-Zorita et al., 2002; Kemper & Rosenau, 1986; see also reviews by Amézketa (1999) and Hu et al. (2023)). While the largest aggregates can be gently isolated by sieving and crushing, small microaggregates and particles (<20 μm) need more advanced techniques for size separation, such as the gravitational split-flow thin-cell (SPLITT) technique. This technique is applied for continuous and preparative size fractionation (Williams, 2022), and has been used to

separate and isolate size fractions of both, marine sediments (Dickens et al., 2006; Keil et al., 1994; Moon et al., 2005) and soils (e.g., Kiem et al., 2002). SPLITT utilizes gravity to differentiate size fractions in a size range of 1–300 μm according to particle settling velocity (Giddings, 1985; Springston et al., 1987).

Dispersion procedures are needed to release microaggregates trapped within macroaggregates (Six et al., 2000a). Traditionally, sonication has been applied for about 40 years (Edwards & Bremner, 1967) to support soil dispersion and isolation of water-stable aggregates. Probe-type ultrasonic systems are mainly used where the ultrasonic probe is inserted into suspensions of soil aggregates. The probe vibrates at an ultrasonic frequency leading to the emission of acoustic pressure waves that cause mechanical straining, disaggregation, and dispersion of soil aggregates (Kaiser & Berhe, 2014). Using calorimetric calibration (North, 1976), the specific dispersive energy released into the suspension can be estimated (Kachanoski et al., 1988). The energy required for dispersion strongly depends on the stability of the investigated aggregates. Using earlier methods such as shaking with glass beads for aggregate dispersion is not recommended as reproducibility among laboratories is limited. Difficulties arose because of the low reliability of commercially available equipment, where deviations of up to 300% had been reported between the displayed and truly measured ultrasonic energy output (Schmidt et al., 1999). However, a recent study showed that after calorimetric calibration, sonication produced reliably replicable disruption of aggregates among nine different laboratories using different sonication devices (Graf-Rosenfellner et al., 2018). Notably, the geometric conditions (probe, container, insertion depth, etc.) and the acoustic pressure relative to the cavitation limit strongly influence the acoustic field, and even a pressure control hardly informs on true dispersion outputs (Amelung & Zech, 1999; Mentler et al., 2004; Schomakers et al., 2011). High-accuracy ultrasonic equipment, initially developed for material testing (Mayer, 1999, 2006), uses the vibration amplitude as a critical parameter for separating soil aggregates of defined stability (Mayer et al., 2002; Mentler et al., 2004). The challenge remains that none of these methods can yet avoid the redistribution of soluble materials among aggregate size fractions, as well as the potential breakdown of microbial cells and particulate organic materials at energy inputs above 60 J mL^{-1} (Amelung & Zech, 1999; Kaiser et al., 2015; Stemmer et al., 1998).

To circumvent the problems with using ultrasonic power for aggregate dispersion, Kristiansen et al. (2006) applied uniaxial crushing to break dry aggregates along "natural planes of mechanical weakness." This type of dry separation has the advantages of circumventing reaggregation and producing microaggregate units by closely simulating destructive forces under field conditions, for example, by mechanical loads from the wheels of agricultural machines or tillage pressure. Generally, dry-sieving yields larger aggregate size fractions than wet-sieving (Bach & Hofmockel, 2014; Blaud et al., 2017; Felde et al., 2021; Nahidan & Nourbakhsh, 2018), probably due to the absence of aggregate slaking in water or even missing aggregate bursts by entrapped air when wetted too fast (Six et al., 2000b). In addition, dry-sieving of field-fresh soil can help differentiate microhabitats within aggregates

of various sizes unless subsequent (air)drying alters microbial community composition (Bach & Hofmockel, 2014; Blaud et al., 2017; Felde et al., 2021). It can also provide information about the impact of wind erosion on aggregates (Chepil, 1962). However, assessing the impact of splash or water erosion requires wet-sieving approaches (Li et al., 2013; Liu et al., 2021).

During the wet sieving, the magnitude of slaking varies, depending on the intensity and velocity of prewetting (e.g., Six et al., 2000c) and the conditions of the sieving, for example, duration, amplitude, and speed of the oscillating (nested) sieve tower. Potentially, following the changes in aggregate moisture status, unwanted reaggregation may occur (Siebers et al., 2018). Unfortunately, we are unaware of any standardized method isolating aggregates by tensile forces under water-unsaturated, that is, more realistic natural conditions.

All the methods mentioned above separate soil particles and aggregates by size and stability. However, these fractions may contain only a few true soil aggregates (Krause et al., 2018; Meyer et al., this issue). Hence, additional techniques such as density isolation of primary particles may be required to separate aggregates from primary particles (Krause et al., 2018), if not even using density fractionation as the primary tool of aggregate fractionation, for example, to separate free from occluded microaggregates (Golchin et al., 1994; John et al., 2005; Six et al., 2000a). In addition, Meyer et al. (this issue) propose a manual separation step that further isolates soil aggregates, for example, after wet-sieving, before obtaining bulk parameters of pooled aggregates, or applying imaging techniques on individual aggregates.

2.2 | Fixation of individual microaggregate

For more detailed analyses of individual aggregate properties, peeling to separate the surfaces and core of aggregates is possible but currently limited to macroaggregates (Amelung & Zech, 1999; Kayser et al., 1994; Sexstone et al., 1985). Argon sputtering can successively eliminate aggregate surfaces at nanoscale resolution as needed for microaggregates (Amelung et al., 2002; Mikutta et al., 2009). However, 2D-mapping approaches or 3D-tomography of aggregates typically require their assessment on the level of individual aggregates. Given that the properties of individual aggregates vary considerably (Lehndorff et al., 2021), developing a methodology to isolate and sample either representatives of specific microaggregate types or microaggregate clusters is mandatory.

Two fixation approaches are commonly applied in studies on the properties of individual microaggregates. Either they are fixed in the entire state on surfaces or embedded in resin and then cut for 2D mapping of properties. For fixation on smooth surfaces, micron-sized soil particles are typically deposited onto adhesive tapes, wafers, or polished metal stubs, or pressed into gold foil or indium pellets. Deposited particles typically maintain their surface properties such as roughness, topographies, or microbial colonies and can be analyzed by electron microscopic or laser ablation techniques. The applicable particle-size range for deposition methods varies with the medium, for example,

15–40 μm for Si wafers up to the millimetre range for C and Kapton tapes. There is generally the risk that larger particles often do not adhere properly to the sample holder's surface and can contaminate the systems operated under high-vacuum conditions, as observed with nanoscale secondary ion mass spectrometry (NanoSIMS). For larger particles like large microaggregates, and also when aiming at the 2D mapping of aggregate thin sections, embedding is usually required to stabilize and prepare a section surface for analysis. The most common approach is to embed the microaggregates in epoxy resin and then cut and polish them to obtain a surface with low topographical differences. Alternative resins are polyester and acryl-based (Tippkötter & Ritz, 1996).

A significant disadvantage of resin embedding is that at least the aggregate surfaces are coated with organic materials, preventing direct assessment of potential carbon accrual at microaggregate surfaces. Other methods include sulfur embedding for synchrotron-based infrared (IR) imaging of microaggregates (Kinyangi et al., 2006). However, the sulfur embedding technique usually requires liquidation of sulfur as a pretreatment operating at above 110−115°C and up to 220°C (Lehmann et al., 2005; Obst et al., 2011), which might pose the risk of alteration of thermally labile aggregate forming materials (Lehmann et al., 2005). In addition, under room temperature, it is challenging and frequently unsuccessful to section the microaggregates embedded in sulfur (Kinyangi et al., 2006). These problems could be addressed by sectioning the hydrated and frozen microaggregates under cryogenic conditions (Kinyangi et al., 2006), and this so-called cryo-thin-sectioning has also been applied to other microscopy and spectroscopy approaches, for example, cryo-scanning transmission electron microscopy (cryo-TEM) combined with electron energy loss spectroscopy (Possinger et al., 2020), to reduce sample damage. Also, the use of water glass for laser ablation-isotope ratio mass spectrometry (LA-IRMS; Vergara Sosa et al., 2021) has been suggested. However, it tends to boil when the vacuum is applied. Tomographic techniques, in turn, may require specific sample preparation techniques, particularly when natural soil moisture conditions should be sustained, such as by inserting microaggregates into a thin-walled 300-μm borosilicate glass capillary, sealed by hard wax with short acclimation (approximately 1 h) for μCT imaging (Voltolini et al., 2017). We must be aware that all fixation methods have advantages and disadvantages, including the risk of structure alteration by sample drying.

With few exceptions, for example, for environmental scanning electron microscopy (ESEM), the samples for the spectromicroscopic approaches must resist high vacuum and be electrically conductive. Electric conductivity can be obtained by, for example, thin-coating with gold or other elements. This procedure is crucial for both SEM and NanoSIMS analyses. While pretreatments for samples can vary with the instrumental technique and the purpose of measurements, preservation of the integrity of aggregate structure and minimization of composition alteration should always be considered during the sample preparation. Furthermore, when integration of results from 2D−3D imaging is planned, attention should be given to the compatibility of sample preparation with measurement requirements of each

instrument in the workflow, as well as the sequence of the measurement, which could be decisive as a prerequisite for a successful 2D–3D image registration.

When aiming at the preservation of whole soil structure or structural units, a thin section of undisturbed soil samples, as commonly used for soil micromorphological analysis, could in principle avoid drawbacks and potential artefacts from the techniques to isolate and then fix individual aggregates. Within these sections, the in situ arrangement of soil (micro) aggregates, pores, and plant fragments can be largely preserved, thus promoting chances to analyze gradients from larger aggregates into soil pores or within the rhizosphere (e.g., Rodionov et al., 2019, 2020). This might help, for instance, to elucidate the complex interplay of such gradients in 3D environments (Kuzyakov & Razavi, 2019; Schnepf et al., 2022; Lippold et al., 2023), whereas aggregate formation inside larger aggregates is likely not seen without fractionation. For thin sections, undisturbed soil blocks have conventionally been sampled by Kubiëna boxes in various sizes and materials (Stoops & Nicosia 2017; Verrecchia & Trombino 2021); nowadays, customized cylinders are increasingly used for undisturbed sampling of soil cores (Lippold et al., 2023; Nunan et al., 2001). Similar to the isolated aggregates, fixation of soil blocks and cores, that is, resin impregnation, is required prior to section (Tippkötter & Ritz, 1996). Correspondingly, structural damage, bubble formation, and the redistribution of particles and/or aggregates should be minimalized and averted in this process.

3 | ASSESSING BULK PROPERTIES OF MICROAGGREGATES

Various techniques can be applied to obtain information on the bulk properties of microaggregates. For instance, gas adsorption, small angle X-ray scattering (SAXS), and the sessile drop method provide information on the specific surface area, porosity, and wettability. In addition, functional groups of minerals and SOM can be acquired by IR spectroscopy (Fultz et al., 2014; Parikh et al., 2014), while the composition and age of SOM can be assessed by nuclear magnetic resonance (NMR) spectroscopy and accelerator mass spectrometry (AMS), respectively. Moreover, mineralogy and elemental composition can be evaluated by X-ray diffraction (XRD; Chenu & Plante, 2006; Fernández-Ugalde et al., 2013; Virto et al., 2008) and energy-dispersive X-ray fluorescence spectroscopy (XRF; Towett et al., 2013). Similarly, microbiome information can be obtained when DNA-based microbial analyses are applied. Again, it must be remembered that soil particles <250 μm usually comprise both, true microaggregates and primary particles. If information is only desired for the former, microaggregates and primary particles must be separated in advance (see Section 2).

Averaged information on specific surface areas across a set of aggregates is commonly obtained using the Brunauer–Emmett–Teller approach applied to N_2 adsorption data (Dixon, 1989). Applying *t-plots* to N_2 adsorption isotherms derives micropores' volume and specific surface area (de Boer et al., 1966). While gas adsorption accesses the porosity in micropores (diameter: 0.4–2 nm) and mesopores (diameter: 2–50 nm) (Macht et al., 2011), the application of mercury porosimetry extends the range of pore sizes from approximately 3 nm to up approximately 900 μm. The role of individual soil constituents on porosities and specific surface area can be assessed after their selective removal, for example, after oxidation of SOM with H_2O_2 or iron oxides and oxide-bound OM by dithionite–citrate–bicarbonate extraction (Eusterhues et al., 2005; Jiang et al., 2013; Kaiser & Guggenberger, 2003). Like the specific surface area, also wettability is usually quantified for a whole set of isolated microaggregates. Wettability assessment relies on the determination of the contact angle (CA; Bachmann et al., 2003) with the sessile drop method (Bachmann et al., 2013; Bachmann et al., 2003; Goebel et al., 2013). The sessile drop method usually involves a thin layer of homogenized soil material (ideally a one-grain layer to avoid capillary forces) (Bachmann et al., 2003). The CA is then measured with a charge-coupled device-equipped CA microscope. The surface wettability of measured soil aggregates is then either classified as wettable (hydrophilic; CA = 0°), subcritically water repellent (CA > 0° and <90°), or nonwettable (hydrophobic; CA ≥ 90°) (Woche et al., 2017). The CA is primarily determined by the polarity and orientation of functional groups on the 0.5−1 nm outer surface layer, the so-called "CA interphase" (Ferguson & Whitesides, 1992). Accordingly, differences in SOM significantly affect the wetting properties of soil aggregates: nonpolar functional groups, such as those involving C-H bonds (e.g., methyl groups), promote the water repellence of microaggregates, whereas the sole presence of polar functional groups that contain either an O-H or C-O bond (e.g., hydroxyl and carboxyl groups) results in a wettable surface (Pronk et al., 2017; Woche et al., 2017). The attachment of bacterial necromass also impacts wetting properties. Schurig et al. (2013), for instance, found a close correlation between the extent of coverage by bacterial cell envelope fragments (containing amino sugars, proteins, and lipids) on mineral particle surfaces and the CA in a soil chronosequence. Achtenhagen et al. (2015) later confirmed that the presence of water- and salt-stressed bacteria on mineral surfaces increased their CA. Under drought conditions, dehydration causes nonpolar functional groups of amphiphilic molecules to point outward, thus increasing CA and hydrophobicity (Bachmann et al., 2021; Doerr et al., 2000). It is also a mechanism that likely contributes to protecting SOM from rapid decay at respective extreme events (Goebel et al., 2011).

Pore structure and pore size distribution of soil microaggregates can be successfully studied by SAXS and ultra SAXS (USAXS) (McCarthy et al., 2008). Unlike N_2 adsorption or Hg porosimetry probing the accessible porosity, X-rays penetrate through the sample. Thus, SAXS provides information on the total porosity of a sample. USAXS can cover a wide range of pore sizes (from 10 Å to 15 μm) (Alberto, 2003). The method is similar to the contrast matching technique such as small angle neutron scattering (SANS; Avdeev et al., 2007) or anomalous SAXS (Bóta & Klumpp, 2005): the change in the contrast is the result of the combustion of the SOM-filled voids, as SAXS takes advantage of differences in X-ray scattering contrast among soil minerals, SOM, air, and water. Data obtained by SAXS/USAXS techniques can be complemented with X-ray computed tomography data for 3D visualization

and quantification of intra-aggregate structures and SOM distribution within soil microaggregates.

For rapid assessment of bulk element contents without significant matrix effects, total XRF was designed with an incidence angle of the incoming beam below the critical angle of total reflection (Dhara & Misra, 2011). This minimizes penetration depth, absorption, and scattering of the incoming beam in the sample matrix (Stosnach, 2007). It also significantly reduced the background noise level (Stosnach, 2005; Stosnach, 2007). When using synchrotron radiation as the excitation source, the background noise decreases further, which increases the sensitivity of XRF (Wobrauschek, 2007). As a result, synchrotron-based XRF is capable of determining elemental concentrations in the ultra-trace range (Sarret et al., 2013).

To analyze the composition of both soil mineral and organic components, vibrational spectroscopy techniques such as Fourier transform infrared (FTIR) and Raman spectroscopy have been applied (Parikh et al., 2014). IR spectroscopy relies on the absorbance of radiation at molecular vibrational frequencies, and most inorganic and organic compounds in the environment are IR-active (Parikh et al., 2014). Much of SOM analyses focus on FTIR, particularly the mid-IR region of light (ca. 4000–400 cm^{-1}), which resolves more bands than near-IR. However, to our knowledge, it is still unavailable at μm-scale resolution. IR spectrometers can be run in transmission, diffuse reflectance, and attenuated total reflectance mode. The total internal reflectance occurs when IR radiation travels through a high refractive index crystal onto the sample surface. This spares attenuated total reflectance–FTIR from water interference, making it a valuable technique for studying solution-solid interfaces.

Using diffuse reflectance IR Fourier transform spectroscopy, Fultz et al. (2014) showed that aggregate-occluded particulate organic matter was enriched in spectral bands related to carboxylates, phenolic C-O, and aliphatic C-H. In contrast, free macro- and microaggregates showed higher signals between 1630 and 1660 cm^{-1}, as typical for fresh plant residues. The data confirmed that microbial alterations of particulate organic matter likely favored their enrichment in aggregates. In the future, FTIR–photoacoustic spectroscopy could be complementary to FTIR, particularly to attenuated total reflectance FTIR, as it has better sensitivity and reproducibility in the 4000−2000 cm^{-1} region (Krivoshein et al., 2022). In the photoacoustic mode, the absorbed energy from the modulated IR beam induces local heating and creates a thermal expansion-driven pressure. This can be detected by a microphone in the form of acoustic signals in the surrounding transfer gas within the photoacoustic cell (Bekiaris et al., 2015; Du et al., 2008). Maximum sensitivity, reproducibility, and signal-to-noise ratio were observed, particularly for clay- and silt-sized microaggregates (Krivoshein et al., 2022).

In contrast to conventional IR, Raman spectroscopy operates at a finer resolution. It utilizes the scattering of incident photons during the transitions between the molecules' quantized rotational and vibrational energy states. Application of Raman spectroscopy to soils can be very challenging due to the typical signal disturbances caused by fluorescence produced from SOM when optical excitation of samples is performed in the visible to near-IR spectral range (Parikh et al., 2014).

Typical applications are therefore restricted to mineral phases without organic moieties. In this case, Raman spectroscopy can be very sensitive, even for tracing isotope exchange (von Sperber et al., 2017).

NMR spectroscopy can be used for deeper insights into bulk SOM composition on liquid or solid samples (Baldock et al., 1997; Baldock et al., 1992; Kögel-Knabner, 1997). Liquid-state NMR has a better resolution of individual signals and has been traditionally applied to, recently, even resolving (labeled) isotopic masses in soil extracts (Wang et al., 2021). Solid-state ^{13}C NMR can be used with minimal sample preparation (Wilson, 2013), although soil samples may have to be pretreated with HCl/HF to improve the signal-to-noise ratio. In addition, it can be used to test for specific interactions between iron and organic matter in variable contact time experiments (Schöning et al., 2005).

A set of microaggregates of a given size range may also be radiocarbon-dated. The first results showed that microaggregates contain carbon being several decades older than those in macroaggregates, with occluded microaggregates containing older carbon than free ones (Buyanovsky et al., 1994). Using AMS, radiocarbon dating is nowadays possible with sample amounts of 0.1–1 mg carbon or even less. However, the required amount of carbon is still too high for the dating of individual microaggregates. Assuming an average size of 100 μm and bulk density of 2.2 g cm^{-3}, a large cubic microaggregate weighs only about 0.7 mg. At a typical carbon content of 1−2%, the total carbon mass within such a microaggregate is below the detection limit of any accelerator mass spectrometer. Hence, microaggregate-specific radiocarbon dating has not yet been achieved. However, mean residence times of microaggregate carbon can be deduced from LA-IRMS (see below and Rodionov et al., 2019).

Similar difficulties in characterizing individual aggregates are usually encountered in studies targeting the soil microbiome. Most studies have been performed on sets of microaggregates of a given size range using amplicon sequencing of the 16S rRNA gene to analyze bacterial community structure. Such studies revealed that micro- and macroaggregates harbor distinct microbial communities (Davinic et al., 2012; Fox et al., 2018) and most distinct communities predominantly occur in the smaller-sized fractions along with the greatest soil microbial diversity and enzymatic activity (Bach et al., 2018; Biesgen et al., 2020; Busto & Perez-Mateos, 2000; Fox et al., 2018). Variations in microbial colonization between aggregates of different sizes are often studied in response to external impacts, such as fertilizer application, tillage, or changes in soil properties (Bach et al., 2018; Fox et al., 2018; Kihara et al., 2012). Occluded microaggregates can be enriched in oligotrophic bacterial taxa, along with better preservation of organic matter, compared with free microaggregates (Biesgen et al., 2020), and surface-colonizing bacteria often differ from those residing inside microaggregates (Mummey & Stahl, 2004). The high-throughput sequencing technologies available today have the potential to provide much more detailed information about colonization preferences. Also, differentiation between intact (viable) versus dead, disintegrated cells or extracellular DNA is also conceivable to be applied to aggregate size fractions (Carini et al., 2016), for example, by separating the two DNA fractions with propidium monoazide, which modifies only extracellular DNA in a way that PCR-amplification is inhibited (Carini et al., 2016;

TABLE 1 Methods for size analysis of microaggregates and their respective sizing limits.

Methodology	Measurement principle	Lower size limit	Upper size limit
Human eye		100 µm	
Laser diffraction	Light scattering translated into volumetric size distribution	10 nm	5000 µm
Dynamic image analyses	High speed camera-based monitoring of moving particles, vibration adds kinetic energy to falling particles or particles in suspension	1 µm	34 mm
Dynamic light scattering	Brownian motion causes fluctuations in light intensity that are correlated to particle size	1 nm	10 µm
Field-flow fractionation	Separation of particles within a fluid based on particles properties such as size, mass, charge, and so on	0.66 nm	100 µm
Scanning electron microscopy	Software (i.e., ImageJ) processing of SEM images, which originate from emitted secondary electrons due to electron interactions	1 nm	200 µm

Heise et al., 2016; Wagner et al., 2015), or by selective removal of extracellular DNA by washing in the presence of phosphate (Alawi et al., 2014; Lever et al., 2015).

4 | SIZE ANALYSES OF MICROAGGREGATES AND FINER PARTICLES

Various methodologies are available to determine the size distribution of individual water-stable aggregates (Table 1). In contrast to sieving, these advanced methods hold the potential to determine the size distribution down to particles and aggregates in a size range of nm to µm, independent of predefined size boundaries.

Laser diffraction (LD) is based on the angular scattering pattern of particles and is capable of fast and reproducibly measuring the particle size distribution (PSD) in a broad size range (Table 1; Bieganowski, Ryżak, et al., 2018; Faé et al., 2019). The PSD measurement by LD is derived from the acquisition of scattered light from measured particles and subsequent calculations according to Mie or Fraunhofer theory (Bieganowski, Ryżak, et al., 2018). Since these theories assume that the shape of the measured particles is spherical, LD is optimized for the PSD measurement of spherical particles. However, previous studies have confirmed the feasibility of applying LD both to wet (Buurman et al., 1997) and dry (Polakowski et al., 2021) microaggregate fractions. For Luvisols, Krause et al. (2018) found that the sizes of small microaggregates followed a gamma distribution, with mean volumetric sizes peaking at about 6 µm. Repeated LD measurements can also evaluate soil aggregate stability (Bieganowski, Zaleski, et al., 2018; Kasmerchak et al., 2019; Mason et al., 2011). For this, the instrument's integrated suspension circulation and stirring function are used to subject the aggregates to a continuous mechanical force. By repeated measurements of the PSD over 10–40 min, information on the stability of aggregates can be derived by shifts in median diameter. A recent study using the slightly modified approach of Mason et al. (2011) found that bare fallow led to the destabilization and disintegration of 53–250 µm soil microaggregates into smaller ones (20–53 µm). This is confirmed by a significantly increased mass of small soil microaggregates compared with a cropped control plot and a significantly decreased median

diameter as identified by continuous LD measurements (Siebers et al., 2024).

Dynamic image analysis (DIA) utilizes a laser-based light source and charge-coupled device camera. It can capture 2D contours of fast-moving, nonspherical particles and aggregates with a speed of up to 450 images per second. Compared with conventional size measurement approaches, the great advantage of the DIA technique is that it provides both size and shape information of particles. In a standard DIA measurement, the camera records a sequence of particle contours when a particle flow passes the light source. As particles circulate within the system, the projected areas of particles are recorded at different orientations over time, thus obtaining representative and more realistic information on particle shape. The application of DIA provides novel ways to quantify soil aggregate size distribution and disentangle soil aggregation at a resolution of several µm (Graf-Rosenfellner et al., 2018; Kayser et al., 2019). Applying DIA to aggregate suspensions provides the opportunity to directly measure size distributions during or after dispersion by sonication or chemical reagents and compare these with control measurements in water. Schweizer et al. (2019) quantified the microaggregate size distributions from soils with clay contents ranging from 16 to 37% before and after dispersion with disodium phosphate. By subtracting the PSD curves, primary particles, not part of the microaggregates but still contained in the size fraction, could be excluded. Irrespective of the different soil textures, most microaggregates were approximately 30 µm diameter. Increasing clay content led to a shift in the mean diameter of large microaggregates from 86 to 94 µm. Felde et al. (2021) analyzed the PSD of dry-crushed microaggregates in a dry state and found bimodal size distributions with peaks at approximately 50 and 150 µm. Sand-sized grains were identified as intact parts of dry-crushed microaggregates using light microscopy and µCT. After water immersion, the aggregate diameters decreased by approximately 60 µm, showing a more unimodal pattern with a peak at ca. 25 µm, as also observed by Schweizer et al. (2019). Hence, applying DIA allows quantifying aggregate sizes in dry, wet, and dispersed states at a resolution of a few µm up to the mm range (Table 1; Felde et al., 2021; Schweizer et al., 2022).

When focusing on particles in the size range of nanoparticles and colloids, the PSD can be measured in suspension using dynamic light

scattering (DLS). The DLS technique measures the intensity fluctuations of laser light scattered by particles randomly moving in the suspension. Brownian motion of the particles causes fluctuations in the scattered light intensity, and the time of these fluctuations is proportional to the particle size. The exact size range that can be analyzed depends on the laser source, scattering angle, and detection system, but DLS is typically most sensitive in the nm to µm range. This is because smaller particles may be difficult to be detected due to limited scattering. In comparison, larger particles may be too large to exhibit significant Brownian motion and thus produce weak scattered light fluctuations. DLS was frequently used to study the aggregation kinetics of soil colloids (Kretzschmar et al., 1998; Nguyen et al., 2013), and helped to identify aggregation at the smallest scale, such as due to coprecipitation of organic molecules with hydroxyl-Al cations (Dultz et al., 2021), homoaggregation of clay minerals, or the heteroaggregation of clay minerals with Fe and Al (hydr)oxides (Zech et al., 2020).

For small soil particles, also field-flow fractionation (FFF) can be used (Baalousha et al., 2011; Jiang et al., 2015; Qureshi & Kok, 2011). One of its outstanding features is its capability to continuously separate colloids and particles over a broad size range that exceeds DIA's (Table 1). The FFF is essentially a nondestructive elution technique separating particulate samples carried by the flow of a liquid within a channel, where a field of force (e.g., gravitational, crossflow, centrifugal, electrical, etc.) is perpendicularly exerted on the sample flow concentrating and retaining particles on the accumulation wall of the channel. This results in different retention time of particles according either directly to their hydrodynamic diameters or to other properties such as mass and electrophoretic mobility, which are also possibly related to the hydrodynamic diameter (Kowalkowski et al., 2006; Ornthai et al., 2016). Accordingly, particles of different sizes will be eluted from the channel at distinct time yielding specific elution profiles, the so-called fractogram (Schimpf et al., 2000; Williams, 2022). Asymmetrical-flow FFF (AF[4]), relying on a crossflow-based field, has been frequently applied to fractionate and characterize natural colloids and nanoparticles in soils and streams (Baalousha et al., 2006; Missong et al., 2018; Wang et al., 2020) and can be coupled to DLS or multiangle light scattering to produce size-profiles of particles. However, analysis of natural colloids spanning a wide size range (1–1000 nm) may hamper the separation process. In practice, colloids up to 200–250 nm can be fractionated well, while colloids eluted in the "release peak," when the cross-flow is zero, are not perfectly separated by size (Jiang et al., 2015; Siebers et al., 2023; Tang et al., 2022). Therefore, AF[4] studies with natural colloids were commonly restricted to a hydrodynamic radius of <500 nm (Baalousha et al., 2011; Missong et al., 2018; Qureshi & Kok, 2011).

The FFF systems can also be coupled to online detectors to characterize the chemical composition. For example, an online coupling to an organic carbon detector and an inductively coupled plasma mass spectrometer (ICP-MS) allows for studying the size-resolved elemental concentrations within particle size fractions (Nischwitz et al., 2016). These element-specific fractograms can be used to calculate elemental ratios, fingerprint geochemical changes in the aggregate structure, or

elucidate, for example, the role of clay particles, iron, and organic carbon in aggregate formation and stability (Krause et al., 2020; Tang et al., 2022). Examining soil fine colloids (<220 nm) in Luvisols by using AF[4] coupled to ICP-MS and an organic carbon detector, Tang et al. (2022) found that, compared with fine water-dispersible colloids, fine colloids occluded inside (micro)aggregates tended to contain more particles in the range of 20–170 nm, which were rich in silicon, aluminum, iron, and organic carbon.

5 | ANALYSES OF INDIVIDUAL AGGREGATES

When deposited or embedded and sliced, several advanced techniques can be used to study the architecture of individual soil microaggregates, all spanning different spatial resolutions (Figure 1). For small or even silt-and clay-sized microaggregates (20–50 µm or even <20 µm) or specific regions of interest (ROIs) thereof, atomic force microscopy (AFM), different electron microscopy techniques with suitable detector systems as well as NanoSIMS provide detailed information on plane properties and composition. Yet, when considering larger microaggregates at the scale of 50–250 µm, for instance, these subsections may not represent the whole architecture. Hence, other techniques operating at coarser resolution but covering larger scales may be needed to explore the properties of the entire microaggregate, such as X-ray photoelectron spectroscopy (XPS), electron probe microanalysis (EPMA), or different laser ablation applications (Figure 1). These analyses can be integrated using tomographic approaches, by appropriate synlocation and synscaling, or even in silico modeling, as outlined below.

5.1 | Mapping topography and nanomechanical properties at the lower end: AFM

After the invention of AFM in 1986 (Binnig et al., 1986), surface-probing has boosted surface metrology and thus the understanding of the topography, mechanical, and thermal properties of soil minerals and organo-mineral particles at unprecedented spatial resolution (Assemi et al., 2004; Fischer et al., 1996; Rennert et al., 2012; Schaumann & Kunhi Mouvenchery, 2012; Totsche et al., 2010; Zhu et al., 2009). AFM employs a tip attached to a cantilever. While the tip is moved across the sample surface in the x–y direction, the tip deflection due to tip–surface interactions is recorded. Height information at a particular location of the sample surface is revealed from the z-movement of the cantilever, which is controlled by keeping the tip–surface interactions constant. Noteworthy, the cantilever tip unit is commonly excited to an oscillation frequency in the lower kHz range. By doing so, not only the height information for a specific location can be revealed, but other tip–sample interactions (e.g., adhesion) and sample properties (e.g., hardness, elasticity, modulus, thermal properties, Hamaker constant) can be determined (Butt et al., 2005) via recording the shifts in height-location, oscillation frequency, amplitude, phase, and higher order harmonic vibrations available through the feedback-loop steering-mechanisms. A strength of AFM is thus to
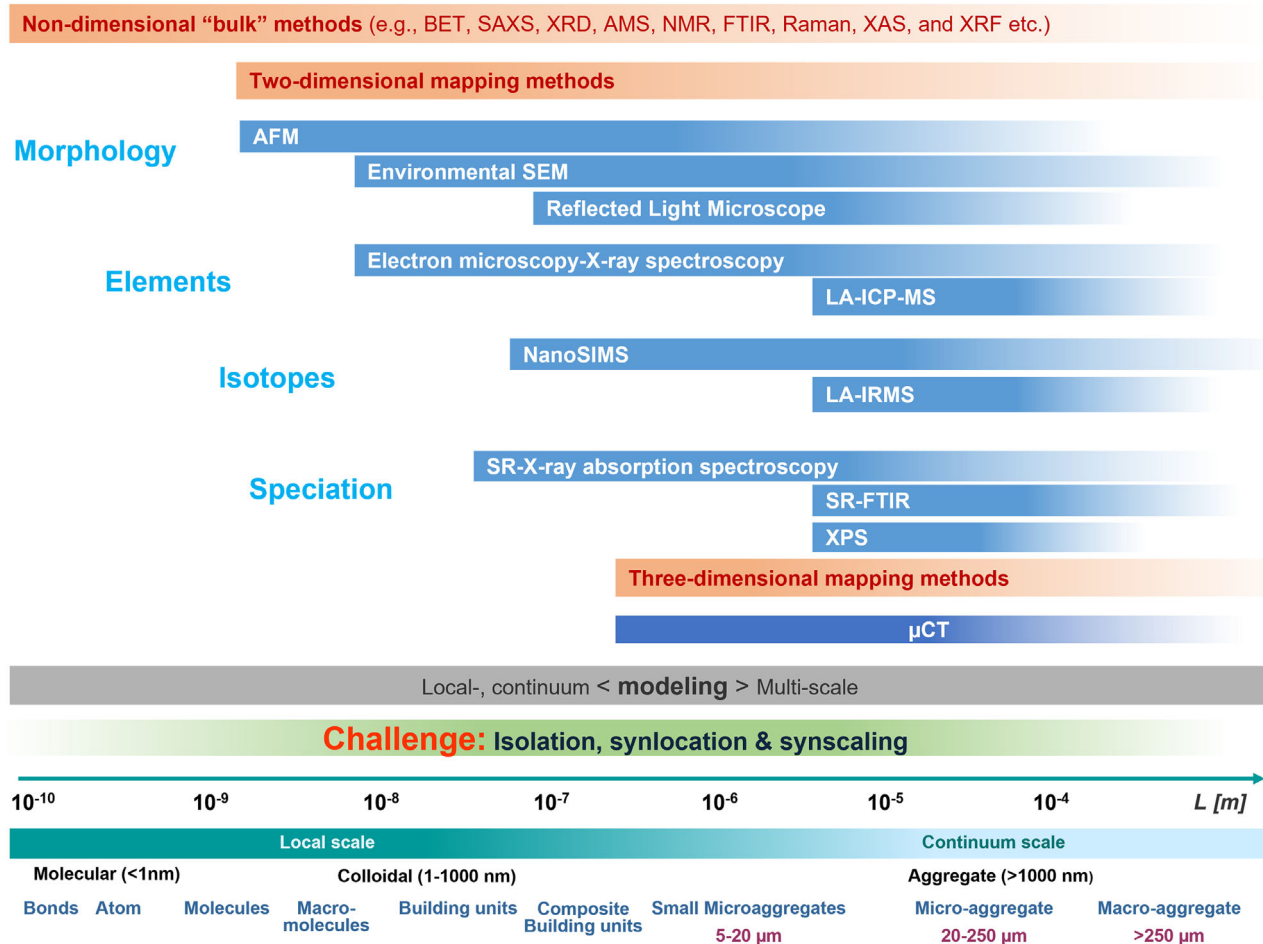
FIGURE 1 Synopsis of instrumental approaches used to explore surface properties, composition, and structure of microaggregates.

provide extremely precise values on the topography of single particles, also including other morphological features like the edge-to-basal surface ratio allowing for calibration of different methods to determine the specific surface area (Macht et al., 2011).

AFM's unequaled planar and height resolution is based on ultra-sharp tips and accurate ceramic piezo elements. Noteworthy, true atomic resolution can only be obtained when extraordinarily flat and rigid sample surfaces are used (Jandt, 2001) and the instruments are run in a vibration-free and acoustically isolated environment.

AFM at the core directly measures the interaction forces between the sample surface and the AFM probe. The interaction results from a superposition of short-range chemical forces and long-range van der Waals, electrostatic, and magnetic dipole forces. Whether the net forces are attractive or repulsive, that is, whether the cantilever will bend into the direction of the sample or away, will depend on the separation distance, the environment (air, vacuum, liquid), and the environmental conditions (e.g., pH, ionic strength, chemical composition).

The tip–sample interactions and, thus, both the force field and the topography depend to a large extent on the geometry of both the sample surfaces and the tip. Therefore, reconstructing the sample surface topography from the force interactions is challenging for relatively rough and structured surfaces like those of natural materials. Standard

AFM probes used for topography mapping use ultra-sharp tips, and thus, the calculation of the geometry of the interfaces is mathematically very demanding. The colloidal probe provided an early solution to this problem (Butt, 1991; Ducker et al., 1991). The interaction forces can be precisely calculated by attaching spherical particles of known radius to the cantilever.

Using functionalized tips by fixing specific materials to the cantilever rather than standard tips was deployed to measure specific interaction forces that govern adhesion directly. Such probes can now be made from various materials, including metals, crystals, and polymers (van Zwol et al., 2008). Even whole microorganisms have been attached to the cantilever (Lower et al., 2000).

With the simultaneous mapping of force–distance relationships and the topography of the contacting surfaces (e.g., Huang et al., 2015), the actual AFM modes of operation provide complete information on the interaction mechanisms that control stability even as a function of the environmental condition: Mosley et al. (2003) were able to show that the interaction forces between minerals and natural organic matter are influenced by pH and salinity.

Since 2010, AFM has been applied beyond life sciences, accepting the challenge using surface probing methods on more complex samples via operating AFM in advanced modes. This includes the

TABLE 2 Advanced mapping and imaging techniques for assessing microaggregate architecture.

Instrumental technique	Information	Common sample pretreatment	Penetration depth[a]	Minimal lateral resolution	Vertical resolution[b]
AFM	Shape, (specific) edge and basal surface area, spatially resolved topology, roughness, adhesion, nano-mechanical properties	Equilibrating at ambient conditions, adhesion to glass slides with, e.g., epoxy glue or tapes	Restricted to the surface	1 nm	1 nm
XPS	Quantitative multielemental composition, C and N species identification, oxidation states	Dehydration, flexible for fixation medium (e.g., deposition on indium foil)	1–10 nm	≈3 µm	1–10 nm
NanoSIMS	Simultaneous mapping of 7 elemental and isotopic distributions, using Cs^+ or O^- primary ion source	Dehydration, polished aggregate section after embedding or deposition of fine particles on flat wafer, conductive thin coating (e.g., Au/Pd)	≈5–20 nm	50–100 nm	≈5–20 nm
LA-IRMS and LA-ICP-MS	Spatio-temporal organic matter gradients, stable isotopes of C and N (natural abundance), hot spots of organic matter turnover/monitoring and mapping of Fe and Si isotopes	Dehydration, embedded in resin or C-free material	4–1000 µm	4–20 µm	4–10 µm
SEM/TEM-EDS, WDS, or EPMA	Size and shape of structural units, hierarchy of the structure, micropore structure, mapping elemental distribution across micro- and nano-aggregates	Dehydration, deposition on surfaces or polished flat aggregate section after embedded	<5 µm	0.1 µm/ 1 nm/~0.5 µm (WDS and EPMA)	≈0.5 µm (EPMA)
Fluorescence microscopy, reflected light microscopy	Spatial localization of individual microbial cells	Deposition on slides	≈1 µm	100–200 nm	20–300 nm
SR-FTIR, µ-XANES, µ-XRF	Mapping functional groups of minerals and organic matter at micron scale/spatially resolved element's oxidation state and its coordination structure/mapping elemental distribution	Fixation and sectioning technique dependent (e.g., hydration and frozen for cryo-sectioning), polished flat aggregate section after embedding	≈2 µm/≈5 µm/ ≈150 µm	10 µm; 30–100 nm; <1 µm (probe depended)	–
µCT	Morphology and topology of 3D pore networks of microaggregate structure	Flexible and fixation technique dependent	Sample thickness	0.35 µm	0.35 µm

[a]The depth at which electromagnetic radiation penetrate into a specimen. Material and beam voltage depended, similar to vertical resolution in case of destructive laser shots, for instance; ejection depth of photoelectrons for XPS.
[b]Resolution for the depth profiling.

simultaneous recording of topography and nanomechanical properties of minerals, microorganisms, and organic matter individually and collectively (Table 2), but also of natural materials separated from soil and sediments (Mouvenchery et al., 2016; Eusterhues et al., submitted; Figure 2) or even soil microaggregates (Gazze et al., 2018).

Using AFM, it has been shown that bacteria-mediated dissolution of minerals severely changes the mineral surface functionality (Maurice et al., 2000). Cheng et al. (2009) successfully used AFM to explain the water-repellency of soils' hydrophilic and hydrophobic surface fractions. They showed that organic polymers modify the hydrophobicity of phyllosilicates and that AFM results are correlated with CA measurements. Gazze et al. (2018) recently reported on

SOM's role in determining soil aggregates' nanomechanical properties. They demonstrated that SOM coverage increases soil materials' roughness and surface variability but decreases stiffness and adhesive properties.

In summary, AFM, with its numerous modes of operation, is a powerful ex situ tool for measuring topographic features of soil particles and for mapping and tracking changes in mechanical and physicochemical surface properties that control and influence particle interactions at ambient conditions. AFM is thus an essential and complementary technique in studying the relation of structure and properties. Furthermore, combining AFM with chemical surface probing techniques (e.g., with NanoSIMS, X-ray absorption spectroscopy, XPS, or TEM) in a
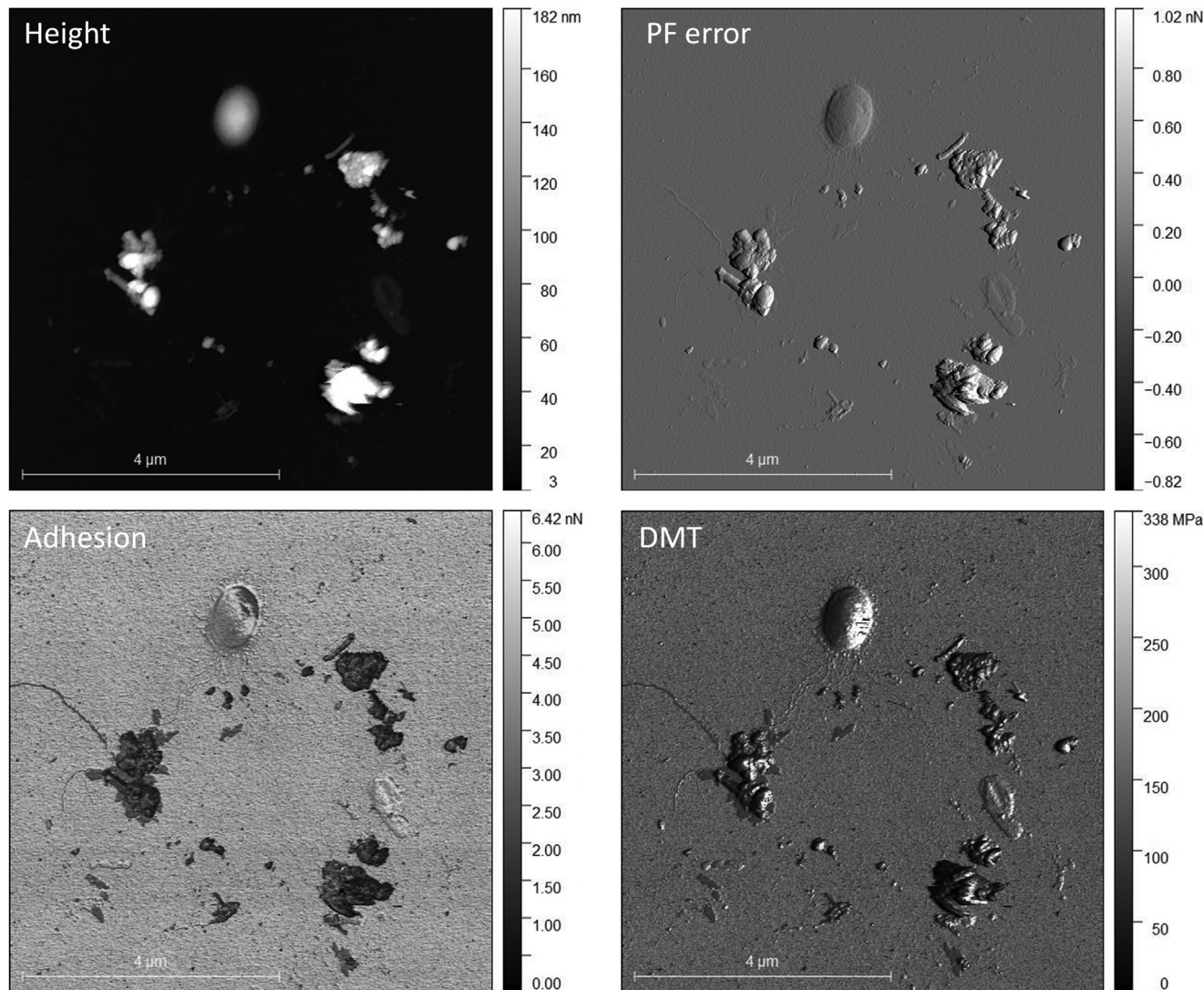
FIGURE 2 AFM images of aggregates and biota present in the sediment of a creek. (A) Height image; (B) peak-force error image ; (C) adhesion map; (D) elastic modulus. A wide variety of mineral, organic, biotic, and aggregated materials are recognized, which differ in morphology and topography, but also in surface (adhesion contrast) and material properties (hardness, DMT). Images were obtained with a standard tip using the quantitative nanomechanical mapping mode (QNM) on a Veeco Multimode operated by a Nanoscope V controller.

joint fashion is now underway and, thanks to the progress made in the coregistration by synlocation and synscaling (see chapter 8), will see an emerging number of studies that help to understand the functioning of the soil. In this regard, a promising but still unexplored option linked to AFM is provided by IR nanospectroscopy. This technique incorporates IR spectroscopy with AFM, thereby allowing for the simultaneous mapping of topography and chemical information in the same run (Reading et al., 2002). Yet, the potential of AFM in the soil sciences has still not been exploited, predominantly because of the presumed limitation to relatively smooth and flat samples and the conception that strong topography contrast, great roughness, and curved samples prohibit the application of AFM to natural aggregated matter (see also Table 3).

Recent advances in sample preparation and tip-cantilever optimization (e.g., Gazze et al., 2018) have shown the potential of AFM to explore even more geometrically demanding objects like intact aggregates. Therefore, one may envisage that with technological progress, particularly in the movement of the sample table (rotational movement, tilting, etc.), also particles/aggregates that are inclined or have a larger-scale roughness can also be investigated by AFM.

5.2 | Two-dimensional mapping of elements and isotopes

5.2.1 | Sample morphology and screening

Before applying other mapping techniques to microaggregates and organo-mineral associations, structural information, such as particle size and particle shape, can be obtained by visualizing samples via

TABLE 3 Examples for options and challenges of advanced mapping and imaging techniques for assessing microaggregate functions.

	Function	Technique	Challenges
I	Control of element cycles, such as • Stabilization of soil organic matter • Nutrient storage • Pollutant immobilization	AFM (I)	Only small areas covered, not necessarily representative, limited to subsections with fairly smooth surfaces, quantitative analyses difficult for steep slopes, soft and loosely attached matter, and undesired forces
		XPS (I, III)	Destructive at depth, semi-quantitative (percentual composition of elements)
		NanoSIMS (I, II, III)	Relatively small coverage, representative sample description requires for multiple areas depending on microspatial heterogeneity, limited to certain elements and isotopes (ionization dependent), difficult technical accessibility and requirement of sample preparation, destructive
II	Habitat function for microorganisms	LA-IRMS (I, II)	Destructive, currently limited to C, MRT calculation eventually hampered by missing controls
		LA-ICP-MS (I)	Destructive, coarse lateral resolution, not optimized for N, P
		SEM/TEM-EDS/WDS and EPMA (I, II, III, V)	Semi-quantitative (EDS), time consuming in high resolution (EPMA), no information on speciation, no preservation of microbes (except for eSEM)
III	Microbial element uptake	SR-FTIR, µ-XRF, µ-NEXAFS (I, III, V)	Limited accessibility to SR source, coarse resolution (SR-FTIR), not optimized for thick samples (µ-XRF), calibration eventually incomplete if not all species occurring in soil are known
IV	Water retention	Fluorescence and reflected light microscopy (II, III)	Sensitive to quenching, not specific for many different taxa, surface sensitive only, relatively low spatial resolution, prone to photobleaching, eventual phototoxicity of the illumination light
V	Provisioning of soil structural units	DNA-based microbial analyses (III)	Not optimized for individual microaggregates, lack of spatial information
		µCT (IV, V)	No direct links to biogeochemistry and biology (except Os staining for C), high computational effort and expertise needed for image processing. Maximum resolution limited depending on sample size, difficult to differentiate between materials with similar X-ray attenuation.

Note: I–V, examples for different microaggregate functions as possible to be evaluated using different spectromicroscopic and imaging techniques.

reflected-light microscopy. Here, a motor-driven cross-table of the microscope enables automated scanning in the x–y plane, thus giving insight into PSD and allowing one to identify and count particles of defined equivalent diameter. In addition, running microscopic analysis with polarized light can help relate the spatial distribution of certain minerals to those of organic matter. Reflected-light microscopy can thus provide highly precise spatial information on microaggregate architecture that will considerably improve the application and understanding of subsequent in-depth spectromicroscopic analyses. Alternatively, polarized light microscopy, which has been frequently performed in micromorphology analysis on soil thin sections (Stoops, 2020), could be a satisfactory substitution for this purpose. Combining its two illumination modes: plane-polarized light and cross-polarized light, pores are able to be distinguished from mineral particles, that is, quartz in images (Stoops, 2020). Therefore, in addition to the basic structural information of particles mentioned above, its application on thin sections of undisturbed soils and/or isolated aggregates could provide information on inter-aggregate and intra-aggregate pores (Guidi et al., 2021; Papadopoulos et al., 2009). However, the minimum size for

pore detection is usually set at 100 µm² (Guidi et al., 2021; Papadopoulos et al., 2009), which appears not to be optimized for detecting intra pores of microaggregates.

5.2.2 | Noninvasive elemental mapping using electron microscopy and X-ray spectroscopy

Electron microscopy allows for studying of microstructures at the nanoscale. In SEM and EPMA, a beam of electrons is directed toward a sample and interacts with the sample's atoms, producing, among others, secondary electrons. These secondary electrons are then collected and used to create an image of the sample, showing the surface features of a material, such as grain boundaries, cracks, and porosity. When a Schottky emitter field-emission gun is utilized as the electron source, the lateral resolution of EPMA can even reach to a nm range. In TEM, a thin sample is placed between the electron source and the imaging device, and electrons are transmitted through the sample. By analyzing the interaction of the electrons with the atoms in the sample,

a high-resolution image of the material's internal structure is obtained. TEM can offer information about the crystalline structure of materials and the presence of defects or impurities in individual crystals; for microaggregates it provides an integrative 2D projection of their composition. With this technique, it is possible to preliminarily identify and localize different aggregate forming materials and microdomains within a single microaggregate (Chenu & Plante, 2006; Watteau & Villemin, 2018; Watteau et al., 2012). Even biological materials such as plant residues and microorganisms are recognizable under TEM. Thus, it is possible to analyze the typology of small soil microaggregates (Watteau & Villemin, 2018; Watteau et al., 2012).

Focused ion beam (FIB)-SEM is a combined sample preparation and imaging technique. In FIB-SEM, a beam of focused ions, typically gallium (Ga^+) ions, is directed onto the sample surface, allowing precise material removal through sputtering. This enables the creation of cross-sectional or site-specific thinning of the sample. Simultaneously, an electron beam scans the surface and collects information about the sample's topography, composition, and structure. The ion beam can be used for various purposes, including sample preparation, milling trenches, or cavities, and removing specific material layers (Gu et al., 2020), and recently was first used to characterize soil structure at the nanoscale (Gerke et al., 2021). When using a broad ion beam (BIB) combined with SEM (BIB-SEM) it is possible to create polished cross-sections for imaging. Here, a broad Ga+ beam is directed towards the sample surface. The ions sputter away the material, gradually milling a flat and smooth cross-section. This process allows for precise and controlled removal of material, revealing the internal structure of the sample allowing to study the pore space morphology at μm down to the nm scale (Hemes et al., 2015; Klaver et al., 2012). Once the desired cross-section is prepared, the sample is transferred to the SEM chamber for imaging. There is growing interest in these techniques for fine-grained geomaterials as they allow for high-resolution characterization of the pore space and microstructure of materials.

A specifically promising microscopic technique to address soil structure-related research questions is ESEM, which basically is SEM without high-vacuum conditions. It allows for analyses with minimum sample pretreatment and, thus, minimum risk of artifacts. One significant advantage is its possibility to image moist samples, albeit at a coarser resolution than conventional SEM. So far, ESEM has rarely been applied to natural soils and their structural subunits. Basic structural features, encrustation of biological materials like the occurrence of roots, fungal hyphae, and bacteria were visualized by Fimmen et al. (2008), while wettability was investigated by Hurraß and Schaumann (2006). Nevertheless, modern instruments offer the opportunity of observing material changes in response to freezing and thawing as well as drying and wetting (e.g., Lin & Cerato, 2014). That means the technique holds much promise to directly study the formation or disruption of soil structures, including microaggregates.

SEM and TEM can be combined with X-ray spectroscopies to generate elemental maps of microaggregates. Element-specific X-rays are emitted, where the primary electron beam hits and ionizes the sample surface and can be detected by either energy dispersive (EDS) or wavelength dispersive (WDS) detectors. Yet, element species are not identified (Table 3). SEM is usually optimized for high-resolution imaging (detecting secondary electrons) and equipped with an EDS for a quick analysis of the spatial distribution of major elements. In comparison, EPMA is inferior in visualization but equipped with several WDSs (up to 5), which offer a higher spectral resolution (5–10 eV) and better detection limits. However, EPMA generally requires longer measurement times, as for WDS detection the characteristic wavelengths of the emission lines have to be adjusted one after the other with a monochromator (Friel & Lyman, 2006). Therefore, it is better suited for accurate elemental mapping.

Elements down to a mass of 4 can be detected at a spatial resolution in the nm to μm ranges (Table 2) by EDS and WDS. The detection limit for WDS is ca. 0.01%, while that of EDS is ca. 0.1%. Results from both techniques can be quantified when matrix effects due to atomic number, absorption, and fluorescence are considered, which is known as ZAF correction. This works best for samples with polished surfaces. Application of SEM/TEM–EDS to soil microaggregates revealed that organic carbon associated with iron, aluminum, and silicon oxides assists soil microaggregate formation, but that organic matter distribution is patchy, with particulate organic matter partly encrusted or coated by fine minerals (Chenu & Plante, 2006; Ladd et al., 1996; Parry et al., 2000).

Applications of EPMA to soil samples are still rare. Lehndorff et al. (2021) applied EPMA to planes of air-dried soil microaggregates. They found highly heterogeneous element patterns, not reproducible for different microaggregates of the same size and soil. However, the presence of microbial debris showed clear evidence of colocations with plant-derived particulate organic matter. Xiao et al. (2019) combined EPMA with synchrotron-based XRF and FTIR to visualize the interiors of intact microaggregates from a Ferralic Cambisol. The authors concluded that the spatial distribution of carbon differed from that of iron and aluminum, and mineral clusters served as nuclei in soil microaggregates (Figure 3).

5.2.3 │ Invasive element mapping using laser-ablation ICP-MS

While EPMA maps reveal the distribution of elements at μm-resolution, coarser element maps, for example, along gradients across and through larger microaggregate sections, can, in principle, also be achieved using laser-ablation with inductively coupled mass spectroscopy (LA-ICP-MS). Laser ablation is achieved by a focused laser beam that induces the release of a plume of material from the sample that is then transported by a carrier gas (He or Ar) to the inductively coupled plasma, where ionization of the sample materials takes place. The charged ions are then separated by their mass-to-charge ratio in the mass analyzer (Wu & Becker, 2012). In the scanning mode for imaging, the laser beam moves stepwise along the sample. The step length and the laser beam diameter (and shape) are adjustable in commercial systems, allowing for various spatial resolutions down to the low μm range. Like ICP-MS, LA-ICP-MS is sensitive to metals and metalloids but can also be applied to nonmetals such as phosphorus, sulfur, and
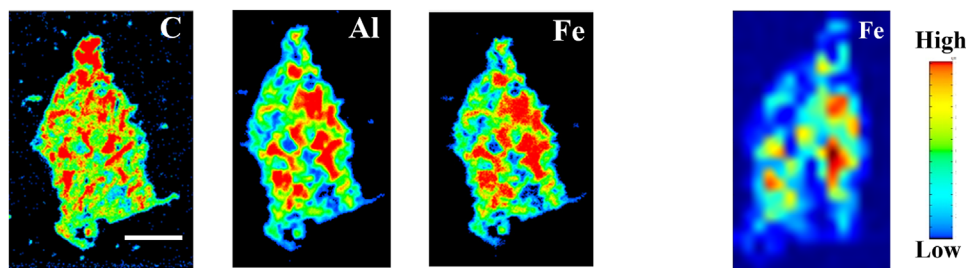
FIGURE 3 Electron probe microanalysis maps of carbon (C), aluminum (Al), and iron (Fe) (left, black framed) and a synchrotron-based X-ray fluorescence map of Fe (right, blue framed) from microaggregates of a Ferralic Cambisol (extracted from Xiao et al. (2019)). Bar (white line) = 50 µm.

carbon. However, quantification of the latter remains challenging. Even multicollector-ICP-MS devices could be used to study the stable isotope composition of elements; however, according to our knowledge, such applications in soil research are still missing.

The LA-ICP-MS technique has been successfully applied in the analyses of soft biological tissues and hard samples such as bones or rocks (Becker et al., 2014). However, the lack of successful applications in soil research is likely related to difficulties in sample preparation: fixed microaggregates are at risk of being blown around by the carrier gas, and microaggregates embedded in the resin can introduce large amounts of organic compounds that hamper the performance of LA-ICP-MS.

Solution-based calibration utilizes a dual-sample introduction system for quantification, where calibration standard solutions are nebulized and introduced to the plasma with the carrier gas carrying the ablated materials. An internal standard element of known concentration is usually needed to determine the relative sensitivity factor, which is later used to calculate the concentration in the sample. The internal standard element does not need to be contained in the soil but can be spiked. A prerequisite for successful quantification is that the plasma conditions are identical during standard and sample analyses. For soil samples fixed on tape, the calibration standards can be prepared similarly, whereas for embedded samples, the elements of the embedding material should be applied as calibration standards (Jantzi & Almirall, 2014). In the future, recent developments of single particle ICP-MS coupled with laser ablation (LA-sp-ICP-MS) might show potential to study soil aggregates. For example, Tuoriniemi et al. (2020) performed a proof-of-concept study using LA-sp-ICP-MS to directly quantify gold nanoparticles spiked to soil with regard to particle frequency and concentration.

5.2.4 | Mapping of elements and isotope enrichment at the NanoSIMS

NanoSIMS enables the measurement and differentiation of elements and isotopes at a lateral resolution of approximately 50−120 nm (Mueller et al., 2022; Nuñez et al., 2018; Pett-Ridge & Weber, 2022). As primary ion sources, Cs^+ and O^- from the new radiofrequency plasma source are used to bombard a sample to stimulate the emission of negatively or positively charged secondary (poly)atomic ions from the sample surface. The secondary ions are detected in a mass spectrometer with a high mass resolution of $M/dM > 5000$, where M is the nominal mass being measured and dM is the mass difference resolvable between neighboring species (Nuñez et al., 2018). NanoSIMS can simultaneously analyze up to seven ion species and can be applied for 2D imaging and depth profiling. To minimize the sample topography, intact soil structures are sectioned and embedded using epoxy resin (Herrmann et al., 2007) or acrylic resin (Kilburn & Clode, 2014). For spectromicroscopic approaches where the introduction of carbon from resin into the sample is to be avoided, soil structures can be prepared using carbon-free media (Kinyangi et al., 2006) or by direct deposition of clay-sized and silt-sized soil structures on semi-conductive wavers (Inagaki et al., 2020; Keiluweit et al., 2012; Yu et al., 2017). ROIs of ca. 30 × 30 µm are selected using light microscopy and SEM (Figures 4A and B). ROIs could be, for example, litter–soil and microbe–soil interfaces or the rhizosphere. Using Cs^+ ion bombardment enables determining the distribution of organic matter-dominated and mineral regions (Figures 4C and D). The normalized CN:C ratio across these surfaces shows an inhomogeneous distribution (Figure 4E); the distribution of ^{15}N indicates the accumulation of the labeled microbial necromass at distinct microsites (Figure 4F). A dual primary ion source approach provides additional information on e.g., calcium, magnesium, potassium, sodium, silicon, aluminum, and iron distributions using the O^- source in combination with the Cs^+ source which jointly enables the spatial differentiation of organo-mineral interactions (Figures 4G–H). As NanoSIMS relies on the ion sputtering of the sample surface, it should be noted that a second measurement is beneath the original surface of the first measurement (see also Table 3). Thus, for the exemplary demonstration of the dual primary ion source approach in Figure 4, information on organic compounds using the Cs+ ion source was obtained before switching to the O^- source, in order to facilitate identification of different soil minerals.

NanoSIMS analyses demonstrated a patchy arrangement of mineral-associated organic matter, which aligns with results obtained by other spectromicroscopic techniques (Schweizer, 2022). Using isotope-labeled organic matter, it has been shown that freshly added organic matter is preferentially retained at preexisting organic matter patches (Vogel et al., 2014). A NanoSIMS-based approach also showed
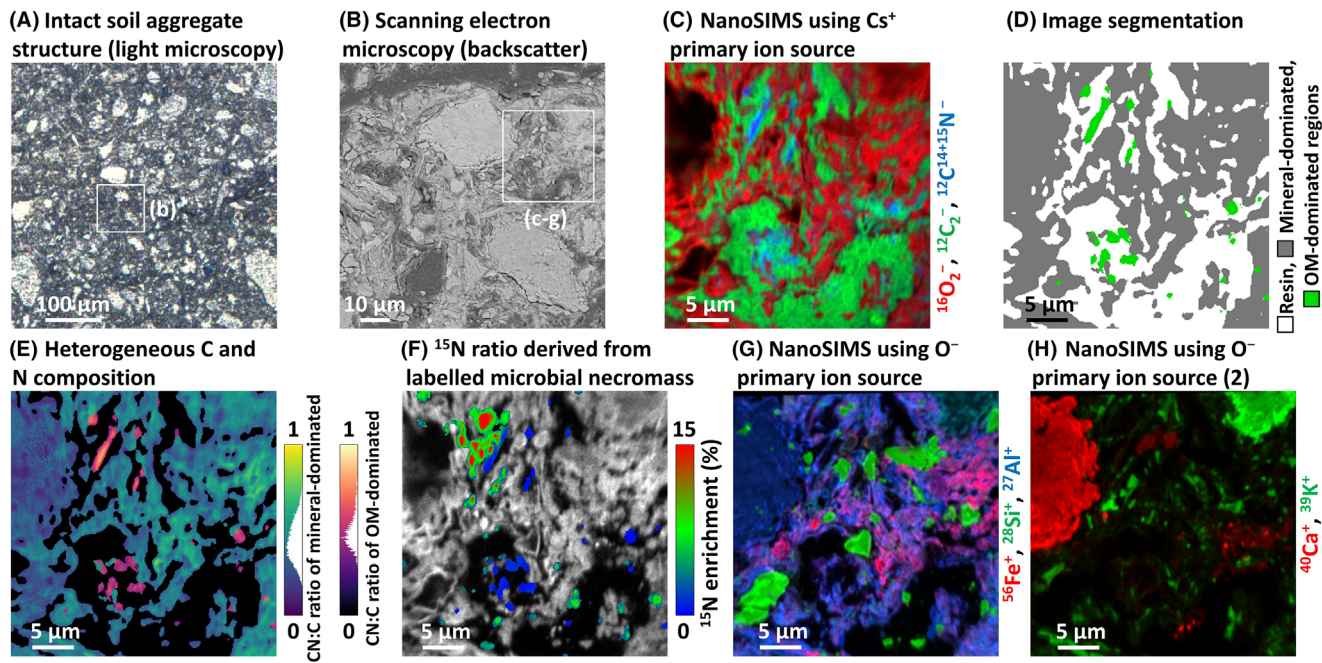
FIGURE 4 Workflow of nanoscale secondary ion mass spectrometry (NanoSIMS) measurements of intact soil aggregates structures using a dual primary ion source at a resolution of approximately 120 nm. (A) Light microscopy and (B) scanning electron microscopy facilitates to select regions of interest in an epoxy-embedded aggregate section. (C) The distribution of O, C, and N by the Cs^+ ion bombardment enables distinguishing (D) the C-rich epoxy resin, as well as O-rich mineral-dominated and N-rich OM-dominated regions by image segmentation. (E) C-rich and N-rich sites are distributed heterogeneously across the soil matrix. (F) ^{15}N-labeled bacterial necromass is located at distinct microsites. (G and H) Bombardment with O^- ions enables analyzing distributions of major elements (Na, Mg, Si, K, Al, and Fe) in soil aggregate structures. Data obtained by using a dual primary ion source approach to facilitate extensive correlative analyses (unpublished data by Schweizer et al. from an isotope labeling experiment to study microaggregate formation).

successive spatial patterns of increasing coverage and connectivity of organic matter patches over time (Schweizer et al., 2018). Analyses of soils from a precipitation gradient showed that the extent to which fresh organic matter was associated with native organic matter patches was correlated with carbon mineralization, suggesting that lower colocalization may result in lower carbon mineralization (Wilhelm et al., 2022). The importance of organic matter interacting with mineral surfaces was highlighted by a more nitrogen-rich composition of organic matter patches colocalized with iron and aluminum phases (Inagaki et al., 2020). Independent of the C:N ratio of added plant litter, nitrogen-rich patches of likely microbial origin comprised most of the newly formed mineral-associated organic matter (Kopittke et al., 2018, 2020). Over the course of soil formation in the Damma glacier forefield, the CN:C ratio of organic matter patches tightly reflected increasing microbial nitrogen assimilation (Schweizer et al., 2018). Considering the overall spatial arrangement of soil components, Steffens et al. (2017) found two recurring types of microdomains linked to the storage or exchange of organic matter and nutrients.

5.2.5 | Mapping the natural abundance of ^{13}C and ^{15}N isotopes with LA-IRMS

LA-IRMS is the only method that allows tracing differences in stable carbon isotope composition at the natural abundance level at a micro-scale resolution in the soil. It enables the localization of carbon stabilization and turnover processes at the scale of individual microaggregates based on natural carbon isotope fractionation. It could also be used for mapping. However, this is usually too time-consuming, so applications focus on specific ROIs. Earlier LA-IRMS set-ups allowed for the analysis of tree rings (Schulze et al., 2004) and soils at a spatial resolution of tens of around 100 µm (Bruneau et al., 2002; Grieve et al., 2006). Recently, Rodionov et al. (2019) developed a set-up suitable for analyzing smaller sample amounts using a microcell and avoiding sample gas losses. This improved the spatial resolution of recording differences in $\delta^{13}C$ natural abundance to 10 µm.

In most biological systems, heavier isotopes are discriminated against their lighter counterparts because of kinetic and thermodynamic processes. Consequently, changes in soil $\delta^{13}C$ values inform on the rate or degree of SOM transformation (Huang et al., 1996; Kramer & Gleixner, 2006; Krull et al., 2007). As C3 plants discriminate more strongly against the heavier ^{13}C isotope than C4 plants, changes in $\delta^{13}C$ natural abundances in soil upon changes in C3/C4 plant input inform on the portions of the remaining former material, that is, on its turnover rates (Derrien & Amelung, 2011; Veldkamp, 1994; Vitorello et al., 1989). First applications to soils showed that the mean residence time of SOM in soil microaggregates is highly variable, ranging from 1—300 years at a spatial scale hardly exceeding 100 µm (Rodionov et al., 2019). It was also shown that SOM turnover is not strictly restricted to aggregate surfaces, but high turnover might also occur in

interior parts (Vergara Sosa et al., 2021). Recent work indicates that it is also possible to detect carbon microbial isotope fractionation processes (Meyer et al., this issue) because microbial use of specific carbon sources also translates into the enrichment of ^{13}C in their residues (Klink et al., 2022; and references therein). The degree of such processes at the scale of microaggregates may be significant (Rodionov et al., 2019), thus likely requiring more complex models rather than one-pool isotope mixing to estimate the carbon turnover in microaggregate fractions induced by vegetation changes, as already critically discussed by Derrien and Amelung (2011). Microbial turnover, however, also leads to changes in SOM quality and changes in C:N:P ratios, the mapping of which requires other techniques, as indicated in Table 3 and outlined below.

5.3 | Mapping of SOM quality

5.3.1 | X-ray photoelectron spectroscopy

XPS characterizes the interface's chemical composition. A monochromatic X-ray beam (e.g., photon energies of Al Kα: 1486.6 eV and Mg Kα: 1253.6 eV) leads to the emission of electrons from the sample. The kinetic energies of these emitted electrons are then measured with an energy-dispersive detector, and the binding energy (BE) is calculated as:

$$BE = h - KE - \Phi, \tag{1}$$

with hν = photon energy, KE = measured kinetic energy, Φ = spectrometer work function.

The obtained BE is characteristic of a given element, including its various core-level electrons, oxidation state, and local chemical environment. It, therefore, provides insight into the chemical composition of the sample. Specific ROIs can be analyzed in spot mode at a spatial resolution of approximately 10 µm. At the same time, the information depth of XPS corresponds to the ejection depth of the photoelectrons from a 1 to 10 nm thin surface layer, thus allowing to link the chemical composition of the biogeochemical interfaces to soil functioning. Applying XPS to soils showed that the increase in water repellency correlates well with changes in the interface chemical composition, especially with a decrease in the interface O/C ratio (Woche et al., 2017). Surface probing by XPS confirmed that, in particular, nonpolar carbon species controlled the CA, and thus, the hydrophobicity of aggregate surfaces (Bachmann et al., 2020; Bachmann et al., 2021; Gaj et al., 2019; Woche et al., 2017), while bulk carbon content was not necessarily linked to CA (Bachmann et al., 2020). Comparing XPS data with bulk data, for example, using particle size fractions or aggregates, allows for assessing the surface enrichment of specific elements (Gerin et al., 2003). It indirectly also enables us to measure the thickness of biogeochemical interfaces. In volcanic ash soils, XPS showed that increasing interfacial carbon content was responsible for larger CA and higher aggregate stability (Bachmann et al.,

2020). In a soil toposequence described by Krause et al. (2018), the surface of free large microaggregates showed increasing concentrations of oxygen and decreasing ones of carbon with increasing amounts of soil clay (Figure 5, left), while carbon contents at the surface of occluded microaggregates increased with increasing amounts of clay (Figure 5, right), coinciding with higher portions of nonpolar C-C and CH bonding forms. Surface-enriched microaggregate carbon prevails mainly in sandier soils, while at high clay contents the surface carbon accrual coincided with increasing occlusion of microaggregates within macroaggregates.

By employing sputter techniques (e.g., with Ar$^+$, fullerenes, or condensed aromatic molecules), XPS becomes destructive (see also Table 3) but extends the insight into the vertical extension of interfaces from the nm-scale to depths of ca. 1 µm. For example, using Ar$^+$ sputtering, Amelung et al. (2002) could demonstrate that organic matter of microaggregates from the Ah and Bh horizons of Chernozems and Podzols, respectively, is concentrated at the particle surface. The same approach was employed by Mikutta et al. (2009) to explore the depth profile of organic matter in organo-mineral associations from A horizons across a mineralogical soil gradient. Their result suggests that aromatic-C is enriched in the proximity of mineral surfaces while amide-C (peptides/proteins) tends to locate in outer regions of organo-mineral associations.

5.3.2 | Vibrational spectroscopic imaging

To capture the laterally resolved 2D distribution of the molecular composition of biological materials or heterogeneous soil at the µm scale, IR-microspectroscopy (µ-FTIR), and Raman imaging at µm-resolution can be applied. For instance, the latter is increasingly used for microplastic counting and identification in soil environments (Araujo et al., 2018; Bläsing & Amelung, 2018), while for SOM screening Raman usually fails due to soil autofluorescence (see Section 3). To improve sensitivity, it is possible to combine FTIR with radiation supplied by synchrotron sources (SR-FTIR; Johnston & Aochi, 1996; Lehmann et al., 2007; Lehmann & Solomon, 2010; Marinkovic et al., 2002). Lehmann et al. (2007) investigated the spatial distribution of organic carbon functional groups in free stable microaggregates from three different soils using near-edge X-ray absorption fine structure (NEXAFS) and SR-FTIR spectroscopies. Their results show that organic carbon groups were unevenly distributed within microaggregates and did not show any discernible gradients from the interior to the exterior of the aggregates, which was also confirmed by Hernandez-Soriano et al. (2018). Furthermore, microbial rather than plant-derived carbon is strongly associated with kaolinitic clay surfaces (Lehmann et al., 2007).

Raman microscopy has been applied in 2D imaging since 1990, when robust dispersive Raman spectroscopy was combined with optical microscopy with a high spatial resolution to analyze single living cells and chromosomes (Puppels et al., 1990). Since then, the technique has been widely used to study, for example, bacteria (Huang et al., 2004;

FIGURE 5 Atomic percentages of oxygen (O) and carbon (C) in the interfaces (approximately 2–10 nm depth) of free and occluded large microaggregates (SMA; 53–250 µm) along a natural clay gradient as revealed by XPS (Woche et al., unpublished).
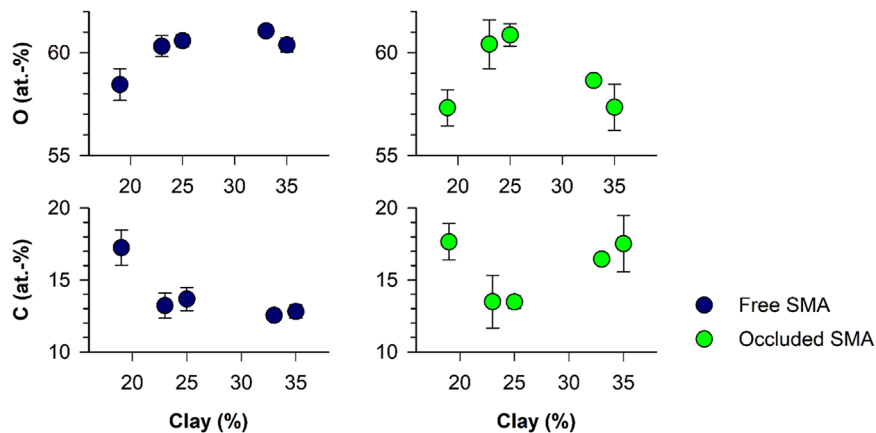
Xie & Li, 2003), ceramics (Durand et al., 2012), and soils (Nkebiwe et al., 2022) with little sample preparation (Toporski et al., 2011). Raman microspectroscopy offers several advantages over dispersive Raman and Fourier transform–Raman, including smaller minimum quantities of the analyte, depth profiling via confocal microscopy, and improved spatial resolution (ca. 300 nm with a 514-nm Raman excitation laser). However, due to the fluorescence interference, the application of Raman microspectroscopy in the visible spectral range is still limited to analyzing soil mineral phases (Vogel et al., 2017). Problems with autofluorescence can be overcome by working with high-energy laser systems that irradiate samples and excite the bands in the deep ultraviolet range (DUV-Raman), that is, outside the fluorescence range (Tarcea et al., 2007; Vogel et al., 2017). Moreover, the spatial resolution of DUV-Raman microspectroscopy is improved as the lateral resolution is proportional to the excitation wavelength (Stewart et al., 2012). These advantages of DUV-Raman microspectroscopy enabled Vogel et al. (2017) to directly detect tiny phosphate particles in soil without the occurrence of sample fluorescence. However, using the UV laser can result in the decomposition of most of the organic material during measurements, impeding the studies of organic matter.

5.3.3 | Synchrotron-based X-ray spectroscopy

Synchrotron radiation has allowed for developing and applying various X-ray analytical techniques for studying soil. The most common X-ray methods are based on the photoelectric effect, where X-ray photons are absorbed by the target element, promoting its core electrons to higher energy levels and emitting photo and Auger electrons. The more advanced synchrotron beamlines now enable the acquisition of 2D information from all three main X-ray spectroscopic techniques: XRF, XAS, and XPS. For 2D imaging at high spatial resolution (µ-XRF), samples are scanned through the beam along a grid pattern that typically has a spot size of 1–10 µm for a microprobe and 50–500 nm for a nanoprobe. This provides qualitative multielement or semi-quantitative single-element maps (e.g., Langner et al., 2013), which can be evaluated for distinct distribution patterns using statistical and geostatistical methods (e.g., Aaron et al., 2018). Frequently, µ-XAS is used as the first step in determining the elemental distribution nonde-

structively and then, based on the results, to select points of interest for complementary spectroscopic methods to obtain spatially resolved details on the chemical state of the elements at the µm to nm scale. For this purpose, a single beamline at a synchrotron radiation facility can be equipped with different microscale techniques, including µ-XRD, µ-XRF, and µ-XAS. In recent years, the two main sections of µ-XAS, that is, µ-XANES (X-ray absorption near edge structure, synonymous with NEXAFS) or µ-EXAFS (extended X-ray absorption fine structure), have become the state-of-the-art techniques in soil science (Baumann et al., 2019; Prietzel et al., 2010; Sharma et al., 2019). While µ-XANES provides spatially resolved information on an element's oxidation state and its coordination structure, including the configuration of the coordination atom, ligand functional groups, and their relative contents, µ-EXAFS offers information on the coordination environment of the absorbing atom, including coordination neighbor atoms, coordination numbers, and coordination bond lengths (e.g., Stöhr, 2013).

Figure 6 shows one example of a combination of µ-XRF with µ-XANES applied to a resin embedded, polished cross section of large soil microaggregates and exemplary Fe-edge XANES spectra of three selected common Fe reference standards. The exposed cross sections (Figure 6, red outlined areas of the light microscopy image) are reflected in the silicon maps. They can therefore be used to distinguish between the inner and outer parts of the particles, depending on their morphology. The comparison of the different elemental maps indicates that some of the microaggregates are primary silicate particles coated with iron and partly phosphorus sorbed to it, meanwhile, evidences the presence of the composite aggregate (Figure 6). The visual inspection of the Fe K-edge µ-XANES spectra of selected locations on the microaggregates suggest that the surface of these microaggregates is enriched in ferric iron species while a mixture of ferric and ferrous iron is present in the interior of the microaggregate. This indicates that the inner part of the microaggregates is encapsulated, and thus readily available electron acceptors such as dissolved oxygen and nitrate are already depleted, favoring the reduction of three-valent iron. However, for a more detailed evaluation of the obtained µ-XANES spectra, linear combination fitting has to be performed using reference spectra of a much broader range of expected species (see Table 3 for challenges). Here, this would allow not only to identify individual Fe species but also to obtain semi-quantitative data.
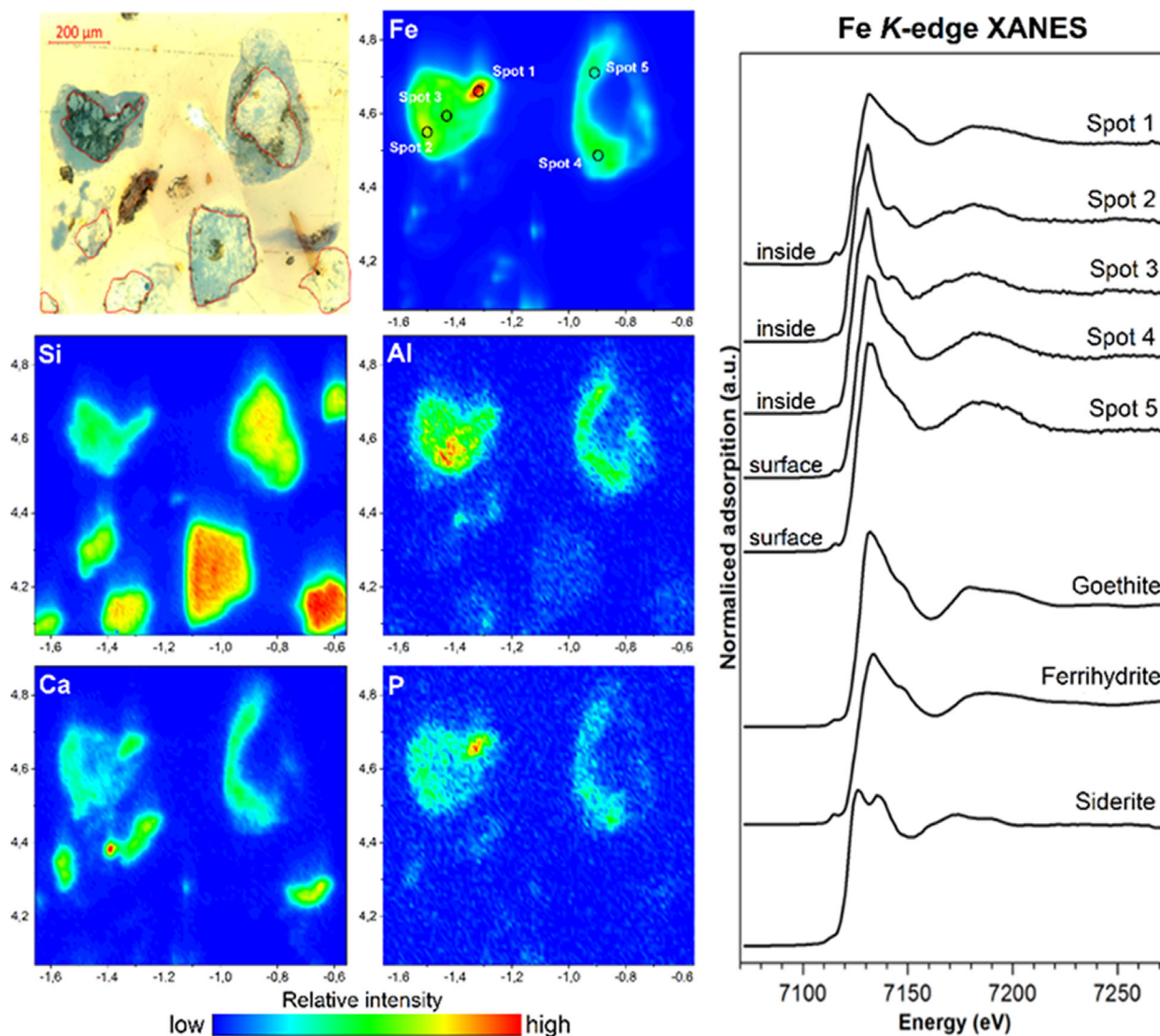
FIGURE 6 Microscopic composite map of large soil microaggregates (53–250 µm) obtained from a Luvisol using reflected and transmitted light microscopic images and respective µ-XRF maps of iron (Fe), silicon (Si), aluminum (Al), calcium (Ca), and phosphorus (P); Fe K-edge µ-XANES spectra of selected spots and exemplary spectra of Fe reference compounds. The µ-XRF maps indicate that the particle in the top left is a composite aggregate, while the rest are primary silicate particles coated with iron and partly phosphorus sorbed to it. Red-bordered parts represent exposed inner parts of aggregates (Kruse et al., unpublished).

When combined with scanning transmission X-ray microscopy (STXM), µ-XAS can be used to create 2D maps with spectral information for each pixel of interest. The pixel-specific intensity of transmitted X-rays is then recorded as a function of energy for a series of frames, which can then be stacked to obtain maps with complete spectral information for each scanned pixel. The technique resolves gradients at the 20-nm scale. It has already been applied for mapping several elements in soil microenvironments (carbon, nitrogen, phosphorus, sulfur, aluminum, silicon, sodium, potassium, calcium, and iron; Obst & Schmid, 2014). Risks of structural alternations of radiation-sensitive compounds can be minimized by using Cryo-STXM. STXM-XANES has been recognized as one of the most effective approaches for investigating soil microaggregates (Stuckey et al., 2017). Applications to samples from the same soil horizon showed that heterogeneity within organic colloids (intraparticle heterogeneity) is smaller than in-between them (interparticle heterogeneity; Schumacher et al., 2005). Likewise, the intraparticle heterogeneity of SOM was also observed within individual microaggregates (Asano et al., 2018; Solomon et al., 2012), being reflected by the variation in molecular compositions among SOM occluded inside the intra-aggregate pores, SOM existing as distinct particles, and the SOM coated on minerals (Kinyangi et al., 2006; Lehmann & Solomon, 2010); specific moieties such as aliphatic carbon play a crucial role in mineral–organic interactions, and thus, carbon stabilization in soil aggregates (Lehmann et al., 2007). Yet, the representativity and scalability of STXM–NEXAFS spectroscopy are often called into question due to the inability to analyze soil samples in replicates and the use of small sample quantities (Dynes et al., 2015).
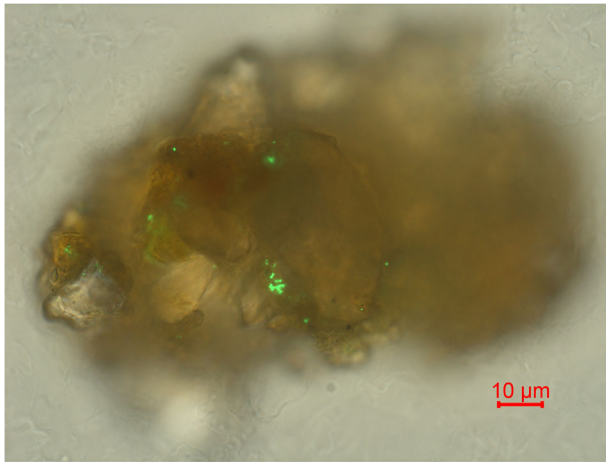
FIGURE 7 Bacterial colonization on the surface of an individual microaggregate. Green fluorescent signals represent bacterial cells. The image was obtained by epi-fluorescence microscope.

6 | MICROBIAL BIOGEOGRAPHY IN AND AT MICROAGGREGATES

Standard molecular methods for the analysis and identification of microbial communities in soil do not provide a resolution down to the μm scale, as they depend on relatively large amounts of sample material so that information on the spatial location of individual organisms relative to each other and to soil components is usually lost. However, such limitations may be overcome by specific microsampling techniques (Dechesne et al., 2003; Grundmann et al., 2001), by use of molecular procedures that are adapted to low sample input (Bailey et al., 2013; Probandt et al., 2018), or by microscopic analysis of polished (thin) sections (Figure 7; Eickhorst & Tippkötter, 2008a; Gutiérrez Castorena et al., 2016; Nunan et al., 2003; Raynaud & Nunan, 2014).

6.1 | DNA-based microbial analyses

Recent advances in microbial analyses are most evident from studies focusing on macroaggregates or larger microaggregates. Successful analyses include measurements of microbial activity on pooled microaggregates (100–300 μm) based on ^{3}H-leucine incorporation (Montgomery et al., 2019). Enzyme assays and subsequent DNA-based community compositional analysis have been applied to macroaggregates (Bailey et al., 2013; Kim et al., 2015), but even then, five to ten aggregates with similar traits had to be pooled because standard procedures typically require between 0.25 and 1 g of soil for DNA extraction (Penton et al., 2016; Young et al., 2014). Very few attempts have been made to analyze individual macroaggregates with DNA-based methods, and we are unaware of any successful application to individual microaggregates (see also Table 3 for general challenges). Szoboszlay and Tebbe (2021) reported on prokaryotic communities associated with individual soil macroaggregates of a size of 2 mm and a mean weight of 5 mg using a commercial kit, while Bailey et al. (2013) were

successful in analyzing individual aggregates down to 0.01−0.05 mg or 250–425 μm in size by applying a specifically adapted procedure for cell lysis and performing random DNA amplification prior to marker gene-targeted PCR for community composition analysis. While providing insight into microbial colonization at a spatial scale that reflects already better the environment a microbial cell perceives, it has to be kept in mind that such approaches are likely to introduce additional bias due to insufficient lysis of some taxa and the introduction of artifacts such as false positive results by whole genome amplification procedures (Kaster & Sobol, 2020). Specific bioinformatic tools have lately been developed to address this problem (Karstens et al., 2019; Liu et al., 2022; C. Wang et al., 2022), but contaminations can lead to substantial loss of sequencing depth after eliminating false-positive data when applying such tools. So far, the studies on individual aggregates have demonstrated that DNA-based methods can reveal valuable information regarding heterogeneity in microbial activities, colonization patterns, and network structures at aggregate size scale. However, these studies did not yet report strong relationships to the individual aggregates' physical, chemical, or biological properties. The link between community structure and aggregate characteristics is either weaker than anticipated, not reflected at the aggregate scale studied so far at a scale above microaggregates, or biased by the heterogeneity among aggregates.

Obtaining taxonomic or functional information with a spatial resolution at the single-cell level is even more challenging but conceivable in the future based on recent advances in single-cell approaches, which could also be suitable for microaggregates. Genomic sequencing of individual cells can successfully be performed, even for soil samples (Aoki et al., 2022; Jing et al., 2021; Kaster & Sobol, 2020). One major challenge will be the sampling of individual cells being associated with aggregates because currently available approaches to select single cells for sequencing rely on cell suspensions. Collecting individual cells from the surfaces of soil particles will be more difficult, especially when the cells are firmly attached to soil particles and thus difficult to remove (Hong et al., 2015). Yet, assuming that single-cell approaches might be combined with complementary microaggregate imaging approaches, context-specific information on ecological niches might soon become available.

6.2 | Microscopy of microorganisms

In contrast to the commonly applied DNA-based analyses, microscopic approaches provide information at the single-cell level. However, microscopic analyses of bacteria in soil and on soil particles are challenging because cells can be difficult to locate due to the low cell-to-soil particle ratio, poor contrast of the cells against the background, and the opaque nature of the soil. Consequently, microbial cells are often fluorescently labeled, either intrinsically, for example, when introducing strains with green or red fluorescent protein into the soil, or by fluorescent staining, for example, via DNA intercalating stains such as 4′,6-diamidino-2-phenylindole, or by using oligonucleotide probes with fluorophors in fluorescence in situ hybridization (FISH). In addition, the

FISH technique can provide taxonomic information about the stained cells, if probes for specific phyla, classes, or genera are applied alone or in combination (e.g., Probandt et al., 2018). A variant of FISH, catalyzed reporter deposition (CARD)-FISH, has been proven very useful in increasing fluorescence signal intensity (e.g., Eickhorst & Tippkötter, 2008b). This improves the detection of bacterial cells of relatively low metabolic activity, which are difficult to detect with standard FISH, and against a background of unspecific fluorescent signals emitted by soil components with autofluorescent properties that often interfere with microbial signals (Li et al., 2004).

Recent technological advances in microscopy and image analysis bear good potential to overcome problems of nonspecific autofluorescence, for example, by reduction of stray light signals, similar to a confocal laser-scanning microscope. On the one hand, specific deconvolution algorithms discriminate scattered unspecific light signals and enhance contrast and resolution. However, the resulting images need to be evaluated carefully compared with the original microscopic images to avoid artifacts. On the other hand, structured illumination may be applied by moving a grid over the sample and acquiring images with the grid structure superimposed in different positions. These images are processed to create one image for the focal plane, eliminating out-of-focus image information as identified based on the superimposed grid structure. A potential disadvantage of structured illumination is the need for a bright and constant fluorescence signal because image acquisition takes more time. Another promising approach is the application of fluorescence lifetime imaging when performing confocal laser scanning fluorescence microscopy. Upon image acquisition, the distinctly different photon arrival times of all photons per pixel are separated in a procedure called phasor plot separation, and fluorescence decay can be visualized. In the first study, clear differences were seen in fluorescence lifetime profiles between the fluorescence signals of microorganisms and the soil matrix, thus demonstrating the applicability of the methods for soil samples (Loeppmann et al., 2023). Potential limitations of this approach are slow image acquisition and long processing times. Furthermore, signal variation due to cell age, metabolic status, and localization as a single cell or in a biofilm may affect the fluorescence lifetime imaging signals and remains to be evaluated (see also Table 3 for additional challenges).

Lee et al. (2022) developed a label-free nondestructive multiphoton microscopy approach with different multiphoton detection modes for autofluorescence imaging of bacteria or fungi associated with roots, minerals, or soil. Imaging with a custom-built multiphoton microscope revealed that different detection modes, including fluorescence lifetime imaging, and applied in combinations, are well suited to visualize microbial cells against background signals. In the future, this might be combined with different omics or mass spectrometry approaches. The combination of methods for correlative imaging has recently been successfully applied in some first studies, including the visualization of microorganisms, though not yet for aggregates. For example, Bandara et al. (2021) performed resin embedding of rhizosphere samples and analyzed the sample surface using CARD-FISH for microbial analysis with SEM with EDS and ToF-SIMS NanoSIMS and µ-RAMAN for chemical mapping. Besides, there is potential to detect metabolically active cells at the single cell level when substrates with stable isotope labels are applied, the incorporation of which being trackable using NanoSIMS or Raman microspectroscopy (Eichorst et al., 2015). Yet, approaching such a single-cell level for habitats at the microaggregate level remains a future vision.

7 | TOMOGRAPHIC APPROACHES

The µCT is a powerful tool to noninvasively prepare 3D maps of X-ray attenuation related to local material densities (Peth, 2010). The process works by taking a series of X-ray images (projections) of an object from different angles, which are then processed by a computer to reconstruct a 3D image. The X-ray images are typically taken using a micro-focus X-ray source and a high-resolution detector, allowing fine details to be captured. During reconstruction, the computer uses algorithms to convert the 2D X-ray projections into a 3D image, which can be visualized and analyzed using specialized software. This enables examination of the object's internal structure without damaging or changing it, making µCT a valuable tool in various fields, including material science, biology, and engineering. It can also be used to infer the spatial distribution of solid soil constituents (mineral and organic) as well as water- and air-filled pores within the individual (micro)aggregates (Figure 8). X-ray CT has already proven a valuable tool for the 3D analysis of soils for a wide range of samples from several centimeters (Capowiez et al., 2011; Gantzer & Anderson, 2002; Kim et al., 2010; Pierret et al., 2002) in diameter down to the aggregate level (Fukumasu et al., 2022; Kravchenko et al., 2015; Menon et al., 2020; Nunan et al., 2006; Zhao et al., 2020).

Among the soil properties that can be analyzed are the total porosity, number of pores, pore shape and size distribution, connectivity and tortuosity of the pore space, pore surface area and surface density, as well as the number of continuous pores that are connected to the surface of an aggregate. Rabbi et al. (2016), for instance, scanned macro- and microaggregates at a voxel resolution between 5.2 and 4.0 µm and found that the rate of substrate decomposition within aggregates was influenced by pore geometry.

Figure 8 shows an example of how a 3D model deriving from a µCT scan can look like and how a pore size distribution can be extracted from it. For the pore size distribution, we chose the four size classes <3, 3–6, 6–10, and >10 µm as key thresholds for different microaggregate functions (representing matrix potentials of −1000, −500, −300 hPa) for the following reasons: the minimum diameter of fungal hyphae is 3 µm (Soufan et al., 2018), pores <6 µm provide protection from predation by protozoa (Wright et al., 1995); also, C turnover was found to be faster in pores >6 µm (Killham et al., 1993). The 10 µm represent the well-known upper threshold for medium-sized pores that are usually air-filled in terrestrial soils.

The best images in terms of spatial resolution, signal-to-noise ratio, and quantitative exploitation are obtained using synchrotron radiation (Baruchel et al., 2006; Indore et al., 2022). This is due to the high-beam energy of synchrotron radiation that allows for a monochromatization of the X-ray beam usually achieved by double crystal monochro-
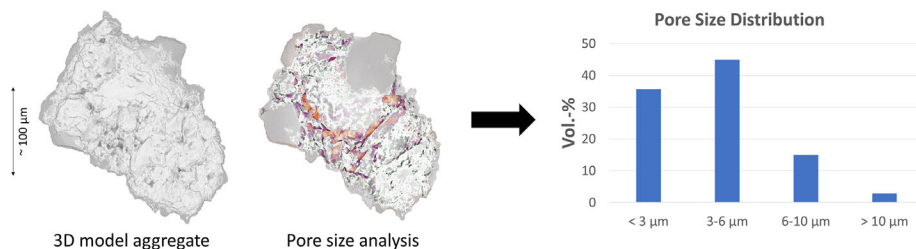
FIGURE 8 µCT supported measurement of the pore size distribution in a large microaggregate (approximately 200 µm diameter) at a resolution of 480 nm. Sample from Felde et al. (2021).

mators (Beckmann et al., 2005) while still delivering a high enough photon flux to ensure excellent image quality. Voltolini et al. (2017) proposed an analysis protocol for the morphometric characterization of complete soil microaggregates. They found significant differences in micro-structures of microaggregates from different soils, some mostly inorganic with mainly interstitial pores while others comprising more organic components within larger pore spaces accessible for microorganisms. With recent advances in X-ray sources, image analysis software, available computing power, and storage capacity, it is now possible to do 4D (time series) tomography with scanning times of a few minutes to seconds for a complete scan (Ferreira et al., 2022).

The application of µCT for in situ discrimination between minerals and SOM within aggregates is challenging because the X-ray attenuation coefficients of organic matter fall between those of pores (water or air-filled) and the mineral matrix. Correspondingly, the X-ray attenuation contrasts of SOM compared with the other compounds are weak, impeding the in situ identification of SOM in natural soil aggregates, where a significant portion of SOM is closely associated with minerals (see also Table 3 for additional challenges). However, the osmium-staining of SOM can overcome this limitation (Peth et al., 2014). The principle is that osmium binds specifically to unsaturated carbon bonds of organic compounds (e.g., present in lipids, lignin, proteins) and at the same time reveals an X-ray absorption edge at higher X-ray energies (74 keV) sufficient to penetrate dense soil material. Thus, osmium is used as a proxy to in situ localize SOM in natural soil aggregates. The method has been applied in various studies (Arai et al., 2019; Rawlins et al., 2016; Schlüter et al., 2022), but so far, not for soil microaggregates.

8 | IN SILICO APPROACHES

Sophisticated numerical tools allow for studying soil microaggregates in silico and visualizing the spatial and temporal dynamics based on model assumptions. For instance, Pot et al. (2015) combined a carbon degradation model with a Lattice-Boltzmann approach into a pore structure from µm to mm. Later, Portell et al. (2018) adapted this model, simulated the influence of heterogeneously distributed organic matter sources on the abundance of microbes, and suggested a strong relation between local properties and soil biodiversity. Zech et al. (2022) followed a similar setting with microbial population dynamics and turnover of particulate organic matter in soil microaggregates. The

CT images of microaggregates obtained from natural soils served as the basis for constraining the simulation domain. The results showed that bacteria and particulate organic matter were heterogeneously distributed so that overall biodegradation kinetics and CO_2 evolution depend strongly on the pore size distribution at the microaggregate scale (< 250 µm).

8.1 | Modeling of explicit aggregate structure dynamics

Modeling the formation of aggregates is fundamental for understanding the functional diversity of soil structure and can test ideas and concepts about what controls the evolution of structure. At the scale of microaggregates, a physically rigorous modeling approach based on the basic mechanisms of transport and physical interaction between particles has been presented by Ritschel and Totsche (2019). They modeled the diffusion of prototypical minerals via a random walk and local particle attachment probabilities using the Derjaguin–Landau–Verwey–Overbeek theory in 3D. Comparable to diffusion/reaction-limited aggregation known from colloidal sciences (Lin et al., 1989; Witten & Sander, 1981), this led to aggregates growing as branched fractals and compact, dense structures in response to the specific physicochemical milieu. Due to the physical framework, the parameters used in this model are available for direct observation, for example, temperature, ionic strength, and zeta potential. Hence, an easy comparison with experimental data is possible. Furthermore, the explicit aggregate structure available in three dimensions permits the estimation of functions based on morphological properties, as exemplified by Ritschel and Totsche (2019) with the derivation of the water retention characteristics from the aggregate pore size distribution.

This approach was extended using sedimentation as an additional transport mechanism by Guhra et al. (2021), who showed how gravity could shape the aggregation dynamics and structural features when aggregates grow and start to settle. Interestingly, gravity can accelerate as well as decelerate aggregate growth through a delicate interplay of different mechanisms (Figure 9). The authors highlighted the strength of mechanistic models to include scenarios that are hard to realize experimentally, for example, no-gravity reference cases or tiny spatiotemporal scales.

A concept of modeling the self-organization of soil structures under microbial activity changes was introduced by Crawford et al. (2011)
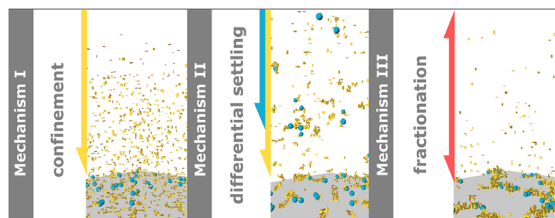
FIGURE 9 Mechanisms of aggregation induced by gravity: increased aggregation due to spatial confinement after sedimentation (left), contact due to different sedimentation velocities (middle), decrease in aggregation rate due to spatial fractionation of potential interaction partners with different sedimentation velocities.

and adopted in a cellular automaton model (CAM) for biofilm development by Tang and Valocchi (2013). Finally, a hybrid discrete-continuum CAM/partial differential equation approach helped to describe and study the structure formation of microaggregates (Rupp et al., 2019; Zech et al., 2020). The model includes a combination of discrete and continuum parts, where in the discrete part a CAM is used to capture the interactions of building units of aggregate, the build-up and break-down of aggregates, the turnover of organic matter, and the resulting alteration of the fluid phases and pore space geometry (Figure 10). Applying this model to building units derived from digital imaging can illustrate, for instance, how the particles dispersed in solution aggregate, thus encrusting particulate organic matter and leaving a scatter of reactive hot spots at the interfaces of larger pores formed (Figure 11).

By modeling the interactions of specific minerals and organic matter, it is possible to identify the mechanisms that control the evolution of structure and establishment of stationary aggregate properties. For example, when subjecting the prototypic building units quartz, goethite, and illite to attractive and repulsive electrostatic interaction forces, the model revealed shielding effects due to charge neutralization and aggregate growth in response to the net system charge (Rupp et al., 2019). Subsequent works included the structural reorganization of the soil architecture spatially and temporally explicitly, based on a dynamic, self-organized rearrangement of solid building units and degrading particulate organic matter with subsequent surface interactions (Zech, et al., 2022). This approach also allows to study the occlusion of organic matter and the fate of different ages or sources of organic matter, for example, by exudation or priming effects, and it can be coupled to macroscale models.

8.2 | Synscaling and synlocation

Tomographic techniques provide a detailed 3D perspective on soil's physical architecture. Recent advances in X-ray μCT resolution permit the investigation at the submicron scale, which is particularly relevant for microaggregates (Voltolini et al., 2017). Yet, μCT only detects local material densities and a comprehensive assessment of microaggregate structure and composition further requires chemical, biological, and mechanical information from other techniques. While

sophisticated instruments increasingly provide 3D data, for example, synchrotron-based μ-XRF (Fittschen & Falkenberg, 2011), they are neither widely available nor fully established. Most other techniques still operate in two dimensions or do not offer a 3D application. Hence, 2D imaging data need to be integrated into the corresponding plane in the 3D tomography dataset to facilitate the combination of data from multiple instruments. However, several of the 2D mapping tools operate with different resolutions (Figure 1 and Table 2) and require the merging of spatial information at different scales (synscaling) and different locations (synlocation), and finally, coregistration of the 2D and 3D information. Difficulties arise because (1) the individual techniques require specific sample preparation, for example, thin sections or embedding, which hamper the application of other techniques to the prepared samples, (2) some techniques, for example, NanoSIMS and LA-IRMS, are consumptive, implying original samples will no longer be available for other studies, (3) the different scales of the field of view frequently diverge, and (4) particularly methods operating at the nanoscale only cover minor parts of the aggregate (or its surface) eventually not representative for the whole microaggregate. To overcome these limitations, each technique must focus on analyzing several preselected regions-of-interest (Abu Quba et al., 2020) located relative to a reference spot, for example, a stained dot on the sample holder, which several methods can easily detect. Hapca et al. (2011) treated image registration as an optimization problem. They matched elemental maps from EDS with μCT data by maximizing their spatial correlation with appropriate spatial rotations and translations. To measure the 2D information inside the soil cores at various locations, they resin-embedded the sample and cut thin sections after μCT measurement, thereby necessarily destroying the sample. Similar embeddings were also applied in studies employing μCT to keep the structure intact while cutting the slices. Hapca et al. (2015) went further by interpolating multiple already aligned 2D maps into 3D space by geostatistical methods. In that way, the 2D distribution of elements could be estimated in 3D using μCT data as a reference frame. Later, Schlüter et al. (2019) also included light microscopy, NanoSIMS, and fluorescence microscopy imaging and approached the challenge of multiple scales in 2D data by individually optimizing rigid transformations (translation, rotation) and scaling using the publicly available ImageJ plugin *elastix* (Klein et al., 2010). With appropriate fluorescence labeling, they could simultaneously locate microorganisms, minerals, and aggregates in 3D space, providing deep insights into the microbial communities and their relation to soil architecture. The combination of μCT with other techniques has shown to be promising for correlating soil pore space and microbial activity by Juyal et al. (2019) using fluorescence microscopy, and by Kravchenko et al. (2019) using zymography. Those recent advances will likely establish correlative imaging for investigating soil microbial habitats in general but still suffer from the diversity and temporal variance of microbial activity and the interdisciplinary expertise required to comprehensively assess data from multiple sources (Védère et al., 2022). To simplify image registration and avoid tedious 3D transformation, Juyal et al. (2019) also carefully adjusted the orientation of the samples, and Kravchenko et al. (2019) placed markers at the sample edges. These preparations will
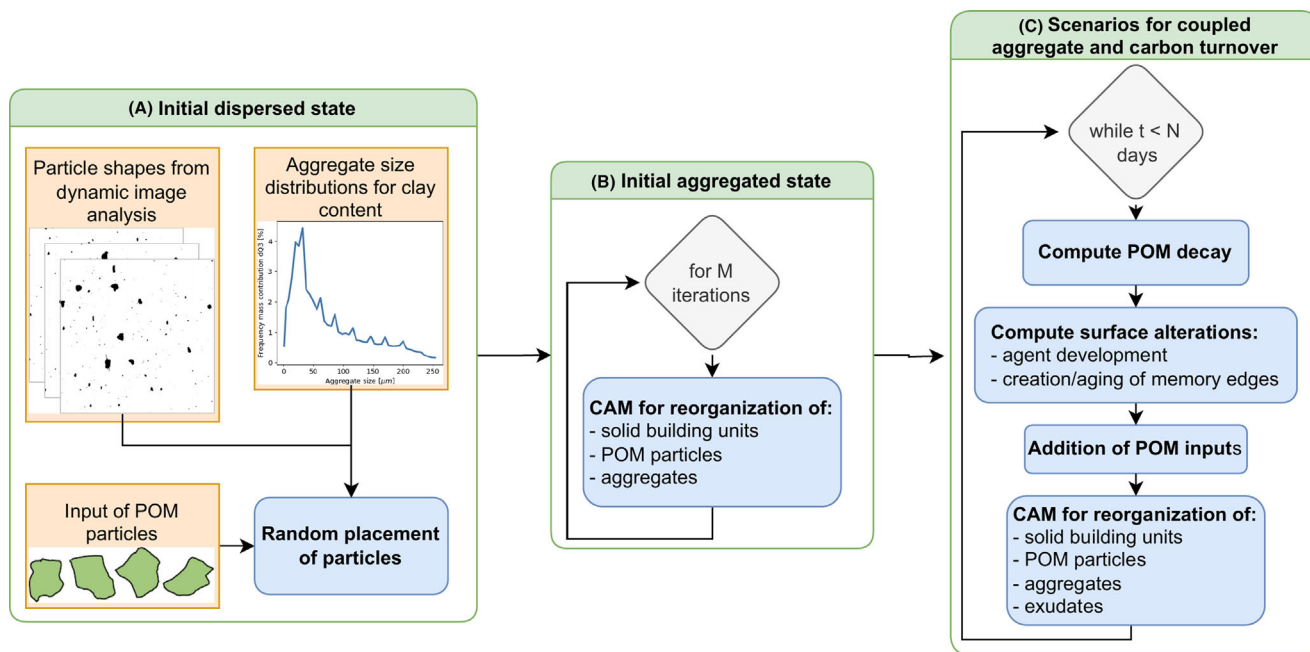
FIGURE 10   Flowchart for a cellular automaton model (CAM) model for aggregate dynamics: first creating an initial dispersed state from a particle shape library (left), second applying CAM rules attaining an aggregated state (middle), and finally iterating the CAM for arbitrary scenarios of temporal and spatial evolution of the aggregates, organic matter, and phases.
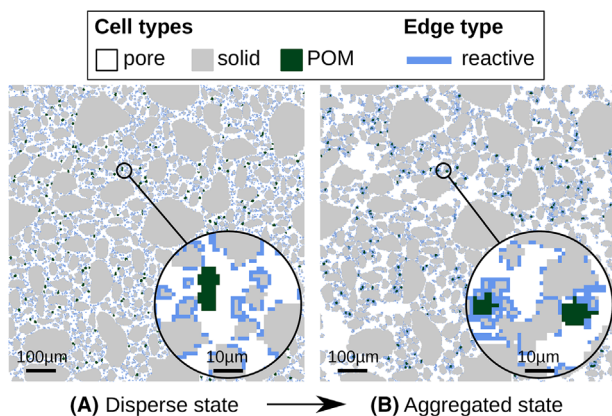

FIGURE 11   Cellular automaton model (CAM) simulations with building units derived from dynamic image analysis of wet-sieved, water-stable aggregates (Schweizer et al., 2019) and particulate organic matter (POM; dark green), creating an initial disperse state (left) and after application of the CAM bonding rules acting on reactive surface sites resulting in an aggregated state (right) with occluded POM.

also accelerate the automated image registration techniques discussed previously.

Based on the results of the above studies, Lippold et al. (2023) recently presented a comprehensive approach to correlative imaging with focus on the rhizosphere. While their general workflow of sample preparation remains similar to previous studies, they include µCT imaging prior to embedding and present a protocol to combine six instrumental techniques (µCT, NanoSIMS, light microscopy, LA-IRMS, SEM, and µ-XRF). All these advances in instrumental and methodological approaches also initiated the development of novel tools for automated image registration that are especially suited for environmental applications (Rohde et al., 2020).

Another promising approach is presented by Ost et al. (2021), which is particularly suited for analysis at the scale of microaggregates. In their study, the authors exploit the availability of 2D techniques that permit image acquisition from multiple perspectives, for example, SEM. By obtaining sufficient coverage of surfaces with different perspectival distortions, they successfully applied photogrammetry to reconstruct the 3D surface of a microaggregate from tilted SEM images and projected NanoSIMS data onto that surface. While this approach does not reveal the internal 3D structure of the sample, it permits correlating surface morphological features, such as curvature, roughness, and specific surface area, to the distribution of elements. This approach is likely also suitable using the imaging techniques already combined with µCT.

9 | LESSONS LEARNED AND OUTLOOK

Novel methodological developments have advanced our understanding of the properties and functions of microaggregates. Each of these methods has technical limitations (Table 3), thus calling for complementary use of these techniques as well as for respective modelling, synscaling and synlocation approaches. At present, we became able to quantify the composition, organization, porosity, and several other properties of individual aggregates. We found that the architecture of microaggregates is highly heterogeneous, even for a given soil, with hot spots of element accrual and microbial life, which vary in position,

and with porosity and materials involved. Consequently, significant challenges remain in the assessment of microaggregates' architecture.

Fractionation, separation, and isolation methods have been refined to obtain soil microaggregates of defined size and stability. The choice of a fractionation method to isolate microaggregates is vital and requires a careful selection of dispersion methods to adequately address the soil structure in question. Under field conditions, influences such as tillage or root growth can directly cause mechanical shearing, whereas the impact of water causes slaking, dispersion, and differential swelling of the soil structure, leading to the conditioning of failure planes. Choosing a suitable quantifiable fractionation technique that captures realistic microaggregate breakdown mechanisms is thus crucial. After fractionation, the different content of (coarse) primary particles inside and outside microaggregates and the diverse building patterns of microaggregates need to be measured and accounted for. To assess the microhabitat functions of microaggregates, the potential dispersion of microbial cells from soil surfaces during fractionation should be minimized but can usually not be entirely avoided. Techniques that can resolve the size distribution and other properties of dispersed soil structures can help adapt and optimize individual fractionation approaches related to the formation and breakdown mechanisms of the analyzed soil structure. Still, it has to be kept in mind that in nature, none of the aggregates exists isolated but as part of the soil structure interwoven by the pore network and other structural components like roots and hyphae; hence, for fully understanding the role of soil (micro)aggregates in the environment, research must remain linked to upscaling and integration into larger scales.

Spectromicroscopic approaches provide opportunities for direct in situ measurements of the properties and functions of microaggregates. Since noninvasive techniques are mostly limited to the morphological assessment of soil structures, various isolation and fixation techniques have emerged. The most widely applied method of fixation in resin enables sectioning and direct probing of microaggregate surfaces. This has led to improved visualization of the biochemical properties within the heterogeneous architecture of soil microaggregates. Nevertheless, the resin matrix may also cause interferences with surface-sensitive techniques such as XPS and AFM.

Further development of embedding techniques, such as cryofixation and sectioning, is warranted to involve surface-sensitive techniques better. To understand microaggregate dynamics, further experimental integration is needed to relate their fate and function to their arrangement within the larger soil structure. Direct observation of the formation and disruption of (micro)aggregates is hardly feasible. However, ESEM promises to enable direct studies examining the factors involved in microaggregate formation, such as drying–wetting or freezing–thawing, under controlled laboratory conditions. Technologies supporting a correlative mapping of whole biomolecules could help better elucidate such processes, but the recently available approaches, such as matrix-assisted laser desorption ionization–mass spectrometry imaging, are still restricted to pure biological matrices.

The actual lifetime of organic matter in individual microaggregates still remains unknown. A given microaggregate may contain organic matter with widely differing turnover times, suggesting residence times ranging from a few weeks to centuries and suggesting that young and old organic matter coexist at distances of only a few tens of micrometers. Nevertheless, microbial isotope discrimination within microaggregates is likely severe, thus hampering the accurate assessment of mean residence times from simply isotope mixing models that operate at natural abundance levels.

Current spectromicroscopic approaches overcame many obstacles to visualize and quantify the architecture of even individual microaggregates. Differences in resolution and sample pretreatment and the degree of destructiveness remain, though, a challenge in synchronizing the respective information. In addition, the high costs and long measurement times do not usually allow for repeated measurements on individual or several microaggregates, thus limiting our understanding of precision and representativeness. Also, no (artificial) microaggregate standards exist for internal spike and accuracy testing.

The application of geostatistical tools to understand the spatiotemporal patterns within and across microaggregates is still developing. This holds particularly true for techniques operating at the 3D resolution but is also valid for those where sequential 2D images can be obtained. On the one hand, classical geostatistical methods known for the macroscale, such as kriging, cannot easily be applied to microaggregates when elements of interest occur patchily in mosaic-like environments. On the other hand, correlating spots of, for example, minerals and organic matter, cannot simply use pixel sizes but must be restricted to contact areas between the target areas of interest and exclude zones where no or less interaction is possible, such as between organic matter and the interior of minerals. Thus, a joint effort is needed to harmonize the evaluation of interactions across scales, within microaggregates, and beyond. Finally, several well-known relationships established for the large (km-) scale across landscapes, such as between SOM and clay content, may not be valid at the scale of individual microaggregates. And even if once established for a given microaggregate, it may not be valid for other microaggregates. Still, it may take major efforts until the techniques presented or future advancements help us to decide what structure of a given microaggregate is representative of the whole set, how this structure is linked to size and stability, as well as to soil-forming factors such as climate, parent material, relief, biota, human activity, and time.

New approaches to explicitly model the temporal and spatial evolution of aggregate structures based on mechanistic principles have evolved. Simulations of scenarios improved our understanding of microaggregate build-up and break-down mechanisms, including, for example, priming effects. Also, the coupling of scales is within reach of the modeling endeavors. When aligned with in situ localization of organic matter and microorganisms, spatially explicit modeling approaches will facilitate a better understanding of interacting mechanisms in microaggregate formation, turnover, and micro-scale soil functioning. Future work now needs to relate the modeling scenarios closer to experimental data to improve the underlying assumptions and to design defined experiments for tangible hypothesis testing; in turn, the input of experimental data may help improve the applicability of numerical simulations in different scenarios.

CONFLICT OF INTEREST STATEMENT

The authors declare no conflict of interest.

DATA AVAILABILITY STATEMENT

Data sharing is not applicable to this article as no datasets were generated or analyzed during the current study.

ORCID

Wulf Amelung https://orcid.org/0000-0002-4920-4667

Ni Tang https://orcid.org/0000-0002-6726-2481

Nina Siebers https://orcid.org/0000-0002-6431-0046

Vincent J. M. N. L. Felde https://orcid.org/0000-0002-1018-2376

Klaus Kaiser https://orcid.org/0000-0001-7376-443X

Ingrid Kögel-Knabner https://orcid.org/0000-0002-7216-8326

Erwin Klumpp https://orcid.org/0000-0002-4810-9414

Claudia Knief https://orcid.org/0000-0001-5259-2675

Robert Mikutta https://orcid.org/0000-0002-7186-6528

Stephan Peth https://orcid.org/0000-0001-9799-212X

Thomas Ritschel https://orcid.org/0000-0002-9922-1107

Steffen A. Schweizer https://orcid.org/0000-0002-9489-1005

Kai U. Totsche https://orcid.org/0000-0002-2692-213X

REFERENCES

Aaron, J. S., Taylor, A. B., & Chew, T.-L. (2018). Image co-localization—co-occurrence versus correlation. *Journal of Cell Science*, 131(3), jcs211847. https://doi.org/10.1242/jcs.211847

Abu Quba, A. A., Schaumann, G. E., Karagulyan, M., & Diehl, D. (2020). A new approach for repeated tip-sample relocation for AFM imaging of nano and micro sized particles and cells in liquid environment. *Ultramicroscopy*, 211, 112945. https://doi.org/10.1016/j.ultramic.2020.112945

Achtenhagen, J., Goebel, M.-O., Miltner, A., Woche, S. K., & Kästner, M. (2015). Bacterial impact on the wetting properties of soil minerals. *Biogeochemistry*, 122(2), 269–280.

Alawi, M., Schneider, B., & Kallmeyer, J. (2014). A procedure for separate recovery of extra- and intracellular DNA from a single marine sediment sample. *Journal of Microbiological Methods*, 104, 36–42.

Alberto, B. (2003). Exploiting the x-ray refraction contrast with an analyser: the state of the art. *Journal of Physics D: Applied Physics*, 36(10A), A24. https://doi.org/10.1088/0022−3727/36/10A/306

Amelung, W., Kaiser, K., Kammerer, G., & Sauer, G. (2002). Organic carbon at soil particle surfaces—Evidence from x-ray photoelectron spectroscopy and surface abrasion. *Soil Science Society of America Journal*, 66(5), 1526–1530.

Amelung, W., & Zech, W. (1999). Minimisation of organic matter disruption during particle-size fractionation of grassland epipedons. *Geoderma*, 92(1), 73–85.

Amézketa, E. (1999). Soil aggregate stability: A review. *Journal of Sustainable Agriculture*, 14(2–3), 83–151.

Aoki, W., Kogawa, M., Matsuda, S., Matsubara, K., Hirata, S., Nishikawa, Y., Hosokawa, M., Takeyama, H., Matoh, T., & Ueda, M. (2022). Massively parallel single-cell genomics of microbiomes in rice paddies. *Frontiers in Microbiology*, 13, 1024640. https://doi.org/10.3389/fmicb.2022.1024640

Arai, M., Uramoto, G.-I., Asano, M., Uematsu, K., Uesugi, K., Takeuchi, A., Morono, Y., & Wagai, R. (2019). An improved method to identify osmium-stained organic matter within soil aggregate structure by electron microscopy and synchrotron X-ray micro-computed tomography. *Soil and Tillage Research*, 191, 275–281.

Araujo, C. F., Nolasco, M. M., Ribeiro, A. M. P., & Ribeiro-Claro, P. J. A. (2018). Identification of microplastics using Raman spectroscopy: Latest developments and future prospects. *Water Research*, 142, 426–440.

Asano, M., Wagai, R., Yamaguchi, N., Takeichi, Y., Maeda, M., Suga, H., & Takahashi, Y. (2018). In search of a binding agent: Nano-scale evidence of preferential carbon associations with poorly-crystalline mineral phases in physically-stable, clay-sized aggregates. *Soil Systems*, 2(2), 32. https://doi.org/10.3390/soilsystems2020032

Assemi, S., Hartley, P. G., Scales, P. J., & Beckett, R. (2004). Investigation of adsorbed humic substances using atomic force microscopy. *Colloids and Surfaces A: Physicochemical and Engineering Aspects*, 248(1), 17–23.

Avdeev, M. V., Aksenov, V. L., & Rosta, L. (2007). Pressure induced changes in fractal structure of detonation nanodiamond powder by small-angle neutron scattering. *Diamond and Related Materials*, 16(12), 2050–2053.

Baalousha, M., Stolpe, B., & Lead, J. R. (2011). Flow field-flow fractionation for the analysis and characterization of natural colloids and manufactured nanoparticles in environmental systems: A critical review. *Journal of Chromatography A*, 1218(27), 4078–4103.

Baalousha, M., Kammer, F. V. D., Motelica-Heino, M., Baborowski, M., Hofmeister, C., & Le Coustumer, P. (2006). Size-based speciation of natural colloidal particles by flow field flow fractionation, inductively coupled plasma-mass spectroscopy, and transmission electron microscopy/X-ray energy dispersive spectroscopy: Colloids—trace element interaction. *Environmental Science & Technology*, 40(7), 2156–2162.

Bach, E. M., & Hofmockel, K. S. (2014). Soil aggregate isolation method affects measures of intra-aggregate extracellular enzyme activity. *Soil Biology and Biochemistry*, 69, 54–62.

Bach, E. M., Williams, R. J., Hargreaves, S. K., Yang, F., & Hofmockel, K. S. (2018). Greatest soil microbial diversity found in micro-habitats. *Soil Biology and Biochemistry*, 118, 217–226.

Bachmann, J., Goebel, M.-O., & Woche, S. K. (2013). Small-scale contact angle mapping on undisturbed soil surfaces. *Journal of Hydrology and Hydromechanics*, 61(1), 3–8.

Bachmann, J., Goebel, M.-O., Krueger, J., Fleige, H., Woche, S. K., Dörner, J., & Horn, R. (2020). Aggregate stability of south Chilean volcanic ash soils—A combined XPS, contact angle, and surface charge analysis. *Geoderma*, 361, 114022. https://doi.org/10.1016/j.geoderma.2019.114022

Bachmann, J., Söffker, S., Sepehrnia, N., Goebel, M.-O., & Woche, S. K. (2021). The effect of temperature and wetting–drying cycles on soil wettability: Dynamic molecular restructuring processes at the solid–water–air interface. *European Journal of Soil Science*, 72(5), 2180–2198.

Bachmann, J., Woche, S. K., Goebel, M. O., Kirkham, M. B., & Horton, R. (2003). Extended methodology for determining wetting properties

of porous media. *Water Resources Research*, *39*(12). https://doi.org/10.1029/2003WR002143

Bailey, V. L., Fansler, S. J., Stegen, J. C., & McCue, L. A. (2013). Linking microbial community structure to β-glucosidic function in soil aggregates. *The ISME Journal*, *7*(10), 2044–2053.

Bailey, V. L., McCue, L. A., Fansler, S. J., Boyanov, M. I., DeCarlo, F., Kemner, K. M., & Konopka, A. (2013). Micrometer-scale physical structure and microbial composition of soil macroaggregates. *Soil Biology and Biochemistry*, *65*, 60–68.

Baldock, J. A., Oades, J. M., Nelson, P. N., Skene, T. M., Golchin, A., & Clarke, P. (1997). Assessing the extent of decomposition of natural organic materials using solid-state ^{13}C NMR spectroscopy. *Soil Research*, *35*(5), 1061–1084.

Baldock, J. A., Oades, J. M., Waters, A. G., Peng, X., Vassallo, A. M., & Wilson, M. A. (1992). Aspects of the chemical structure of soil organic materials as revealed by solid-state^{13}C NMR spectroscopy. *Biogeochemistry*, *16*(1), 1–42.

Bandara, C. D., Schmidt, M., Davoudpour, Y., Stryhanyuk, H., Richnow, H. H., & Musat, N. (2021). Microbial identification, high-resolution microscopy and spectrometry of the rhizosphere in its native spatial context. *Frontiers in Plant Science*, *12*, 668929. https://doi.org/10.3389/fpls.2021.668929

Baruchel, J., Buffiere, J.-Y., Cloetens, P., Di Michiel, M., Ferrie, E., Ludwig, W., Maire, E., & Salvo, L. (2006). Advances in synchrotron radiation microtomography. *Scripta Materialia*, *55*(1), 41–46.

Baumann, K., Siebers, M., Kruse, J., Eckhardt, K.-U., Hu, Y., Michalik, D., Siebers, N., Kar, G., Karsten, U., & Leinweber, P. (2019). Biological soil crusts as key player in biogeochemical P cycling during pedogenesis of sandy substrate. *Geoderma*, *338*, 145–158.

Baveye, P. C. (2006). Comment on "Soil structure and management: A review" by C.J. Bronick and R. Lal. *Geoderma*, *134*(1), 231–232.

Baveye, P. C. (2021). Bypass and hyperbole in soil research: Worrisome practices critically reviewed through examples. *European Journal of Soil Science*, *72*(1), 1–20.

Becker, J. S., Matusch, A., & Wu, B. (2014). Bioimaging mass spectrometry of trace elements—Recent advance and applications of LA-ICP-MS: A review. *Analytica Chimica Acta*, *835*, 1–18.

Beckmann, F., Vollbrandt, J., Donath, T., Schmitz, H. W., & Schreyer, A. (2005). Neutron and synchrotron radiation tomography: New tools for materials science at the GKSS-Research Center. *Nuclear Instruments and Methods in Physics Research Section A: Accelerators, Spectrometers, Detectors and Associated Equipment*, *542*(1), 279–282.

Bekiaris, G., Lindedam, J., Peltre, C., Decker, S. R., Turner, G. B., Magid, J., & Bruun, S. (2015). Rapid estimation of sugar release from winter wheat straw during bioethanol production using FTIR-photoacoustic spectroscopy. *Biotechnology for Biofuels*, *8*(1), 85. https://doi.org/10.1186/s13068-015-0267-2

Bieganowski, A., Ryżak, M., Sochan, A., Barna, G., Hernádi, H., Beczek, M., Polakowski, C., & Makó, A. (2018). Chapter Five—Laser diffractometry in the measurements of soil and sediment particle size distribution. In D. L. Sparks (Ed.), *Advances in agronomy* (Vol. 151, pp. 215–279). Academic Press.

Bieganowski, A., Zaleski, T., Kajdas, B., Sochan, A., Józefowska, A., Beczek, M., Lipiec, J., Turski, M., & Ryżak, M. (2018). An improved method for determination of aggregate stability using laser diffraction. *Land Degradation & Development*, *29*(5), 1376–1384.

Biesgen, D., Frindte, K., Maarastawi, S., & Knief, C. (2020). Clay content modulates differences in bacterial community structure in soil aggregates of different size. *Geoderma*, *376*, 114544. https://doi.org/10.1016/j.geoderma.2020.114544

Binnig, G., Quate, C. F., & Gerber, C. (1986). Atomic force microscope. *Physical Review Letters*, *56*(9), 930. https://doi.org/10.1103/PhysRevLett.56.930

Bläsing, M., & Amelung, W. (2018). Plastics in soil: Analytical methods and possible sources. *Science of The Total Environment*, *612*, 422–435.

Blaud, A., Menon, M., van der Zaan, B., Lair, G. J., & Banwart, S. A. (2017). Effects of dry and wet sieving of soil on identification and interpretation of microbial community composition. In S. A. Banwart & D. L. Sparks (Eds.), *Advances in agronomy* (pp. 119–142). Academic Press.

Bóta, A., & Klumpp, E. (2005). Effects of contaminants on biological model membranes: The advantage of the ASAXS method for the study of the location of copper ions and dihalogenated phenol molecules. *Colloids and Surfaces A: Physicochemical and Engineering Aspects*, *265*(1), 124–130.

Bruneau, P. M. C., Ostle, N., Davidson, D. A., Grieve, I. C., & Fallick, A. E. (2002). Determination of rhizosphere 13C pulse signals in soil thin sections by laser ablation isotope ratio mass spectrometry. *Rapid Communications in Mass Spectrometry*, *16*(23), 2190–2194.

Busto, M. D., & Perez-Mateos, M. (2000). Characterization of β-d-glucosidase extracted from soil fractions. *European Journal of Soil Science*, *51*(2), 193–200.

Butt, H.-J., Cappella, B., & Kappl, M. (2005). Force measurements with the atomic force microscope: Technique, interpretation and applications. *Surface Science Reports*, *59*(1), 1–152.

Butt, H.-J. (1991). Electrostatic interaction in atomic force microscopy. *Biophysical Journal*, *60*(4), 777–785.

Buurman, P., de Boer, K., & Pape, T. (1997). Laser diffraction grain-size characteristics of andisols in perhumid Costa Rica: The aggregate size of allophane. *Geoderma*, *78*(1), 71–91.

Buyanovsky, G. A., Aslam, M., & Wagner, G. H. (1994). Carbon turnover in soil physical fractions. *Soil Science Society of America Journal*, *58*(4), 1167–1173.

Capowiez, Y., Sammartino, S., & Michel, E. (2011). Using X-ray tomography to quantify earthworm bioturbation non-destructively in repacked soil cores. *Geoderma*, *162*(1), 124–131.

Carini, P., Marsden, P. J., Leff, J. W., Morgan, E. E., Strickland, M. S., & Fierer, N. (2016). Relic DNA is abundant in soil and obscures estimates of soil microbial diversity. *Nature Microbiology*, *2*(3), 16242. https://doi.org/10.1038/nmicrobiol.2016.242

Cheng, S., Bryant, R., Doerr, S. H., Wright, C. J., & Williams, P. R. (2009). Investigation of surface properties of soil particles and model materials with contrasting hydrophobicity using atomic force microscopy. *Environmental Science & Technology*, *43*(17), 6500–6506.

Chenu, C., & Plante, A. F. (2006). Clay-sized organo-mineral complexes in a cultivation chronosequence: revisiting the concept of the 'primary organo-mineral complex'. *European Journal of Soil Science*, *57*(4), 596–607.

Chepil, W. S. (1962). A compact rotary sieve and the importance of dry sieving in physical soil analysis. *Soil Science Society of America Journal*, *26*(1), 4–6.

Crawford, J. W., Deacon, L., Grinev, D., Harris, J. A., Ritz, K., Singh, B. K., & Young, I. (2011). Microbial diversity affects self-organization of the soil–microbe system with consequences for function. *Journal of The Royal Society Interface*, *9*(71), 1302–1310. https://doi.org/10.1098/rsif.2011.0679

Davinic, M., Fultz, L. M., Acosta-Martinez, V., Calderón, F. J., Cox, S. B., Dowd, S. E., Allen, V. G., Zak, J. C., & Moore-Kucera, J. (2012). Pyrosequencing and mid-infrared spectroscopy reveal distinct aggregate stratification of soil bacterial communities and organic matter composition. *Soil Biology and Biochemistry*, *46*, 63–72.

de Boer, J. H., Lippens, B. C., Linsen, B. G., Broekhoff, J. C. P., van den Heuvel, A., & Osinga, T. J. (1966). Thet-curve of multimolecular N_2-adsorption. *Journal of Colloid and Interface Science*, *21*(4), 405–414.

Dechesne, A., Pallud, C., Debouzie, D., Flandrois, J. P., Vogel, T. M., Gaudet, J. P., & Grundmann, G. L. (2003). A novel method for characterizing the microscale 3D spatial distribution of bacteria in soil. *Soil Biology and Biochemistry*, *35*(12), 1537–1546.

Derrien, D., & Amelung, W. (2011). Computing the mean residence time of soil carbon fractions using stable isotopes: impacts of the model framework. *European Journal of Soil Science*, *62*(2), 237–252.

Dexter, A. R. (1988). Advances in characterization of soil structure. *Soil and Tillage Research*, 11(3), 199–238.

Dhara, S., & Misra, N. L. (2011). Application of total reflection X-ray fluorescence spectrometry for trace elemental analysis of rainwater. *Pramana*, 76(2), 361–366.

Díaz-Zorita, M., Perfect, E., & Grove, J. H. (2002). Disruptive methods for assessing soil structure. *Soil and Tillage Research*, 64(1), 3–22.

Dickens, A. F., Baldock, J. A., Smernik, R. J., Wakeham, S. G., Arnarson, T. S., Gélinas, Y., & Hedges, J. I. (2006). Solid-state 13C NMR analysis of size and density fractions of marine sediments: Insight into organic carbon sources and preservation mechanisms. *Geochimica et Cosmochimica Acta*, 70(3), 666–686.

Dixon, J. B. (1989). Kaolin and serpentine group minerals. In J. B. Dixon, & S. B. Weed (Eds.), *Minerals in soil environments* (pp. 467–525). SS.

Doerr, S. H., Shakesby, R. A., & Walsh, R. P. D. (2000). Soil water repellency: its causes, characteristics and hydro-geomorphological significance. *Earth-Science Reviews*, 51(1), 33–65.

Du, C., Linker, R., & Shaviv, A. (2008). Identification of agricultural Mediterranean soils using mid-infrared photoacoustic spectroscopy. *Geoderma*, 143(1), 85–90.

Ducker, W. A., Senden, T. J., & Pashley, R. M. (1991). Direct measurement of colloidal forces using an atomic force microscope. *Nature*, 353(6341), 239–241.

Dultz, S., Mikutta, R., Kara, S. N. M., Woche, S. K., & Guggenberger, G. (2021). Effects of solution chemistry on conformation of self-aggregated tannic acid revealed by laser light scattering. *Science of The Total Environment*, 754, 142119. https://doi.org/10.1016/j.scitotenv.2020.142119

Durand, J.-C., Jacquot, B., Salehi, H., Fages, M., Margerit, J., & Cuisinier, F. J. G. (2012). Confocal Raman microscopic analysis of the zirconia/feldspathic ceramic interface. *Dental Materials*, 28(6), 661–671.

Dynes, J. J., Regier, T. Z., Snape, I., Siciliano, S. D., & Peak, D. (2015). Validating the scalability of soft X-ray spectromicroscopy for quantitative soil ecology and biogeochemistry research. *Environmental Science & Technology*, 49(2), 1035–1042.

Edwards, A. P., & Bremner, J. M. (1967). Dispersion of soil paricles by sonic vibration. *Journal of Soil Science*, 18(1), 47–63.

Eichorst, S. A., Strasser, F., Woyke, T., Schintlmeister, A., Wagner, M., & Woebken, D. (2015). Advancements in the application of NanoSIMS and Raman microspectroscopy to investigate the activity of microbial cells in soils. *FEMS Microbiology Ecology*, 91(10). https://doi.org/10.1093/femsec/fiv106

Eickhorst, T., & Tippkötter, R. (2008a). Detection of microorganisms in undisturbed soil by combining fluorescence in situ hybridization (FISH) and micropedological methods. *Soil Biology and Biochemistry*, 40(6), 1284–1293.

Eickhorst, T., & Tippkötter, R. (2008b). Improved detection of soil microorganisms using fluorescence in situ hybridization (FISH) and catalyzed reporter deposition (CARD-FISH). *Soil Biology and Biochemistry*, 40(7), 1883–1891.

Eusterhues, K., Rumpel, C., & Kögel-Knabner, I. (2005). Stabilization of soil organic matter isolated via oxidative degradation. *Organic Geochemistry*, 36(11), 1567–1575.

Faé, G. S., Montes, F., Bazilevskaya, E., Añó, R. M., & Kemanian, A. R. (2019). Making soil particle size analysis by laser diffraction compatible with standard soil texture determination methods. *Soil Science Society of America Journal*, 83(4), 1244–1252.

Felde, V. J. M. N. L., Schweizer, S. A., Biesgen, D., Ulbrich, A., Uteau, D., Knief, C., Graf-Rosenfellner, M., Kögel-Knabner, I., & Peth, S. (2021). Wet sieving versus dry crushing: Soil microaggregates reveal different physical structure, bacterial diversity and organic matter composition in a clay gradient. *European Journal of Soil Science*, 72(2), 810–828.

Ferguson, G. S., & Whitesides, G. M. (1992). Thermal reconstruction of the functionalized interface of polyethylene carboxylic acid and its derivatives. In M. E. Schrader & G. I. Loeb (Eds.), *Modern approaches to wettability: Theory and applications* (pp. 143–177). Springer US.

Fernández-Ugalde, O., Barré, P., Hubert, F., Virto, I., Girardin, C., Ferrage, E., Caner, L., & Chenu, C. (2013). Clay mineralogy differs qualitatively in aggregate-size classes: clay-mineral-based evidence for aggregate hierarchy in temperate soils. *European Journal of Soil Science*, 64(4), 410–422.

Ferreira, T. R., Pires, L. F., & Reichardt, K. (2022). 4D X-ray computed tomography in soil science: An overview and future perspectives at Mogno/Sirius. *Brazilian Journal of Physics*, 52(2), 33. https://doi.org/10.1007/s13538-021–01043-x

Fimmen, R. L., Richter, D. d., Vasudevan, D., Williams, M. A., & West, L. T. (2008). Rhizogenic Fe–C redox cycling: a hypothetical biogeochemical mechanism that drives crustal weathering in upland soils. *Biogeochemistry*, 87(2), 127–141.

Fischer, L., Mühlen, E. Z., Brümmer, G. W., & Niehus, H. (1996). Atomic force microscopy (AFM) investigations of the surface topography of a multidomain porous goethite. *European Journal of Soil Science*, 47(3), 329–334.

Fittschen, U. E. A., & Falkenberg, G. (2011). Trends in environmental science using microscopic X-ray fluorescence. *Spectrochimica Acta Part B: Atomic Spectroscopy*, 66(8), 567–580.

Fox, A., Ikoyi, I., Torres-Sallan, G., Lanigan, G., Schmalenberger, A., Wakelin, S., & Creamer, R. (2018). The influence of aggregate size fraction and horizon position on microbial community composition. *Applied Soil Ecology*, 127, 19–29.

Friel, J. J., & Lyman, C. E. (2006). Tutorial review: X-ray mapping in electron-beam instruments. *Microscopy and Microanalysis*, 12(1), 2–25.

Fukumasu, J., Jarvis, N., Koestel, J., Kätterer, T., & Larsbo, M. (2022). Relations between soil organic carbon content and the pore size distribution for an arable topsoil with large variations in soil properties. *European Journal of Soil Science*, 73(1), e13212. https://doi.org/10.1111/ejss.13212

Fultz, L. M., Moore-Kucera, J., Calderón, F., & Acosta-Martínez, V. (2014). Using Fourier-transform mid-infrared spectroscopy to distinguish soil organic matter composition dynamics in aggregate fractions of two agroecosystems. *Soil Science Society of America Journal*, 78(6), 1940–1948.

Gaj, M., Lamparter, A., Woche, S. K., Bachmann, J., McDonnell, J. J., & Stange, C. F. (2019). The role of matric potential, solid interfacial chemistry, and wettability on isotopic equilibrium fractionation. *Vadose Zone Journal*, 18(1), 180083. https://doi.org/10.2136/vzj2018.04.0083

Gantzer, C. J., & Anderson, S. H. (2002). Computed tomographic measurement of macroporosity in chisel-disk and no-tillage seedbeds. *Soil and Tillage Research*, 64(1), 101–111.

Gazze, S. A., Hallin, I., Quinn, G., Dudley, E., Matthews, G. P., Rees, P., van Keulen, G., Doerr, S. H., & Francis, L. W. (2018). Organic matter identifies the nano-mechanical properties of native soil aggregates. *Nanoscale*, 10(2), 520–525.

Gerin, P. A., Genet, M. J., Herbillon, A. J., & Delvaux, B. (2003). Surface analysis of soil material by X-ray photoelectron spectroscopy. *European Journal of Soil Science*, 54(3), 589–604.

Gerke, K. M., Korostilev, E. V., Romanenko, K. A., & Karsanina, M. V. (2021). Going submicron in the precise analysis of soil structure: A FIB-SEM imaging study at nanoscale. *Geoderma*, 383, 114739. https://doi.org/10.1016/j.geoderma.2020.114739

Gerzabek, M. H., Aquino, A. J. A., Balboa, Y. I. E., Galicia-Andrés, E., Grančič, P., Oostenbrink, C., Petrov, D., & Tunega, D. (2022). A contribution of molecular modeling to supramolecular structures in soil organic matter. *Journal of Plant Nutrition and Soil Science*, 185, 44–59.

Giddings, J. C. (1985). A system based on split-flow lateral-transport thin (SPLITT) separation cells for rapid and continuous particle fractionation. *Separation Science and Technology*, 20(9–10), 749–768.

Goebel, M.-O., Bachmann, J., Reichstein, M., Janssens, I. A., & Guggenberger, G. (2011). Soil water repellency and its implications for organic matter decomposition–is there a link to extreme climatic events? *Global Change Biology*, 17(8), 2640–2656.

Goebel, M.-O., Woche, S. K., Abraham, P. M., Schaumann, G. E., & Bachmann, J. (2013). Water repellency enhances the deposition of negatively charged hydrophilic colloids in a water-saturated sand matrix. *Colloids and Surfaces A: Physicochemical and Engineering Aspects*, *431*, 150–160.

Golchin, A., Oades, J., Skjemstad, J., & Clarke, P. (1994). Study of free and occluded particulate organic matter in soils by solid state ^{13}C Cp/MAS NMR spectroscopy and scanning electron microscopy. *Soil Research*, *32*(2), 285–309.

Graf-Rosenfellner, M., Kayser, G., Guggenberger, G., Kaiser, K., Büks, F., Kaiser, M., Mueller, C. W., Schrumpf, M., Rennert, T., Welp, G., & Lang, F. (2018). Replicability of aggregate disruption by sonication—An inter-laboratory test using three different soils from Germany. *Journal of Plant Nutrition and Soil Science*, *181*(6), 894–904.

Grieve, I. C., Davidson, D. A., Ostle, N. J., Bruneau, P. M. C., & Fallick, A. E. (2006). Spatial heterogeneity in the relocation of added ^{13}C within the structure of an upland grassland soil. *Soil Biology and Biochemistry*, *38*(2), 229–234.

Grundmann, G. L., Dechesne, A., Bartoli, F., Flandrois, J. P., Chassé, J. L., & Kizungu, R. (2001). Spatial modeling of nitrifier microhabitats in soil. *Soil Science Society of America Journal*, *65*(6), 1709–1716.

Gu, L., Wang, N., Tang, X., & Changela, H. G. (2020). Application of FIB-SEM techniques for the advanced characterization of earth and planetary materials. *Scanning*, *2020*, 8406917. https://doi.org/10.1155/2020/8406917

Guhra, T., Ritschel, T., & Totsche, K. U. (2021). The mechanisms of gravity-constrained aggregation in natural colloidal suspensions. *Journal of Colloid and Interface Science*, *597*, 126–136.

Guidi, P., Falsone, G., Wilson, C., Cavani, L., Ciavatta, C., & Marzadori, C. (2021). New insights into organic carbon stabilization in soil macroaggregates: An in situ study by optical microscopy and SEM-EDS technique. *Geoderma*, *397*, 115101. https://doi.org/10.1016/j.geoderma.2021.115101

Gutiérrez Castorena, E. V., Gutiérrez-Castorena, M. D. C., González Vargas, T., Cajuste Bontemps, L., Delgadillo Martínez, J., Suástegui Méndez, E., & Ortiz Solorio, C. A. (2016). Micromapping of microbial hotspots and biofilms from different crops using digital image mosaics of soil thin sections. *Geoderma*, *279*, 11–21.

Hapca, S. M., Wang, Z. X., Otten, W., Wilson, C., & Baveye, P. C. (2011). Automated statistical method to align 2D chemical maps with 3D X-ray computed micro-tomographic images of soils. *Geoderma*, *164*(3–4), 146–154.

Hapca, S., Baveye, P. C., Wilson, C., Lark, R. M., & Otten, W. (2015). Three-dimensional mapping of soil chemical characteristics at micrometric scale by combining 2D SEM-EDX data and 3D X-ray CT images. *Plos One*, *10*(9), e0137205. https://doi.org/10.1371/journal.pone.0137205

Hemes, S., Desbois, G., Urai, J. L., Schröppel, B., & Schwarz, J.-O. (2015). Multi-scale characterization of porosity in Boom Clay (HADES-level, Mol, Belgium) using a combination of X-ray μ-CT, 2D BIB-SEM and FIB-SEM tomography. *Microporous and Mesoporous Materials*, *208*, 1–20.

Heise, J., Nega, M., Alawi, M., & Wagner, D. (2016). Propidium monoazide treatment to distinguish between live and dead methanogens in pure cultures and environmental samples. *Journal of Microbiological Methods*, *121*, 11–23.

Hernandez-Soriano, M. C., Dalal, R. C., Warren, F. J., Wang, P., Green, K., Tobin, M. J., Menzies, N. W., & Kopittke, P. M. (2018). Soil organic carbon stabilization: mapping carbon speciation from intact microaggregates. *Environmental Science & Technology*, *52*(21), 12275–12284.

Herrmann, A. M., Ritz, K., Nunan, N., Clode, P. L., Pett-Ridge, J., Kilburn, M. R., Murphy, D. V., O'Donnell, A. G., & Stockdale, E. A. (2007). Nano-scale secondary ion mass spectrometry—A new analytical tool in biogeochemistry and soil ecology: A review article. *Soil Biology and Biochemistry*, *39*(8), 1835–1850.

Hong, Z., Chen, W., Rong, X., Cai, P., Tan, W., & Huang, Q. (2015). Effects of humic acid on adhesion of Bacillus subtilis to phyllosilicates and goethite. *Chemical Geology*, *416*, 19–27.

Hu, W., Cichota, R., Beare, M., Müller, K., Drewry, J., & Eger, A. (2023). Soil structural vulnerability: Critical review and conceptual development. *Geoderma*, *430*, 116346. https://doi.org/10.1016/j.geoderma.2023.116346

Huang, Q., Wu, H., Cai, P., Fein, J. B., & Chen, W. (2015). Atomic force microscopy measurements of bacterial adhesion and biofilm formation onto clay-sized particles. *Scientific Reports*, *5*(1), 16857. https://doi.org/10.1038/srep16857

Huang, Y.-S., Karashima, T., Yamamoto, M., Ogura, T., & Hamaguchi, H.-O. (2004). Raman spectroscopic signature of life in a living yeast cell. *Journal of Raman Spectroscopy*, *35*(7), 525–526.

Huang, Y., Bol, R., Harkness, D. D., Ineson, P., & Eglinton, G. (1996). Post-glacial variations in distributions, ^{13}C and ^{14}C contents of aliphatic hydrocarbons and bulk organic matter in three types of British acid upland soils. *Organic Geochemistry*, *24*(3), 273–287.

Hurraß, J., & Schaumann, G. E. (2006). Properties of soil organic matter and aqueous extracts of actually water repellent and wettable soil samples. *Geoderma*, *132*(1), 222–239.

Inagaki, T. M., Possinger, A. R., Grant, K. E., Schweizer, S. A., Mueller, C. W., Derry, L. A., Lehmann, J., & Kögel-Knabner, I. (2020). Subsoil organomineral associations under contrasting climate conditions. *Geochimica et Cosmochimica Acta*, *270*, 244–263.

Indore, N. S., Karunakaran, C., & Jayas, D. S. (2022). Synchrotron tomography applications in agriculture and food sciences research: a review. *Plant Methods*, *18*(1), 101. https://doi.org/10.1186/s13007-022-00932-9

Jandt, K. D. (2001). Atomic force microscopy of biomaterials surfaces and interfaces. *Surface Science*, *491*(3), 303–332.

Jantzi, S. C., & Almirall, J. R. (2014). Elemental analysis of soils using laser ablation inductively coupled plasma mass spectrometry (LA-ICP-MS) and laser-induced breakdown spectroscopy (LIBS) with multivariate discrimination: tape mounting as an alternative to pellets for small forensic transfer specimens. *Applied Spectroscopy*, *68*(9), 963–974.

Jarvis, S., Tisdall, J., Oades, M., Six, J., Gregorich, E., & Kögel-Knabner, I. (2012). Landmark papers. *European Journal of Soil Science*, *63*(1), 1–21.

Jastrow, J. D., Miller, R. M., & Boutton, T. W. (1996). Carbon dynamics of aggregate-associated organic matter estimated by carbon–13 natural abundance. *Soil Science Society of America Journal*, *60*(3), 801–807.

Jiang, C., Séquaris, J.-M., Vereecken, H., & Klumpp, E. (2013). Diffusion-controlled mobilization of water-dispersible colloids from three German silt loam topsoils: Effect of temperature. *European Journal of Soil Science*, *64*(6), 777–786.

Jiang, X., Bol, R., Nischwitz, V., Siebers, N., Willbold, S., Vereecken, H., Amelung, W., & Klumpp, E. (2015). Phosphorus containing water dispersible nanoparticles in arable soil. *Journal of Environmental Quality*, *44*(6), 1772–1781.

Jing, X., Gong, Y., Xu, T., Meng, Y., Han, X., Su, X., Wang, J., Ji, Y., Li, Y., Jia, Z., Ma, B., & Xu, J. (2021). One-cell metabolic phenotyping and sequencing of soil microbiome by Raman-activated gravity-driven encapsulation (RAGE). *mSystems*, *6*(3), e00181–00121. https://doi.org/10.1128/mSystems.00181-21

John, B., Yamashita, T., Ludwig, B., & Flessa, H. (2005). Storage of organic carbon in aggregate and density fractions of silty soils under different types of land use. *Geoderma*, *128*(1), 63–79.

Johnston, C. T., & Aochi, Y. O. (1996). Fourier transform infrared and Raman spectroscopy. In A. Klute (Ed.), *Methods of soil analysis* (pp. 269–321). SSSA.

Juyal, A., Otten, W., Falconer, R., Hapca, S., Schmidt, H., Baveye, P. C., & Eickhorst, T. (2019). Combination of techniques to quantify the distribution of bacteria in their soil microhabitats at different spatial scales. *Geoderma*, *334*, 165–174.

Kachanoski, R. G., Voroney, R. P., & Gregorich, E. G. (1988). Ultrasonic dispersion of aggregates: distribution of organic matter in size fractions. *Canadian Journal of Soil Science*, *68*(2), 395–403.

Kaiser, K., & Guggenberger, G. (2003). Mineral surfaces and soil organic matter. *European Journal of Soil Science*, *54*(2), 219–236.

Kaiser, M., & Berhe, A. (2014). How does sonication affect the mineral and organic constituents of soil aggregates?—A review. *Journal of Plant Nutrition and Soil Science*, *177*(4), 479–495.

Kaiser, M., Berhe, A. A., Sommer, M., & Kleber, M. (2012). Application of ultrasound to disperse soil aggregates of high mechanical stability. *Journal of Plant Nutrition and Soil Science*, *175*(4), 521–526.

Kaiser, M., Kleber, M., & Berhe, A. A. (2015). How air-drying and rewetting modify soil organic matter characteristics: An assessment to improve data interpretation and inference. *Soil Biology and Biochemistry*, *80*, 324–340.

Karstens, L., Asquith, M., Davin, S., Fair, D., Gregory, W. T., Wolfe, A. J., Braun, J., & McWeeney, S. (2019). Controlling for contaminants in low-biomass 16S rRNA gene sequencing experiments. *mSystems*, *4*(4), e00290–00219. https://doi.org/10.1128/mSystems.00290–19

Kasmerchak, C. S., Mason, J. A., & Liang, M. (2019). Laser diffraction analysis of aggregate stability and disintegration in forest and grassland soils of northern Minnesota, USA. *Geoderma*, *338*, 430–444.

Kaster, A.-K., & Sobol, M. S. (2020). Microbial single-cell omics: the crux of the matter. *Applied Microbiology and Biotechnology*, *104*(19), 8209–8220.

Kayser, A. T., Wilcke, W., Kaupenjohann, M., & Joslin, J. D. (1994). Small scale heterogeneity of soil chemical properties. I. A technique for rapid aggregate fractionation. *Zeitschrift für Pflanzenernährung und Bodenkunde*, *157*(6), 453–458.

Kayser, G., Graf-Rosenfellner, M., Schack-Kirchner, H., & Lang, F. (2019). Dynamic imaging provides novel insight into the shape and stability of soil aggregates. *European Journal of Soil Science*, *70*(3), 454–465.

Keil, R. G., Tsamakis, E., Fuh, C. B., Giddings, J. C., & Hedges, J. I. (1994). Mineralogical and textural controls on the organic composition of coastal marine sediments: Hydrodynamic separation using SPLITT-fractionation. *Geochimica et Cosmochimica Acta*, *58*(2), 879–893.

Keiluweit, M., Bougoure, J. J., Zeglin, L. H., Myrold, D. D., Weber, P. K., Pett-Ridge, J., Kleber, M., & Nico, P. S. (2012). Nano-scale investigation of the association of microbial nitrogen residues with iron (hydr)oxides in a forest soil O-horizon. *Geochimica et Cosmochimica Acta*, *95*, 213–226.

Kemper, W. D., & Rosenau, R. C. (1986). Aggregate stability and size distribution. In A. Klute (Ed.), *Methods of soil analysis* (pp. 425–442). SSSA.

Kiem, R., Knicker, H., & Kögel-Knabner, I. (2002). Refractory organic carbon in particle-size fractions of arable soils I: Distribution of refractory carbon between the size fractions. *Organic Geochemistry*, *33*(12), 1683–1697.

Kihara, J., Martius, C., Bationo, A., Thuita, M., Lesueur, D., Herrmann, L., Amelung, W., & Vlek, P. L. G. (2012). Soil aggregation and total diversity of bacteria and fungi in various tillage systems of sub-humid and semi-arid Kenya. *Applied Soil Ecology*, *58*, 12–20.

Kilburn, M. R., & Clode, P. L. (2014). Elemental and isotopic imaging of biological samples using NanoSIMS. In J. Kuo (Ed.), *Electron microscopy. Methods in molecular biology* (p. 1117). Humana Press.

Killham, K., Amato, M., & Ladd, J. N. (1993). Effect of substrate location in soil and soil pore-water regime on carbon turnover. *Soil Biology and Biochemistry*, *25*, 57–62.

Kim, H., Anderson, S. H., Motavalli, P. P., & Gantzer, C. J. (2010). Compaction effects on soil macropore geometry and related parameters for an arable field. *Geoderma*, *160*(2), 244–251.

Kim, H., Nunan, N., Dechesne, A., Juarez, S., & Grundmann, G. (2015). The spatial distribution of exoenzyme activities across the soil micro-landscape, as measured in micro- and macro-aggregates, and ecosystem processes. *Soil Biology and Biochemistry*, *91*, 258–267.

Kinyangi, J., Solomon, D., Liang, B., Lerotic, M., Wirick, S., & Lehmann, J. (2006). Nanoscale biogeocomplexity of the organomineral assemblage in soil. *Soil Science Society of America Journal*, *70*(5), 1708–1718.

Klaver, J., Desbois, G., Urai, J. L., & Littke, R. (2012). BIB-SEM study of the pore space morphology in early mature Posidonia Shale from the Hils area, Germany. *International Journal of Coal Geology*, *103*, 12–25.

Klein, S., Staring, M., Murphy, K., Viergever, M. A., & Pluim, J. P. W. (2010). *elastix*: A toolbox for intensity-based medical image registration. Medical Imaging. *IEEE Transactions*, *29*(1), 196–205.

Klink, S., Keller, A. B., Wild, A. J., Baumert, V. L., Gube, M., Lehndorff, E., Meyer, N., Mueller, C. W., Phillips, R. P., & Pausch, J. (2022). Stable isotopes reveal that fungal residues contribute more to mineral-associated organic matter pools than plant residues. *Soil Biology and Biochemistry*, *168*, 108634. https://doi.org/10.1016/j.soilbio.2022.108634

Kögel-Knabner, I. (1997). ^{13}C and ^{15}N NMR spectroscopy as a tool in soil organic matter studies. *Geoderma*, *80*(3), 243–270.

Kopittke, P. M., Dalal, R. C., Hoeschen, C., Li, C., Menzies, N. W., & Mueller, C. W. (2020). Soil organic matter is stabilized by organo-mineral associations through two key processes: The role of the carbon to nitrogen ratio. *Geoderma*, *357*, 113974. https://doi.org/10.1016/j.geoderma.2019.113974

Kopittke, P. M., Hernandez-Soriano, M. C., Dalal, R. C., Finn, D., Menzies, N. W., Hoeschen, C., & Mueller, C. W. (2018). Nitrogen-rich microbial products provide new organo-mineral associations for the stabilization of soil organic matter. *Global Change Biology*, *24*(4), 1762–1770.

Kowalkowski, T., Buszewski, B., Cantado, C., & Dondi, F. (2006). Field-flow fractionation: Theory, techniques, applications and the challenges. *Critical Reviews in Analytical Chemistry*, *36*(2), 129–135.

Kramer, C., & Gleixner, G. (2006). Variable use of plant- and soil-derived carbon by microorganisms in agricultural soils. *Soil Biology and Biochemistry*, *38*(11), 3267–3278.

Krause, L., Klumpp, E., Nofz, I., Missong, A., Amelung, W., & Siebers, N. (2020). Colloidal iron and organic carbon control soil aggregate formation and stability in arable Luvisols. *Geoderma*, *374*, 114421. https://doi.org/10.1016/j.geoderma.2020.114421

Krause, L., Rodionov, A., Schweizer, S. A., Siebers, N., Lehndorff, E., Klumpp, E., & Amelung, W. (2018). Microaggregate stability and storage of organic carbon is affected by clay content in arable Luvisols. *Soil and Tillage Research*, *182*, 123–129.

Kravchenko, A. N., Guber, A. K., Razavi, B. S., Koestel, J., Blagodatskaya, E. V., & Kuzyakov, Y. (2019). Spatial patterns of extracellular enzymes: Combining X-ray computed micro-tomography and 2D zymography. *Soil Biology and Biochemistry*, *135*, 411–419.

Kravchenko, A. N., Negassa, W. C., Guber, A. K., & Rivers, M. L. (2015). Protection of soil carbon within macro-aggregates depends on intra-aggregate pore characteristics. *Scientific Reports*, *5*(1), 16261. https://doi.org/10.1038/srep16261

Kretzschmar, R., Holthoff, H., & Sticher, H. (1998). Influence of pH and humic acid on coagulation kinetics of kaolinite: A dynamic light scattering study. *Journal of Colloid and Interface Science*, *202*(1), 95–103.

Kristiansen, S. M., Schjønning, P., Thomsen, I. K., Olesen, J. E., Kristensen, K., & Christensen, B. T. (2006). Similarity of differently sized macro-aggregates in arable soils of different texture. *Geoderma*, *137*(1), 147–154.

Krivoshein, P. K., Volkov, D. S., Rogova, O. B., & Proskurnin, M. A. (2022). FTIR photoacoustic and ATR spectroscopies of soils with aggregate size fractionation by dry sieving. *ACS Omega*, *7*(2), 2177–2197.

Krull, E., Bray, S., Harms, B. E. N., Baxter, N., Bol, R., & Farquhar, G. (2007). Development of a stable isotope index to assess decadal-scale vegetation change and application to woodlands of the Burdekin catchment, Australia. *Global Change Biology*, *13*(7), 1455–1468.

Kuzyakov, Y., & Razavi, B. S. (2019). Rhizosphere size and shape: Temporal dynamics and spatial stationarity. *Soil Biology and Biochemistry*, *135*, 343–360.

Ladd, J., Foster, R., Nannipieri, P., & Oades, J. (1996). Soil structure and biological activity. *Soil Biochemistry*, *9*, 23–78.

Langner, P., Mikutta, C., Suess, E., Marcus, M. A., & Kretzschmar, R. (2013). Spatial distribution and speciation of arsenic in peat studied with microfocused X-ray fluorescence spectrometry and X-ray absorption spectroscopy. *Environmental Science & Technology*, *47*(17), 9706–9714.

Lee, J., Hestrin, R., Nuccio, E. E., Morrison, K. D., Ramon, C. E., Samo, T. J., Pett-Ridge, J., Ly, S. S., Laurence, T. A., & Weber, P. K. (2022). Label-free multiphoton imaging of microbes in root, mineral, and soil matrices with time-gated coherent Raman and fluorescence lifetime imaging. *Environmental Science & Technology*, 56(3), 1994–2008.

Lehmann, J., Kinyangi, J., & Solomon, D. (2007). Organic matter stabilization in soil microaggregates: implications from spatial heterogeneity of organic carbon contents and carbon forms. *Biogeochemistry*, 85(1), 45–57.

Lehmann, J., Liang, B., Solomon, D., Lerotic, M., Luizão, F., Kinyangi, J., Schäfer, T., Wirick, S., & Jacobsen, C. (2005). Near-edge X-ray absorption fine structure (NEXAFS) spectroscopy for mapping nano-scale distribution of organic carbon forms in soil: Application to black carbon particles. *Global Biogeochemical Cycles*, 19(1). https://doi.org/10.1029/2004GB002435

Lehmann, J., & Solomon, D. (2010). Organic carbon chemistry in soils observed by synchrotron-based spectroscopy. In B. Singh & M. Gräfe (Eds.), *Developments in soil science* (pp. 289–312). Elsevier.

Lehndorff, E., Rodionov, A., Plümer, L., Rottmann, P., Spiering, B., Dultz, S., & Amelung, W. (2021). Spatial organization of soil microaggregates. *Geoderma*, 386, 114915. https://doi.org/10.1016/j.geoderma.2020.114915

Letey, J. (1991). The study of soil structure—Science or art. *Soil Research*, 29(6), 699–707.

Lever, M. A., Torti, A., Eickenbusch, P., Michaud, A. B., Šantl-Temkiv, T., & Jørgensen, B. B. (2015). A modular method for the extraction of DNA and RNA, and the separation of DNA pools from diverse environmental sample types. *Frontiers in Microbiology*, 6, https://doi.org/10.3389/fmicb.2015.00476

Li, Y., Dick, W. A., & Tuovinen, O. H. (2004). Fluorescence microscopy for visualization of soil microorganisms—A review. *Biology and Fertility of Soils*, 39, 301–311.

Li, Z., Yang, W., Cai, C., & Wang, J. (2013). Aggregate mechanical stability and relationship with aggregate breakdown under simulated rainfall. *Soil Science*, 178(7). https://doi.org/10.1097/SS.0b013e3182a74255

Lin, B., & Cerato, A. B. (2014). Applications of SEM and ESEM in microstructural investigation of shale-weathered expansive soils along swelling-shrinkage cycles. *Engineering Geology*, 177, 66–74.

Lin, M. Y., Lindsay, H. M., Weitz, D. A., Ball, R. C., Klein, R., & Meakin, P. (1989). Universality in colloid aggregation. *Nature*, 339(6223), 360–362. h.

Lippold, E., Schlüter, S., Mueller, C. W., Höschen, C., Harrington, G., Kilian, R., Gocke, M. I., Lehndorff, E., Mikutta, R., & Vetterlein, D. (2023). Correlative imaging of the rhizosphere—A multimethod workflow for targeted mapping of chemical gradients. *Environmental Science & Technology*, 57(3), 1538–1549.

Liu, J., Xu, C., Hu, F., Wang, Z., Ma, R., & Zhao, S. (2021). Effect of soil internal forces on fragment size distributions after aggregate breakdown and their relations to splash erosion. *European Journal of Soil Science*, 72(5), 2088–2101.

Liu, Y., Elworth, R. A. L., Jochum, M. D., Aagaard, K. M., & Treangen, T. J. (2022). De novo identification of microbial contaminants in low microbial biomass microbiomes with Squeegee. *Nature Communications*, 13(1), 6799. https://doi.org/10.1038/s41467-022-34409-z

Loeppmann, S., Tegtmeier, J., Shi, Y., de la Fuente, A. A., Boy, J., Guggenberger, G., Fulterer, A., Fritsch, M., & Spielvogel, S. (2023). Using fluorescence lifetime imaging to disentangle microbes from the heterogeneous soil matrix. *Biology and Fertility of Soils*, 59(2), 249–260.

Lower, S. K., Tadanier, C. J., & Hochella, M. F. (2000). Measuring interfacial and adhesion forces between bacteria and mineral surfaces with biological force microscopy. *Geochimica et Cosmochimica Acta*, 64(18), 3133–3139.

Macht, F., Eusterhues, K., Pronk, G. J., & Totsche, K. U. (2011). Specific surface area of clay minerals: Comparison between atomic force microscopy measurements and bulk-gas (N_2) and -liquid (EGME) adsorption methods. *Applied Clay Science*, 53(1), 20–26.

Marinkovic, N. S., Huang, R., Bromberg, P., Sullivan, M., Toomey, J., Miller, L. M., Sperber, E., Moshe, S., Jones, K. W., Chouparova, E., Lappi, S., Franzen, S., & Chance, M. R. (2002). Center for Synchrotron Bio■sciences' U2B beamline: an international resource for biological infrared spectroscopy. *Journal of Synchrotron Radiation*, 9(4), 189–197.

Mason, J. A., Greene, R. S. B., & Joeckel, R. M. (2011). Laser diffraction analysis of the disintegration of aeolian sedimentary aggregates in water. *Catena*, 87(1), 107–118.

Maurice, P. A., Lee, Y. J., & Hersman, L. E. (2000). Dissolution of Al-substituted goethites by an aerobic *Pseudomonas mendocina* var. *bacteria*. *Geochimica et Cosmochimica Acta*, 64(8), 1363–1374.

Mayer, H. (1999). Fatigue crack growth and threshold measurements at very high frequencies. *International Materials Reviews*, 44(1), 1–34.

Mayer, H. (2006). Ultrasonic torsion and tension–compression fatigue testing: Measuring principles and investigations on 2024-T351 aluminium alloy. *International Journal of Fatigue*, 28(11), 1446–1455.

Mayer, H., Mentler, A., Papakyriacou, M., Rampazzo, N., Marxer, Y., & Blum, W. (2002). Influence of vibration amplitude on the ultrasonic dispersion of soils. *International Agrophysics*, 16(1), 52–60.

McCarthy, J. F., Ilavsky, J., Jastrow, J. D., Mayer, L. M., Perfect, E., & Zhuang, J. (2008). Protection of organic carbon in soil microaggregates via restructuring of aggregate porosity and filling of pores with accumulating organic matter. *Geochimica et Cosmochimica Acta*, 72(19), 4725–4744.

Menon, M., Mawodza, T., Rabbani, A., Blaud, A., Lair, G. J., Babaei, M., Kercheva, M., Rousseva, S., & Banwart, S. (2020). Pore system characteristics of soil aggregates and their relevance to aggregate stability. *Geoderma*, 366, 114259. https://doi.org/10.1016/j.geoderma.2020.114259

Mentler, A., Mayer, H., Strauß, P., & Blum, W. (2004). Characterisation of soil aggregate stability by ultrasonic dispersion. *International Agrophysics*, 18(1), 39–45.

Mikutta, R., Schaumann, G. E., Gildemeister, D., Bonneville, S., Kramer, M. G., Chorover, J., Chadwick, O. A., & Guggenberger, G. (2009). Biogeochemistry of mineral–organic associations across a long-term mineralogical soil gradient (0.3–4100kyr), Hawaiian Islands. *Geochimica et Cosmochimica Acta*, 73(7), 2034–2060.

Missong, A., Bol, R., Nischwitz, V., Krüger, J., Lang, F., Siemens, J., & Klumpp, E. (2018). Phosphorus in water dispersible-colloids of forest soil profiles. *Plant and Soil*, 427(1), 71–86.

Montgomery, M. T., Fulmer, P. A., Gaston, J. D., Pirlo, R. K., & Ringeisen, B. R. (2019). Heterotrophic bacterial production measured on soil microaggregates sampled using a biological laser printer. *Soil Biology and Biochemistry*, 131, 176–181.

Moon, M. H., Yang, S. G., Lee, J. Y., & Lee, S. (2005). Combination of gravitational SPLITT fractionation and field-flow fractionation for size-sorting and characterization of sea sediment. *Analytical and Bioanalytical Chemistry*, 381(6), 1299–1304.

Mosley, L. M., Hunter, K. A., & Ducker, W. A. (2003). Forces between colloid particles in natural waters. *Environmental Science & Technology*, 37(15), 3303–3308.

Mouvenchery, Y. K., Miltner, A., Schurig, C., Kästner, M., & Schaumann, G. E. (2016). Linking atomic force microscopy with nanothermal analysis to assess microspatial distribution of material characteristics in young soils. *Journal of Plant Nutrition and Soil Science*, 179(1), 48–59.

Mueller, C. W., Hoeschen, C., & Koegel-Knabner, I. (2022). Understanding of soil processes at the microscale—Use of NanoSIMS in soil science. In S. Elias (Ed.), *Reference module in earth systems and environmental sciences*. Elsevier.

Mummey, D. L., & Stahl, P. D. (2004). Analysis of soil whole- and inner-microaggregate bacterial communities. *Microbial Ecology*, 48(1), 41–50.

Nahidan, S., & Nourbakhsh, F. (2018). Distribution pattern of amidohydrolase activities among soil aggregates: Effect of soil aggregates isolation methods. *Applied Soil Ecology*, 125, 250–256.

Nguyen, M. N., Dultz, S., Tran, T. T. T., & Bui, A. T. K. (2013). Effect of anions on dispersion of a kaolinitic soil clay: A combined study of dynamic light scattering and test tube experiments. *Geoderma*, *209–210*, 209–213.

Nischwitz, V., Gottselig, N., Missong, A., Meyn, T., & Klumpp, E. (2016). Field flow fractionation online with ICP-MS as novel approach for the quantification of fine particulate carbon in stream water samples and soil extracts. *Journal of Analytical Atomic Spectrometry*, *31*(9), 1858–1868.

Nkebiwe, P. M., Sowoidnich, K., Maiwald, M., Sumpf, B., Hartmann, T. E., Wanke, D., & Müller, T. (2022). Detection of calcium phosphate species in soil by confocal μ-Raman spectroscopy. *Journal of Plant Nutrition and Soil Science*, *185*(2), 221–231.

North, P. F. (1976). Towards an absolute measurement of soil structural stability using ultrasound. *Journal of Soil Science*, *27*(4), 451–459.

Nunan, N., Ritz, K., Crabb, D., Harris, K., Wu, K., Crawford, J. W., & Young, I. M. (2001). Quantification of the in situ distribution of soil bacteria by large-scale imaging of thin sections of undisturbed soil. *FEMS Microbiology Ecology*, *37*(1), 67–77.

Nunan, N., Ritz, K., Rivers, M., Feeney, D. S., & Young, I. M. (2006). Investigating microbial micro-habitat structure using X-ray computed tomography. *Geoderma*, *133*(3), 398–407.

Nunan, N., Wu, K., Young, I. M., Crawford, J. W., & Ritz, K. (2003). Spatial distribution of bacterial communities and their relationships with the micro-architecture of soil. *FEMS Microbiology Ecology*, *44*(2), 203–215.

Nuñez, J., Renslow, R., CliffIII, J. B., & Anderton, C. R. (2018). NanoSIMS for biological applications: Current practices and analyses. *Biointerphases*, *13*(3), 03B301. https://doi.org/10.1116/1.4993628

Oades, J. M., & Waters, A. G. (1991). Aggregate hierarchy in soils. *Soil Research*, *29*(6), 815–828.

Obst, M., Grathwohl, P., Kappler, A., Eibl, O., Peranio, N., & Gocht, T. (2011). Quantitative high-resolution mapping of phenanthrene sorption to black carbon particles. *Environmental Science & Technology*, *45*(17), 7314–7322.

Obst, M., & Schmid, G. (2014). 3D Chemical Mapping: Application of scanning transmission (soft) X-ray microscopy (STXM) in combination with angle-scan tomography in bio-, geo-, and environmental sciences. In J. Kuo (Ed.), *Electron microscopy: Methods and protocols* (pp. 757–781). Humana Press.

Ornthai, M., Siripinyanond, A., & Gale, B. K. (2016). Biased cyclical electrical field-flow fractionation for separation of submicron particles. *Analytical and Bioanalytical Chemistry*, *408*(3), 855–863.

Ost, A. D., Wu, T., Höschen, C., Mueller, C. W., Wirtz, T., & Audinot, J.-N. (2021). 4D surface reconstructions to study microscale structures and functions in soil biogeochemistry. *Environmental Science & Technology*, *55*(13), 9384–9393.

Papadopoulos, A., Bird, N. R. A., Whitmore, A. P., & Mooney, S. J. (2009). Investigating the effects of organic and conventional management on soil aggregate stability using X-ray computed tomography. *European Journal of Soil Science*, *60*(3), 360–368.

Parikh, S. J., Goyne, K. W., Margenot, A. J., Mukome, F. N. D., & Calderón, F. J. (2014). Soil chemical insights provided through vibrational spectroscopy. In D. L. Sparks (Ed.), *Advances in agronomy* (pp. 1–148). Academic Press.

Parry, S., Renault, P., Chadœuf, J., Chenu, C., & Lensi, R. (2000). Particulate organic matter as a source of variation in denitrification in clods of soil. *European Journal of Soil Science*, *51*(2), 271–281.

Peerlkamp, P. (1959). A visual method of soil structure evaluation. *Meded. vd Landbouwhogeschool en Opzoekingsstations van de Staat te Gent*, *24*(24), 216–221.

Penton, C. R., Gupta, V. V. S. R., Yu, J., & Tiedje, J. M. (2016). Size matters: Assessing optimum soil sample size for fungal and bacterial community structure analyses using high throughput sequencing of rRNA Gene amplicons. *Frontiers in Microbiology*, *7*, https://doi.org/10.3389/fmicb.2016.00824

Peth, S. (2010). Applications of microtomography in soils and sediments. In B. Singh & M. Gräfe (Eds.), *Developments in soil science* (pp. 73–101). Elsevier.

Peth, S., Chenu, C., Leblond, N., Mordhorst, A., Garnier, P., Nunan, N., Pot, V., Ogurreck, M., & Beckmann, F. (2014). Localization of soil organic matter in soil aggregates using synchrotron-based X-ray microtomography. *Soil Biology and Biochemistry*, *78*, 189–194.

Pett-Ridge, J., & Weber, P. K. (2022). NanoSIP: NanoSIMS applications for microbial biology. In A. Navid (Ed.), *Microbial systems biology: Methods and protocols* (pp. 91–136). Springer US.

Pierret, A., Capowiez, Y., Belzunces, L., & Moran, C. J. (2002). 3D reconstruction and quantification of macropores using X-ray computed tomography and image analysis. *Geoderma*, *106*(3), 247–271.

Polakowski, C., Sochan, A., Ryżak, M., Beczek, M., Mazur, R., Majewska, K., Turski, M., & Bieganowski, A. (2021). Measurement of soil dry aggregate size distribution using the laser diffraction method. *Soil and Tillage Research*, *211*, 105023. https://doi.org/10.1016/j.still.2021.105023

Portell, X., Pot, V., Garnier, P., Otten, W., & Baveye, P. C. (2018). Microscale heterogeneity of the spatial distribution of organic matter can promote bacterial biodiversity in soils: Insights from computer simulations. *Frontiers in Microbiology*, *9*, https://doi.org/10.3389/fmicb.2018.01583

Possinger, A. R., Zachman, M. J., Enders, A., Levin, B. D. A., Muller, D. A., Kourkoutis, L. F., & Lehmann, J. (2020). Organo–organic and organo–mineral interfaces in soil at the nanometer scale. *Nature Communications*, *11*(1), 6103. https://doi.org/10.1038/s41467–020–19792–9

Pot, V., Peth, S. O. L. A. P. L. M. F., Monga, O., Vogel, L. E., Genty, A., Garnier, P., Vieublé-Gonod, L., Ogurreck, M., Beckmann, F., & Baveye, P. C. (2015). Three-dimensional distribution of water and air in soil pores: comparison of two-phase two-relaxation-times lattice-Boltzmann and morphological model outputs with synchrotron X-ray computed tomography data. *Advances in Water Resources*, *84*, 87–102.

Prietzel, J., Thieme, J., & Salomé, M. (2010). Assessment of sulfur and iron speciation in a soil aggregate by combined S and Fe micro-XANES: microspatial patterns and relationships. *Journal of Synchrotron Radiation*, *17*(2), 166–172.

Probandt, D., Eickhorst, T., Ellrott, A., Amann, R., & Knittel, K. (2018). Microbial life on a sand grain: from bulk sediment to single grains. *The ISME Journal*, *12*(2), 623–633.

Pronk, G. J., Heister, K., Vogel, C., Babin, D., Bachmann, J., Ding, G.-C., Ditterich, F., Gerzabek, M. H., Giebler, J., Hemkemeyer, M., Kandeler, E., Kunhi Mouvenchery, Y., Miltner, A., Poll, C., Schaumann, G. E., Smalla, K., Steinbach, A., Tanuwidjaja, I., Tebbe, C. C., … Kögel-Knabner, I. (2017). Interaction of minerals, organic matter, and microorganisms during biogeochemical interface formation as shown by a series of artificial soil experiments. *Biology and Fertility of Soils*, *53*(1), 9–22.

Puppels, G. J., de Mul, F. F. M., Otto, C., Greve, J., Robert-Nicoud, M., Arndt-Jovin, D. J., & Jovin, T. M. (1990). Studying single living cells and chromosomes by confocal Raman microspectroscopy. *Nature*, *347*(6290), 301–303.

Qureshi, R. N., & Kok, W. T. (2011). Application of flow field-flow fractionation for the characterization of macromolecules of biological interest: a review. *Analytical and Bioanalytical Chemistry*, *399*(4), 1401–1411.

Rabbi, S. M. F., Daniel, H., Lockwood, P. V., Macdonald, C., Pereg, L., Tighe, M., Wilson, B. R., & Young, I. M. (2016). Physical soil architectural traits are functionally linked to carbon decomposition and bacterial diversity. *Scientific Reports*, *6*(1), 33012. https://doi.org/10.1038/srep33012

Rabot, E., Wiesmeier, M., Schlüter, S., & Vogel, H. J. (2018). Soil structure as an indicator of soil functions: A review. *Geoderma*, *314*, 122–137.

Rawlins, B. G., Wragg, J., Reinhard, C., Atwood, R. C., Houston, A., Lark, R. M., & Rudolph, S. (2016). Three-dimensional soil organic matter distribution, accessibility and microbial respiration in macroaggregates using osmium staining and synchrotron X-ray computed tomography. *Soil*, *2*(4), 659–671.

Ray, N., Rupp, A., & Prechtel, A. (2017). Discrete-continuum multiscale model for transport, biomass development and solid restructuring in porous media. *Advances in Water Resources*, *107*, 393–404.

Raynaud, X., & Nunan, N. (2014). Spatial ecology of bacteria at the microscale in soil. *Plos One*, *9*(1), e87217. https://doi.org/10.1371/journal.pone.0087217

Reading, M., Grandy, D., Hammiche, A., Bozec, L., & Pollock, H. M. (2002). Thermally assisted nanosampling and analysis using micro-IR spectroscopy and other analytical methods. *Vibrational Spectroscopy*, *29*(1), 257–260.

Rennert, T., Totsche, K. U., Heister, K., Kersten, M., & Thieme, J. (2012). Advanced spectroscopic, microscopic, and tomographic characterization techniques to study biogeochemical interfaces in soil. *Journal of Soils and Sediments*, *12*(1), 3–23.

Ritschel, T., & Totsche, K. U. (2019). Modeling the formation of soil microaggregates. *Computers & Geosciences*, *127*, 36–43.

Rodionov, A., Bauke, S. L., von Sperber, C., Hoeschen, C., Kandeler, E., Kruse, J., Lewandowski, H., Marhan, S., Mueller, C. W., Simon, M., Tamburini, F., Uhlig, D., von Blanckenburg, F., Lang, F., & Amelung, W. (2020). Biogeochemical cycling of phosphorus in subsoils of temperate forest ecosystems. *Biogeochemistry*, *150*, 313–328.

Rodionov, A., Lehndorff, E., Stremtan, C. C., Brand, W. A., Königshoven, H.-P., & Amelung, W. (2019). Spatial microanalysis of natural $^{13}C/^{12}C$ abundance in environmental samples using laser ablation-isotope ratio mass spectrometry. *Analytical Chemistry*, *91*(9), 6225–6232.

Rohde, F., Braumann, U.-D., & Schmidt, M. (2020). Correlia: an ImageJ plug-in to co-register and visualise multimodal correlative micrographs. *Journal of Microscopy*, *280*(1), 3–11.

Rupp, A., Guhra, T., Meier, A., Prechtel, A., Ritschel, T., Ray, N., & Totsche, K. U. (2019). Application of a cellular automaton method to model the structure formation in soils under saturated conditions: A mechanistic approach. *Frontiers in Environmental Science*, *7*, 170. https://doi.org/10.3389/fenvs.2019.00170

Soufan, R., Delaunay, Y., Gonod, L. V., Shor, L. M., Garnier, P., Otten, W., & Baveye, P. C. (2018). Pore-scale monitoring of the effect of microarchitecture on fungal growth in a two-dimensional soil-like micromodel. *Frontiers in Environmental Science*, *6*, 68. https://doi.org/10.3389/fenvs.2018.00068

Sarret, G., Smits, E. A. H. P., Michel, H. C., Isaure, M. P., Zhao, F. J., & Tappero, R. (2013). Use of synchrotron-based techniques to elucidate metal uptake and metabolism in plants. In D. L. Sparks (Ed.), *Advances in agronomy* (pp. 1–82). Academic Press.

Schaumann, G. E., & Kunhi Mouvenchery, Y. (2012). Erratum to: Potential of AFM–nanothermal analysis to study the microscale thermal characteristics in soils and natural organic matter (NOM). *Journal of Soils and Sediments*, *12*(1), 115–115.

Schaumann, G. E., & Thiele-Bruhn, S. (2011). Molecular modeling of soil organic matter: Squaring the circle? *Geoderma*, *166*(1), 1–14.

Schimpf, M. E., Caldwell, K., & Giddings, J. C. (2000). *Field-flow fractionation handbook*. Wiley.

Schlüter, S., Eickhorst, T., & Mueller, C. W. (2019). Correlative imaging reveals holistic view of soil microenvironments. *Environmental Science & Technology*, *53*(2), 829–837.

Schlüter, S., Leuther, F., Albrecht, L., Hoeschen, C., Kilian, R., Surey, R., Mikutta, R., Kaiser, K., Mueller, C. W., & Vogel, H.-J. (2022). Microscale carbon distribution around pores and particulate organic matter varies with soil moisture regime. *Nature Communications*, *13*(1), 2098. https://doi.org/10.1038/s41467-022-29605-w

Schmidt, M. W. I., Rumpel, C., & Kögel-Knabner, I. (1999). Evaluation of an ultrasonic dispersion procedure to isolate primary organomineral complexes from soils. *European Journal of Soil Science*, *50*(1), 87–94.

Schnepf, A., Carminati, A., Ahmed, M. A., Ani, M., Benard, P., Bentz, J., Bonkowski, M., Knott, M., Diehl, D., Duddek, P., Kröner, E., Javaux, M., Landl, M., Lehndorff, E., Lippold, E., Lieu, A., Mueller, C., Oburger, E., Otten, W., … Vetterlein, D. (2022). Linking rhizosphere processes across scales: Opinion. *Plant Soil*, *478*, 5–42.

Schomakers, J., Mentler, A., Steurer, T., Klik, A., & Mayer, H. (2011). Characterization of soil aggregate stability using low intensity ultrasonic vibrations. *International Agrophysics*, *25*(2), 165–172.

Schöning, I., Knicker, H., & Kögel-Knabner, I. (2005). Intimate association between O/N-alkyl carbon and iron oxides in clay fractions of forest soils. *Organic Geochemistry*, *36*(10), 1378–1390.

Schulze, B., Wirth, C., Linke, P., Brand, W. A., Kuhlmann, I., Horna, V., & Schulze, E.-D. (2004). Laser ablation-combustion-GC-IRMS—A new method for online analysis of intra-annual variation of $\delta^{13}C$ in tree rings. *Tree Physiology*, *24*(11), 1193–1201.

Schumacher, M., Christl, I., Scheinost, A. C., Jacobsen, C., & Kretzschmar, R. (2005). Chemical heterogeneity of organic soil colloids investigated by scanning transmission X-ray microscopy and C-1s NEXAFS microspectroscopy. *Environmental Science & Technology*, *39*(23), 9094–9100.

Schurig, C., Smittenberg, R. H., Berger, J., Kraft, F., Woche, S. K., Goebel, M.-O., Heipieper, H. J., Miltner, A., & Kaestner, M. (2013). Microbial cell-envelope fragments and the formation of soil organic matter: a case study from a glacier forefield. *Biogeochemistry*, *113*(1), 595–612.

Schweizer, S. A. (2022). Perspectives from the Fritz-Scheffer Awardee 2021: Soil organic matter storage and functions determined by patchy and piled-up arrangements at the microscale. *Journal of Plant Nutrition and Soil Science*, *185*(6), 694–706.

Schweizer, S. A., Bucka, F. B., Graf-Rosenfellner, M., & Kögel-Knabner, I. (2019). Soil microaggregate size composition and organic matter distribution as affected by clay content. *Geoderma*, *355*, 113901. https://doi.org/10.1016/j.geoderma.2019.113901

Schweizer, S. A., Graf-Rosenfellner, M., Bhat, N. A., Kayser, G., Sisodia, B. S., Kirchhof, G., Zikeli, S., Cadisch, G., & Bhullar, G. S. (2022). Responses of soil organic carbon, aggregate diameters, and hydraulic properties to long-term organic and conventional farming on a Vertisol in India. *Land Degradation & Development*, *33*(5), 785–797.

Schweizer, S. A., Hoeschen, C., Schlüter, S., Kögel-Knabner, I., & Mueller, C. W. (2018). Rapid soil formation after glacial retreat shaped by spatial patterns of organic matter accrual in microaggregates. *Global Change Biology*, *24*(4), 1637–1650.

Sexstone, A. J., Revsbech, N. P., Parkin, T. B., & Tiedje, J. M. (1985). Direct measurement of oxygen profiles and denitrification rates in soil aggregates. *Soil Science Society of America Journal*, *49*(3), 645–651.

Sharma, A., Muyskens, A., Guinness, J., Polizzotto, M. L., Fuentes, M., Tappero, R. V., Chen-Wiegart, Y.-c. K., Thieme, J., Williams, G. J., Acerbo, A. S., & Hesterberg, D. (2019). Multi-element effects on arsenate accumulation in a geochemical matrix determined using μ-XRF, μ-XANES and spatial statistics. *Journal of Synchrotron Radiation*, *26*(6), 1967–1979. https://doi.org/10.1107/S1600577519012785

Siebers, N., Abdelrahman, H., Krause, L., & Amelung, W. (2018). Bias in aggregate geometry and properties after disintegration and drying procedures. *Geoderma*, *313*, 163–171.

Siebers, N., Kruse, J., Jia, Y., Lennartz, B., & Koch, S. (2023). Loss of subsurface particulate and truly dissolved phosphorus during various flow conditions along a tile drain–ditch–brook continuum. *Science of The Total Environment*, *866*, 161439. https://doi.org/10.1016/j.scitotenv.2023.161439

Siebers, N., Voggenreiter, E., Joshi, P., Rethemeyer, J., & Wang, L. (2024). Synergistic relationships between the age of soil organic matter, Fe speciation, and aggregate stability in an arable Luvisol. *Journal of Plant Nutrition and Soil Science*, *187*, https://doi.org/10.1002/jpln.202300020

Six, J., Elliott, E. T., & Paustian, K. (2000a). Soil macroaggregate turnover and microaggregate formation: a mechanism for C sequestration under no-tillage agriculture. *Soil Biology and Biochemistry*, *32*(14), 2099–2103.

Six, J., Elliott, E. T., & Paustian, K. (2000b). Soil structure and soil organic matter II. A normalized stability index and the effect of mineralogy. *Soil Science Society of America Journal*, *64*(3), 1042–1049.

Six, J., Paustian, K., Elliott, E. T., & Combrink, C. (2000c). Soil structure and organic matter I. distribution of aggregate-size classes and aggregate-

associated carbon. *Soil Science Society of America Journal*, 64(2), 681–689.

Soil Science Society of America. (1997). *Glossary of soil science terms*. Soil Science Society of America.

Solomon, D., Lehmann, J., Harden, J., Wang, J., Kinyangi, J., Heymann, K., Karunakaran, C., Lu, Y., Wirick, S., & Jacobsen, C. (2012). Micro- and nano-environments of carbon sequestration: Multi-element STXM–NEXAFS spectromicroscopy assessment of microbial carbon and mineral associations. *Chemical Geology*, 329, 53–73.

Springston, S. R., Myers, M. N., & Giddings, J. C. (1987). Continuous particle fractionation based on gravitational sedimentation in split-flow thin cells. *Analytical Chemistry*, 59(2), 344–350.

Steffens, M., Rogge, D. M., Mueller, C. W., Höschen, C., Lugmeier, J., Kölbl, A., & Kögel-Knabner, I. (2017). Identification of distinct functional microstructural domains controlling C storage in soil. *Environmental Science & Technology*, 51(21), 12182–12189.

Stemmer, M., Gerzabek, M. H., & Kandeler, E. (1998). Organic matter and enzyme activity in particle-size fractions of soils obtained after low-energy sonication. *Soil Biology and Biochemistry*, 30(1), 9–17.

Stewart, S., Priore, R. J., Nelson, M. P., & Treado, P. J. (2012). Raman imaging. *Annual Review of Analytical Chemistry*, 5(1), 337–360.

Stöhr, J. (2013). *NEXAFS spectroscopy* (Vol. 25). Springer Science & Business Media.

Stoops, G. (2020). *Guidelines for analysis and description of soil and regolith thin sections*. ASA, CSSA, SSSA.

Stoops, G., & Nicosia, C. (2017). Sampling for soil micromorphology. In C. Nicosia, & G. Stoops (Eds.), *Archaeological soil and sediment micromorphology* (pp. 383–391). Wiley.

Stosnach, H. (2005). Environmental trace-element analysis using a bench-top total reflection X-ray fluorescence spectrometer. *Analytical Sciences*, 21(7), 873–876.

Stosnach, H. (2007). S2 PICOFOX total reflection X-ray fluorescence spectroscopy—Working principles. *Lab report. Bruker AXS Microanalysis GmbH*.

Stuckey, J. W., Yang, J., Wang, J., & Sparks, D. L. (2017). Advances in scanning transmission X-ray microscopy for elucidating soil biogeochemical processes at the submicron scale. *Journal of Environmental Quality*, 46(6), 1166–1174.

Szoboszlay, M., & Tebbe, C. C. (2021). Hidden heterogeneity and co-occurrence networks of soil prokaryotic communities revealed at the scale of individual soil aggregates. *MicrobiologyOpen*, 10(1), e1144. https://doi.org/10.1002/mbo3.1144

Tang, N., Siebers, N., Leinweber, P., Eckhardt, K. U., Dultz, S., Nischwitz, V., & Klumpp, E. (2022). Implications of free and occluded fine colloids for organic matter preservation in arable soils. *Environmental Science & Technology*, 56(19), 14133–14145.

Tang, Y., & Valocchi, A. J. (2013). An improved cellular automaton method to model multispecies biofilms. *Water Research*, 47(15), 5729–5742.

Tarcea, N., Harz, M., Rösch, P., Frosch, T., Schmitt, M., Thiele, H., Hochleitner, R., & Popp, J. (2007). UV Raman spectroscopy—A technique for biological and mineralogical in situ planetary studies. *Spectrochimica Acta Part A: Molecular and Biomolecular Spectroscopy*, 68(4), 1029–1035.

Tippkötter, R., & Ritz, K. (1996). Evaluation of polyester, epoxy and acrylic resins for suitability in preparation of soil thin sections for in situ biological studies. *Geoderma*, 69(1), 31–57.

Tisdall, J. M., & Oades, J. M. (1982). Organic matter and water-stable aggregates in soils. *Journal of Soil Science*, 33(2), 141–163.

Toporski, J., Dieing, T., & Hollricher, O. (2011). *Confocal raman microscopy* (Vol. 158). Springer.

Totsche, K. U., Amelung, W., Gerzabek, M. H., Guggenberger, G., Klumpp, E., Knief, C., Lehndorff, E., Mikutta, R., Peth, S., Prechtel, A., Ray, N., & Kögel-Knabner, I. (2018). Microaggregates in soils. *Journal of Plant Nutrition and Soil Science*, 181(1), 104–136.

Totsche, K. U., Rennert, T., Gerzabek, M. H., Kögel-Knabner, I., Smalla, K., Spiteller, M., & Vogel, H.-J. (2010). Biogeochemical interfaces in soil: The interdisciplinary challenge for soil science. *Journal of Plant Nutrition and Soil Science*, 173(1), 88–99.

Towett, E. K., Shepherd, K. D., & Cadisch, G. (2013). Quantification of total element concentrations in soils using total X-ray fluorescence spectroscopy (TXRF). *Science of The Total Environment*, 463–464, 374–388.

Tuoriniemi, J., Holbrook, T. R., Cornelis, G., Schmitt, M., Stärk, H.-J., & Wagner, S. (2020). Measurement of number concentrations and sizes of Au nano-particles spiked into soil by laser ablation single particle ICPMS. *Journal of Analytical Atomic Spectrometry*, 35(8), 1678–1686.

Upton, R. N., Bach, E. M., & Hofmockel, K. S. (2019). Spatio-temporal microbial community dynamics within soil aggregates. *Soil Biology and Biochemistry*, 132, 58–68.

van Zwol, P. J., Palasantzas, G., van de Schootbrugge, M., de Hosson, J. T. M., & Craig, V. S. J. (2008). Roughness of microspheres for force measurements. *Langmuir*, 24(14), 7528–7531.

Védère, C., Vieublé Gonod, L., Nunan, N., & Chenu, C. (2022). Opportunities and limits in imaging microorganisms and their activities in soil microhabitats. *Soil Biology and Biochemistry*, 174, 108807. https://doi.org/10.1016/j.soilbio.2022.108807

Veldkamp, E. (1994). Organic carbon turnover in three tropical soils under pasture after deforestation. *Soil Science Society of America Journal*, 58(1), 175–180.

Vergara Sosa, M., Lehndorff, E., Rodionov, A., Gocke, M., Sandhage-Hofmann, A., & Amelung, W. (2021). Micro-scale resolution of carbon turnover in soil—Insights from laser ablation isotope ratio mass spectrometry on water-glass embedded aggregates. *Soil Biology and Biochemistry*, 159, 108279. https://doi.org/10.1016/j.soilbio.2021.108279

Verrecchia, E. P., Trombino, L. (2021). Observation of soils: From the field to the microscope. In E. P. Verrecchia, & L. Trombino (Eds.), *A visual atlas for soil micromorphologists* (pp. 1–17). Springer. https://doi.org/10.1007/978–3–030–67806–7_1

Vidal, A., Hirte, J., Bender, S. F., Mayer, J., Gattinger, A., Höschen, C., Schädler, S., Iqbal, T. M., & Mueller, C. W. (2018). Linking 3D soil structure and plant–microbe–soil carbon transfer in the rhizosphere. *Frontiers in Environmental Science*, 6, https://doi.org/10.3389/fenvs.2018.00009

Virto, I., Barré, P., & Chenu, C. (2008). Microaggregation and organic matter storage at the silt-size scale. *Geoderma*, 146(1), 326–335.

Vitorello, V. A., Cerri, C. C., Andreux, F., Feller, C., & Victória, R. L. (1989). Organic matter and natural Carbon–13 distribution in forested and cultivated Oxisols. *Soil Science Society of America Journal*, 53(3), 773–778.

Vogel, C., Mueller, C. W., Höschen, C., Buegger, F., Heister, K., Schulz, S., Schloter, M., & Kögel-Knabner, I. (2014). Submicron structures provide preferential spots for carbon and nitrogen sequestration in soils. *Nature Communications*, 5(1), 2947. https://doi.org/10.1038/ncomms3947

Vogel, C., Ramsteiner, M., Sekine, R., Doolette, A., & Adam, C. (2017). Characterization of phosphorus compounds in soils by deep ultraviolet (DUV) Raman microspectroscopy. *Journal of Raman Spectroscopy*, 48(6), 867–871.

Vogel, H.-J., Balseiro-Romero, M., Kravchenko, A., Otten, W., Pot, V., Schlüter, S., Weller, U., & Baveye, P. C. (2022). A holistic perspective on soil architecture is needed as a key to soil functions. *European Journal of Soil Science*, 73(1), e13152. https://doi.org/10.1111/ejss.13152

Voltolini, M., Taş, N., Wang, S., Brodie, E. L., & Ajo-Franklin, J. B. (2017). Quantitative characterization of soil micro-aggregates: New opportunities from sub-micron resolution synchrotron X-ray microtomography. *Geoderma*, 305, 382–393.

von Sperber, C., Lewandowski, H., Tamburini, F., Bernasconi, S. M., Amelung, W., & Frossard, E. (2017). Kinetics of enzyme-catalysed oxygen isotope exchange between phosphate and water revealed by Raman spectroscopy. *Journal of Raman Spectroscopy*, 48(3), 368–373.

Wagner, A. O., Praeg, N., Reitschuler, C., & Illmer, P. (2015). Effect of DNA extraction procedure, repeated extraction and ethidium monoazide (EMA)/propidium monoazide (PMA) treatment on overall DNA yield and impact on microbial fingerprints for bacteria, fungi and archaea in a reference soil. *Applied Soil Ecology*, 93, 56–64.

Wang, C., Heraty, L. J., Wallace, A. F., Liu, C., Li, X., McGovern, G. P., Horita, J., Fuller, M. E., Hatzinger, P. B., & Sturchio, N. C. (2021). Position-specific isotope effects during alkaline hydrolysis of 2,4-dinitroanisole resolved by compound-specific isotope analysis, ^{13}C NMR, and density-functional theory. *Chemosphere*, *280*, 130625. https://doi.org/10.1016/j.chemosphere.2021.130625

Wang, C., Zhang, L., Jiang, X., Ma, W., Geng, H., Wang, X., & Li, M. (2022). Toward efficient and high-fidelity metagenomic data from sub-nanogram DNA: evaluation of library preparation and decontamination methods. *BMC Biology*, *20*(1), 225. https://doi.org/10.1186/s12915-022-01418-9

Wang, L., Missong, A., Amelung, W., Willbold, S., Prietzel, J., & Klumpp, E. (2020). Dissolved and colloidal phosphorus affect P cycling in calcareous forest soils. *Geoderma*, *375*, 114507. https://doi.org/10.1016/j.geoderma.2020.114507

Watteau, F., & Villemin, G. (2018). Soil microstructures examined trough transmission electron microscopy reveal soil–microorganisms interactions. *Frontiers in Environmental Science*, *6*, https://doi.org/10.3389/fenvs.2018.00106

Watteau, F., Villemin, G., Bartoli, F., Schwartz, C., & Morel, J. L. (2012). 0–20 μm aggregate typology based on the nature of aggregative organic materials in a cultivated silty topsoil. *Soil Biology and Biochemistry*, *46*, 103–114.

Weng, Z., Lehmann, J., Van Zwieten, L., Joseph, S., Archanjo, B. S., Cowie, B., Thomsen, L., Tobin, M. J., Vongsvivut, J., Klein, A., Doolette, C. L., Hou, H., Mueller, C. W., Lombi, E., & Kopittke, P. M. (2022). Probing the nature of soil organic matter. *Critical Reviews in Environmental Science and Technology*, *52*(22), 4072–4093.

Wilhelm, R. C., Lynch, L., Webster, T. M., Schweizer, S., Inagaki, T. M., Tfaily, M. M., Kukkadapu, R., Hoeschen, C., Buckley, D. H., & Lehmann, J. (2022). Susceptibility of new soil organic carbon to mineralization during dry-wet cycling in soils from contrasting ends of a precipitation gradient. *Soil Biology and Biochemistry*, *169*, 108681. https://doi.org/10.1016/j.soilbio.2022.108681

Williams, P. S. (2022). Chapter 18 - Theoretical principles of field-flow fractionation and SPLITT fractionation. In C. Contado (Ed.), *Particle separation techniques* (pp. 579–620). Elsevier.

Wilson, M. A. (2013). *NMR techniques & applications in geochemistry & soil chemistry*. Elsevier.

Witten, T. A., & Sander, L. M. (1981). Diffusion-limited aggregation, a kinetic critical phenomenon. *Physical Review Letters*, *47*(19), 1400–1403.

Wobrauschek, P. (2007). Total reflection x-ray fluorescence analysis—A review. *X-Ray Spectrometry*, *36*(5), 289–300.

Woche, S. K., Goebel, M.-O., Mikutta, R., Schurig, C., Kaestner, M., Guggenberger, G., & Bachmann, J. (2017). Soil wettability can be explained by the chemical composition of particle interfaces—An XPS study. *Scientific Reports*, *7*(1), 42877. https://doi.org/10.1038/srep42877

Wright, D. A., Killham, K., Glover, L. A., & Prosser, J. I. (1995). Role of pore size location in determining bacterial activity during predation by protozoa in soil. *Applied and Environmental Microbiology*, *61*, 3537–3543.

Wu, B., & Becker, J. S. (2012). Imaging techniques for elements and element species in plant science. *Metallomics*, *4*(5), 403–416.

Xiao, J., Wen, Y.-L., Dou, S., Bostick, B. C., He, X.-H., Ran, W., Yu, G.-H., & Shen, Q.-R. (2019). A new strategy for assessing the binding microenvironments in intact soil microaggregates. *Soil and Tillage Research*, *189*, 123–130.

Xie, C., & Li, Y.-Q. (2003). Confocal micro-Raman spectroscopy of single biological cells using optical trapping and shifted excitation difference techniques. *Journal of Applied Physics*, *93*(5), 2982–2986.

Young, I. M., & Crawford, J. W. (2004). Interactions and self-organization in the soil-microbe complex. *Science*, *304*(5677), 1634–1637.

Young, J. M., Rawlence, N. J., Weyrich, L. S., & Cooper, A. (2014). Limitations and recommendations for successful DNA extraction from forensic soil samples: A review. *Science & Justice*, *54*(3), 238–244.

Yu, G., Xiao, J., Hu, S., Polizzotto, M. L., Zhao, F., McGrath, S. P., Li, H., Ran, W., & Shen, Q. (2017). Mineral availability as a key regulator of soil carbon storage. *Environmental Science & Technology*, *51*, 4960–4969.

Zech, S., Dultz, S., Guggenberger, G., Prechtel, A., & Ray, N. (2020). Microaggregation of goethite and illite evaluated by mechanistic modeling. *Applied Clay Science*, *198*, 105845. https://doi.org/10.1016/j.clay.2020.105845

Zech, S., Ritschel, T., Ray, N., Totsche, K. U., & Prechtel, A. (2022). How water connectivity and substrate supply shape the turnover of organic matter—Insights from simulations at the scale of microaggregates. *Geoderma*, *405*, 115394. https://doi.org/10.1016/j.geoderma.2021.115394

Zech, S., Schweizer, S. A., Bucka, F. B., Ray, N., Kögel-Knabner, I., & Prechtel, A. (2022). Explicit spatial modeling at the pore scale unravels the interplay of soil organic carbon storage and structure dynamics. *Global Change Biology*, *28*(15), 4589–4604.

Zhao, Y., Hu, X., & Li, X. (2020). Analysis of the intra-aggregate pore structures in three soil types using X-ray computed tomography. *Catena*, *193*, 104622. https://doi.org/10.1016/j.catena.2020.104622

Zhu, J., Zhu, L., Zhu, R., Tian, S., & Li, J. (2009). Surface microtopography of surfactant modified montmorillonite. *Applied Clay Science*, *45*(1), 70–75.